MULTIPLEXED PROTEIN BIOMARKER ANALYSIS ON SILICON PHOTONIC MICRORING RESONATORS: TRANSLATION TOWARDS CLINICAL DIAGNOSTICS

BY

WINNIE W. SHIA

DISSERTATION

Submitted in partial fulfillment of the requirements
for the degree of Doctor of Philosophy in Chemistry
in the Graduate College of the
University of Illinois at Urbana-Champaign, 2016

Urbana, Illinois

Doctoral Committee:

Professor Ryan C. Bailey, Chair
Professor Catherine J. Murphy
Professor Kenneth S. Suslick
Professor Jonathan V. Sweedler

Abstract

Protein biomarkers are valuable indicators of human physiological states. In clinical practice, they play a strong role in presymptomatic diagnosis of various diseases, as well as evaluation of disease prognosis and aid in treatment decisions making. Due to the importance of biomarkers, much efforts were made towards the discovery of good biomarker candidates, analytical methodologies for biomarker detection and quantitation, and ultimately, translation of the developed analytical platform to detect novel biomarkers in clinical practice.

This dissertation places stronger emphasis on the latter two aspects of protein biomarker research: detection of biomarkers through immunoassays development, and translation of optimized assays to clinical samples analysis. For the immunoassays development aspect, assays described in this thesis were developed on a platform based on silicon photonic microring resonator technology. This sensing technology has high potential for clinical diagnostics utility, as sensor chips of this platform can be cheaply manufactured through a highly scalable process. Moreover, continuous improvements in sensor chip designs allowed rapid increase of biomarkers that can be detected simultaneously in a multiplexed panel. Multiplexed measurements are desirable due to the heterogeneity of the human population, and in many instances quantitation of multiple biomarkers are necessary to identify the disease state. Additionally, the latest generation sensing platforms have integrated fluidic systems that can be programmed for immunoassay automation, which shortens intensive training required for clinical laboratory personnel to perform assay runs.

For the translational aspect of applying novel biomarker detection to the clinical laboratory, collaborations have been established with hospital physicians for access to clinical samples from diseased patients. Blood serum or plasma samples from these patients have been evaluated by the immunoassays developed on the microring resonator platform, and results from the platform's measurements are then evaluated against other established immunoassay techniques to assess assay performance. Translational research in clinical diagnostics is a trial and error process. Good immunoassays developed for novel biomarkers might not have good diagnostics value once placed into clinical evaluations, and thus the biomarker discovery and assay development research phases repeats through again.

This doctoral dissertation describes the progress of immunoassay development throughout the continuous improvements in the microring resonator platform, and eventually translates some of the developed assays to clinical samples analysis. Chapter 1 contains an introduction to protein biomarker immunoassays and their translational research value, with a more in depth description of microring resonators operation principles and the progression of the sensing platform development. Chapter 2 describes a simple detection of ricin toxin to illustrate the utility of microring resonators for protein analysis. Chapter 3 focuses on the development of an 8-plex panel to detect cancer biomarker that utilizes a protein multilayer strategy to improve assay signals. Chapter 4 explores the clinical utility of the platform by detecting monocyte chemactic protein-1 in human serum matrix. Chapter 5 describes the detection and quantitation of cardiac troponin I in serum samples from cardiac disease patients. Chapter 6 demonstrates the development of a multiplexed assay panel to detect 12 immunoregulatory markers associated with sepsis, as well as application of the panel to test plasma samples from septic patients at the intensive care unit of a local hospital. Finally, Chapter 7 outlines the future work related to the cardiac troponins project and the sepsis project described in the previous two chapters.

Acknowledgments

I would like to acknowledge all the help and support from many people throughout my graduate work at UIUC. First, I must thank my advisor Prof. Ryan Bailey for his mentorship and support to my professional development throughout the years. I would also like to thank the rest of my thesis committee members, Prof. Catherine Murphy, Prof. Kenneth Suslick, and Prof. Jonathan Sweedler for their guidance to my research progress.

I would like to thank the American Heart Association for their predoctoral fellowship that supported my final two years of graduate school. This fellowship provided great flexibility to my work and inspired my interest to establish a career related to clinical chemistry and human healthcare.

I greatly enjoyed working with the past and present members of the Bailey Group. Everyone I have worked with have been wonderful colleagues, providing helpful feedback when I encountered challenges in research, moral support in my times of frustration, and often the source of humor (especially with the contributions to the Bailey Group "Quote Wall").

I also want to express my gratitude to Furong Sun, Dr. Haijun Yao, and Dr. Kevin Tucker at the Mass Spectrometry Laboratory for giving me the opportunity to gain experience in LC-MS analysis to prepare for my upcoming job in Atlanta.

Finally, I want to thank my parents and Vincent for their endless love and support, as well as my friends Alvaro, Christine and Maria that I met in Austin, my former classmates at YWGS in Hong Kong, for continuously motivating me to finish my PhD.

Table of Contents

Chapter 1:

Introduction to Microring Resonators for Multiplexed Diagnostics

1.1 Protein biomarkers immunoassays

Starting with the invention of an radioimmunoassay against blood insulin by Berson and Yalow in the 1950s,(1) protein biomarkers have played an increasingly important role in clinical diagnostics due to their predictive value in identifying disease types and progression. In protein biomarkers immunoassays, antibodies are utilized to detect low quantities of the target analyte biomarker in a sample of interest. These antibodies can be generated with high affinity and outstanding specificity against a wide range of biomolecules (known as antigens), which is crucial to the success of immunoassays.(2)

Immunoassays can be classified as limited reagent and excess reagents formats.(3) Assays in limited reagent format are known as competitive binding assays, where a limited amount of antibodies is immobilized on a solid phase, typically a microwell plate. Subsequently, a mixture is introduced to compete for the limited binding sites of the immobilized antibodies; the mixture consists of the sample containing the analyte of interest, and a fix amount of antigen labeled with a signal molecule. As the analyte concentration in the sample increases, less of the labeled antigen can bind to the antibodies, resulting in a decrease of measured signal. Thus, in a competitive binding assay, the analyte concentration is inversely related to the generated signal in a calibration curve.

Assays in excess reagent format are known as sandwich immunoassays. Similar to competitive binding assays, capture antibodies are immobilized on a solid phase, and the sample containing the analyte is allowed to incubate and bind to the capture antibodies. Afterwards, excess amounts of tracer antibodies labeled with signal molecules are added. Both the capture and tracer antibodies can specifically bind to two different non-interfering epitopes of the analyte molecule, effectively forming a “sandwich”. In this type of assay, the analyte concentration is proportional to the generated signal.

As mentioned earlier, the very first type of immunoassays utilized radioactive labels, but later they were modified to using enzyme labels that catalyze conversion of substrates to colorimetric signals.(4) This type of assay signaling format, known as enzyme-linked immunosorbent assays (ELISAs), turned out to be the most commonly adopted assay configuration. While this method is considered a gold standard for immunoassays, its main drawbacks for clinical

utility are in the large patients' sample volume required, the laborious assay rinse steps, and the long incubation time to acquiring test results.(5) Moreover, traditionally ELISAs are used to target single biomarker analyte per sample, but a diagnosis based on detection of one single biomarker is often unreliable due to the inherent complexity of different diseases, and often multiple biomarker analysis is required.(6-8)

In the 1980s, Roger Ekins first conceived the idea of multi-analyte immunoassays, which are built upon traditional immunoassay principles of utilizing multiple high affinity capture/tracer agents to detect biomarkers of interest.(9) More importantly, he proposed that miniaturization of immunoassay systems can improve sensitivity and selectivity due to shortening the diffusion distances, thus overcoming drawbacks of traditional ELISAs. This miniaturization theory also revolutionized clinical diagnostics, as it enables biomarker analysis from small volumes of clinical samples.(10) In the current era of personalized medicine, multiplexed biomarker immunoassays become essential for differentiating between individual patient's characteristics among various disease states. This is because for many complex diseases such as inflammatory diseases and cancers, the underlying cell-signaling pathway induced by the disease is different even if patients are exhibiting similar physiological symptoms, and monitoring changes in multiple biomarkers involved in this intricate cell-signaling network is crucial to make an informative diagnosis and treatment decisions.(11, 12)

1.2 Contemporary multiplexed biomarker immunoassays

According to Tighe *et al.*,(13) current multiplexed biomarker immunoassays are generally categorized into two types: planar-based assays or suspension-based assays. As its name implies, planar-based assays consist of a planar surface immobilized with multiple capture agents to target biomarker analytes in the sample flowing across the surface. Fluorescent or chemiluminescent-tagged tracer molecules targeting the captured analytes are commonly used as the reporter signal.(14) The classic example of this assay type are microarrays on glass slides, though there are other assays utilizing detection strategies outside of fluorescent or chemiluminescent labels, for example surface plasmon resonance (SPR), quartz crystal microbalance, or electrochemical sensing methodologies can also be classified as planar-based assays if a planar geometry is adopted.(15-19) In suspension-based assays, rather than utilizing a planar surface for immunoassay platform, unique fluorescent/chemiluminscent-coded beads conjugated with capture agents are

suspended into the sample to capture biomarker analytes. After incubation and rinsing steps, tracer molecules with fluorescent/chemiluminescent tags dissimilar to the ones used by the beads are added in to detect the analyte bound on the beads surface. Each of these beads can then be uniquely identified by flow cytometry principles.(20) A common example for suspension-based assays is the Luminex® system.

Both the planar and suspension-based assay platforms have their advantages and limitations. Suspension-based assays have better precision due to their capabilities to have a large number of beads (50-100) for replicate measurements,(21) while precision of planar assays are limited by the spot density of capture agents on the planar platform. In terms of inter-assay precision, suspension assays have manufacturing variations of beads size, which can account for up to 32% difference in fluorescent readings,(22) whereas for planar assays the variability depends on the reproducibility of array spots from different automated printing techniques.(23) Both systems have cross-reactivity issues that arise from multiplexing, but suspension assays potentially have higher cross-reactivity due to the circulation of beads in sample that can freely interact with protein components and cross-link with one another.(13) For clinical applications, the capacity to automate the system is critical as well. In this regard, suspension assays are well integrated with automated flow cytometry techniques, while planar arrays are simpler to integrate microfluidics automation. Integration with microfluidics adds potential for manufacturing smaller, point-of-care devices that is important for translation of clinical diagnostics from bench to bedside.

1.3 Introduction to microring resonators operation principles

Since this dissertation is centered on microring resonator sensors, it is important to describe the background theory of this technology and its operation principles. Microring resonators belong to a class of sensors known as whispering gallery mode (WGM) sensors. This terminology came from the phenomenon first observed by Lord Rayleigh at the dome of St. Paul's Cathedral in London. He noticed that whispers from one end of the dome were audible at specific positions around the structure, and later on discovered that this phenomenon is due to resonance based on acoustic wave interference throughout the dome. Eventually, it was revealed that electromagnetic waves also exhibit similar resonance qualities, and many WGM optical sensors of various geometries were developed, as discussed in the comprehensive review by Vollmer and Arnold.(24) In the case of microring resonators, the geometry of the sensor is in a ring format. These structures

are fabricated via photolithographic patterning and reactive ion etching of features on silicon-on-insulator (SOI) wafers. These features consist of 30-µm diameter circular waveguides etched adjacent to linear waveguides (200 nm × 500 nm cross section dimensions), with grating couplers at either end. Light from a tunable diode laser centered at 1550 nm is directed to the linear waveguides via the grating couplers, and couple to the microring structures upon optical resonance conditions governed by the following equation:

$$m\lambda = 2\pi r n_{eff}$$

where m is an integer, λ is the wavelength of light, r is the radius of the microring, and n_{eff} is the effective refractive index of the optical mode. From the equation, it is apparent that the wavelength is sensitive to changes in refractive index at near proximity to the microring. Thus, any molecular binding events near the microring surface, for example antibodies immobilization on microrings and subsequent antibody-analyte interactions for assays described in this thesis, can alter the local refractive index and correspondingly cause a shift in resonance wavelength, which is monitored from the output light intensity in real time, as illustrated in Figure 1.1.(25, 26)

1.4 Progression of the microring resonator platform development

The microring resonator chip arrays and instrumentation used in this thesis work were developed in collaboration with Genalyte, Inc. (San Diego, CA), and have undergone many iterations since the beginning of the dissertation. The first generation design was described in comprehensive detail by Iqbal,(25) and later design generations were built upon this work. Some key points to note for this first generation system is that the sensor chip array consists of 32 individually addressable microrings on a 6 mm × 6 mm chip size, and the entire chip is spin coated with a perfluoropolymer cladding. Annular openings are etched off for 24 of the microrings, allowing them to actively interact with assay solutions to monitor binding interactions. The remaining 8 microrings are left covered by the perfluoropolymer and only respond to temperature fluctuations, effectively serving as thermal controls rings. To run an immunoassay experiment, a sensor chip immobilized with capture antibodies on the microrings is assembled in a cartridge consisting of an aluminum chip holder, a Mylar gasket that has fluidic cut-outs that direct solution flow over the microrings, and a Teflon piece with screwed in ports linking inlet fluidic tubings to assay reagents and the waste outlet to external syringe pumps. This first generation instrument was

used to perform ricin detection experiments described in Chapter 2. In the second generation design, named as Maverick M1 system, peristaltic fluidic pumps and an assay reagent holder stage were integrated into the instrument, and these components can be controlled by a connected computer uploaded with a pre-programed immunoassay recipe. This design greatly improved fluidic automation for assay runs. The sensor chip performance for the Maverick M1 system also greatly improved as well. In the initial "beta testing" design, the chip dimensions were altered down to 4 mm × 6 mm, while the number of microrings increased to 34 sensors, with 2 rings kept covered by the perfluoropolymer as thermal controls. This instrument version was used for the work of developing the 8-plex cancer biomarker panel described in Chapter 3. In the later version of the instrument, the number of microrings on each sensor chip further increased to 132 total rings, 4 rings serving as thermal controls and the remaining 128 active sensor rings were grouped into 32 clusters of 4 rings, which enables 4 replicate measurements for each cluster. This later instrument version was used for experiments described in Chapters 4 and 5. The latest generation instrument of the instrument is the Maverick M24 system. The sensor chips used in this system are identical to the 132-microrings sensors used in the later M1 design, but rather than manually assembling an individual chip to a cartridge prior to each experiment, these chips come pre-assembled in a cartridge of 12 chips array, with the inlet/outlet ports and microfluidic channels integrated within the rack. This new set-up enables performing 12 consecutive experiments without interruptions, which greatly shortens preparation time and facilitates clinical samples testing for experiments described in Chapter 6 for sepsis diagnostics applications.

1.5 Objective of thesis: Translation of microring resonator assays to clinical diagnostics

The underlying theme of this dissertation is to translate protein immunoassays developed on the microring resonator platform to clinical diagnostics applications. As described by multiple literature sources, translational science is a cyclic process involving interconnection of four different research phases illustrated in Figure 1.2: discovery, development, delivery, and outcome.(3, 27-29) For the case of translating biomarkers immunoassays to clinical diagnostics, the discovery phase is the identification of novel biomarkers relevant to disease diagnosis, the development phase involves biomarker immunoassay development and validation on a clinical platform, the delivery phase is to apply the developed platform to evaluate clinical samples, and

finally the outcome phase involves interpretation of clinical results and assessment of public health outcomes upon implementing a new assay. Predictive analytics, a statistical method that utilizes a large volume of health data set to predict individual patient's outcome, is often utilized to interpret clinical results.(30, 31) As shown in the diagram in Figure 1.2, these four research phases often interact with one another in no particular order.

This dissertation mainly focuses on the development and delivery phases in translational research. For the development phase, our group has repeatedly demonstrated detection of various clinical protein biomarkers on microring resonator sensor platforms in the past,(26, 32-36) and this thesis work added upon that by optimizing assays for additional markers and expanding the number of biomarkers detectable on a multiplexed panel. The motivation behind utilizing this sensor platform comes from the many superior qualities over other multiplexed immunoassay platforms. Firstly, microring resonator arrays have well-established fabrication process through standard semiconductor processing technologies that enables mass-production of many devices in bulk for clinical use. Secondly, unlike immunoassays that are solely based on fluorescent/colorimetric endpoint signals, microring resonators can monitor each individual binding step of the assay in real-time, beginning from analyte binding to capture agents, tracer molecules binding to analyte, to later stages of incorporating amplification strategies. As selection of sensitive and selective capture agents play a highly important role to develop a sensitive immunoassay, this real-time monitoring of molecular interactions is highly useful in the initial stages of assay development, where multiple capture agents can be evaluated on their binding affinity to the analyte of interest, as well as their potential cross-reactivity to other assay components.

Regarding the delivery phase focus in translational research, the work described in this thesis initiated the next step of translating protein biomarker assays to actual clinical utility. This was aided by the collaboration with clinicians and physicians from multiple hospitals, who were able to provide valuable patients' samples to evaluate and optimize the performance of microring arrays immunoassays. The work developed in this dissertation has focused on developing immunoassays that have the ability to monitor disease onset, predict prognosis and treatment efficacy. This is also the fundamental goal of integrating analytical chemistry with translational

medicine, which aims to improve human health through translating findings from clinical diagnostic tools and implementing them to real-world practice.

1.6 Outline of thesis

The chapters of this thesis document the concurrent innovation in assay design through the progressive improvements in the microring resonator platform setup. Chapter 2 describes the initial work of protein detection on microring resonators, using ricin toxin as a model. This chapter illustrates that different antibodies against the same molecular target can have dissimilar binding affinities, and microring resonators have the multiplexed capabilities to evaluate optimal antibodies for immunoassay development. Chapter 3 demonstrates multiplexed detection of cancer biomarkers in a complex human serum matrix, and also documents the use of protein multilayers to amplify signals for sandwich immunoassays. Chapter 4 focuses on the validation of clinical utility of the microring resonator platform through the detection and quantitation of clinically relevant concentration of monocyte chemotactic protein-1 in serum. Chapter 5 describes the detection and quantitation of cardiac troponin I in cardiac disease patients' serum samples. Chapter 6 illustrates the development of a 14-plex biomarker panel to monitor the fluctuation of immunoregulatory markers in septic patients' plasma samples. Finally, Chapter 7 discusses the future direction of clinical immunoassays on the microring resonator platform.

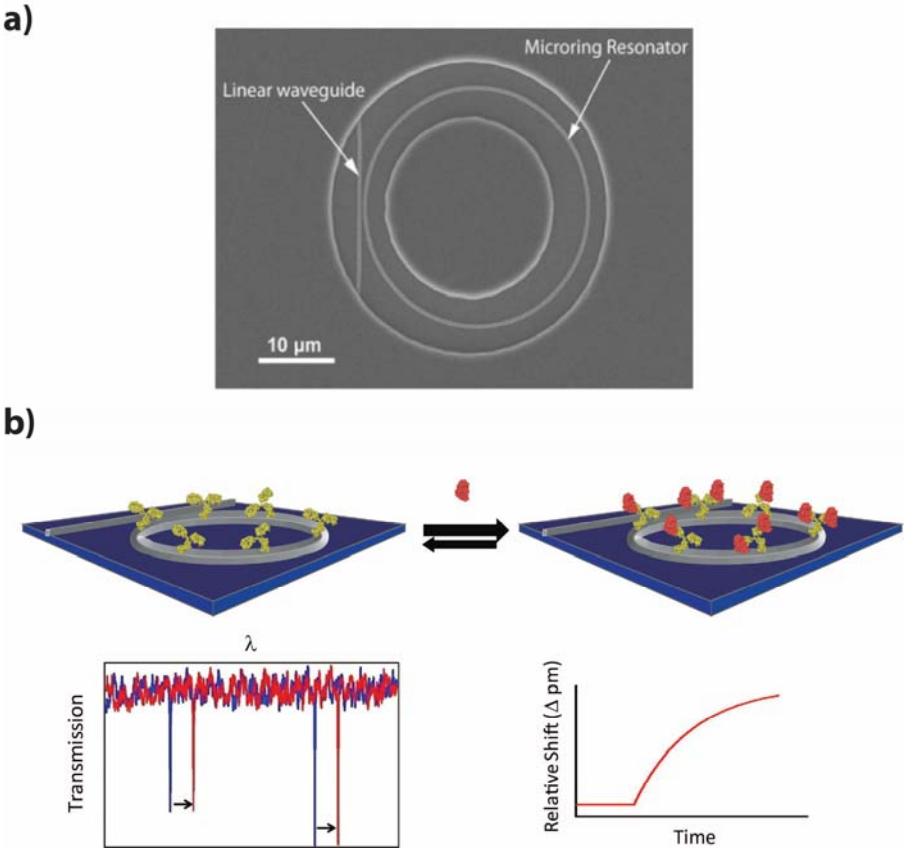

Figure 1.1 a) Scanning electron microscopy image of a microring. Light from a tunable diode laser is directed through the linear waveguide and couples to the circular microring resonator when resonance conditions are met. **b)** Schematic diagram illustrating capture antibodies (yellow) immobilized on a microring, along with the transmission spectrum showing the characteristic dips at the resonance wavelength. Upon analyte (red) binding to capture antibodies on the microring surface, changes in refractive index leads to a shift in the transmission spectrum (from blue to red traces). The microring resonator instrumentation monitors the relative wavelength shift to produce the output sensogram in real-time. Figure adapted from Washburn, *et al.*(26)

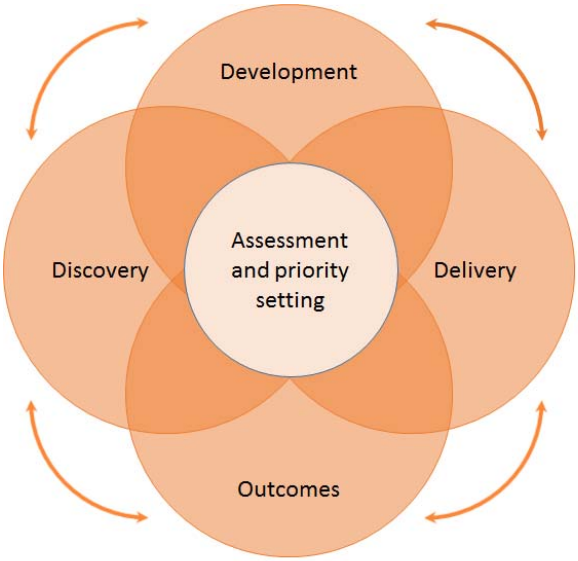

Figure 1.2 Diagram illustrating the four different phases of translational research, where each phase in the process are interconnected with one another through constant assessment at each phase.

1.7 References

1. Yalow RS, Berson SA. Immunoassay of endogenous plasma insulin in man. The Journal of Clinical Investigation 1960;39:1157-75.
2. Wild D. Chapter 1.2 - immunoassay for beginners. In: Wild D, ed. The immunoassay handbook (fourth edition), Vol. Oxford: Elsevier, 2013:7-10.
3. Rai AJ. Biomarkers in translational research: Focus on discovery, development and translation of protein biomarkers to clinical immunoassays. Expert Review of Molecular Diagnostics 2007;7:545+.
4. Engvall E, Perlmann P. Enzyme-linked immunosorbent assay (elisa) quantitative assay of immunoglobulin g. Immunochemistry 1971;8:871-4.
5. Aydin S. A short history, principles, and types of elisa, and our laboratory experience with peptide/protein analyses using elisa. Peptides.
6. Humpel C. Identifying and validating biomarkers for alzheimer's disease. Trends in Biotechnology 2011;29:26-32.
7. Harris VK, Sadiq SA. Disease biomarkers in multiple sclerosis: Potential for use in therapeutic decision making. Mol Diagn Ther 2009;13:225-44.
8. Gupta VB, Sundaram R, Martins RN. Multiplex biomarkers in blood. Alzheimer's Research & Therapy 2013;5:31-.
9. Ekins RP. Multi-analyte immunoassay. Journal of Pharmaceutical and Biomedical Analysis 1989;7:155-68.
10. Kohler K, Seitz H. Validation processes of protein biomarkers in serum--a cross platform comparison. Sensors (Basel) 2012;12:12710-28.
11. Chan IS, Ginsburg GS. Personalized medicine: Progress and promise. Annual Review of Genomics and Human Genetics 2011;12:217-44.
12. Yu X, Schneiderhan-Marra N, Joos TO. Protein microarrays for personalized medicine. Clinical Chemistry 2010;56:376-87.
13. Tighe PJ, Ryder RR, Todd I, Fairclough LC. Elisa in the multiplex era: Potentials and pitfalls. Proteomics – Clinical Applications 2015;9:406-22.
14. Herbáth M, Papp K, Balogh A, Matkó J, Prechl J. Exploiting fluorescence for multiplex immunoassays on protein microarrays. Methods and Applications in Fluorescence 2014;2:032001.
15. Vashist SK, Schneider EM, Luong JHT. A rapid and highly-sensitive surface plasmon resonance (spr)-based immunoassay procedure for human fetuin a. 2014.
16. Kim YK, Lim S-I, Choi S, Cho I-S, Park E-H, An D-J. A novel assay for detecting canine parvovirus using a quartz crystal microbalance biosensor. Journal of Virological Methods 2015;219:23-7.
17. Chandra P, Noh H-B, Pallela R, Shim Y-B. Ultrasensitive detection of drug resistant cancer cells in biological matrixes using an amperometric nanobiosensor. Biosensors and Bioelectronics 2015;70:418-25.
18. Liu J, Wang L, Ouyang W, Wang W, Qin J, Xu Z, et al. Fabrication of pmma nanofluidic electrochemical chips with integrated microelectrodes. Biosensors and Bioelectronics 2015;72:288-93.
19. Dahlin AB, Jönsson P, Jonsson MP, Schmid E, Zhou Y, Höök F. Synchronized quartz crystal microbalance and nanoplasmonic sensing of biomolecular recognition reactions. ACS Nano 2008;2:2174-82.

20. Varro R, Chen R, Sepulveda H, Apgar J. Bead-based multianalyte flow immunoassays. In: Albitar M, ed. Monoclonal antibodies, Vol. 378: Humana Press, 2007:125-52.
21. Ellington AA, Kullo IJ, Bailey KR, Klee GG. Antibody-based protein multiplex platforms: Technical and operational challenges. Clinical Chemistry 2010;56:186-93.
22. Hanley B, Xing L, Cheng R. Variance in multiplex suspension array assays: Microsphere size variation impact. Theor Biol Med Model 2007;4:1-8.
23. Kricka L, Master S. Validation and quality control of protein microarray-based analytical methods. Mol Biotechnol 2008;38:19-31.
24. Vollmer F, Arnold S. Whispering-gallery-mode biosensing: Label-free detection down to single molecules. Nat Meth 2008;5:591-6.
25. Iqbal M, Gleeson MA, Spaugh B, Tybor F, Gunn WG, Hochberg M, et al. Label-free biosensor arrays based on silicon ring resonators and high-speed optical scanning instrumentation. Selected Topics in Quantum Electronics, IEEE Journal of 2010;16:654-61.
26. Washburn AL, Gunn LC, Bailey RC. Label-free quantitation of a cancer biomarker in complex media using silicon photonic microring resonators. Analytical Chemistry 2009;81:9499-506.
27. Kelley M, Edwards K, Starks H, Fullerton SM, James R, Goering S, et al. Values in translation: How asking the right questions can move translational science toward greater health impact. Clinical and Translational Science 2012;5:445-51.
28. Callard F, Rose D, Wykes T. Close to the bench as well as at the bedside: Involving service users in all phases of translational research. Health Expectations 2012;15:389-400.
29. Khoury MJ, Gwinn M, Yoon PW, Dowling N, Moore CA, Bradley L. The continuum of translation research in genomic medicine: How can we accelerate the appropriate integration of human genome discoveries into health care and disease prevention? Genet Med 2007;9:665-74.
30. Raghupathi W, Raghupathi V. Big data analytics in healthcare: Promise and potential. Health Inf Sci Syst 2014;2:1-10.
31. Simpao A, Ahumada L, Gálvez J, Rehman M. A review of analytics and clinical informatics in health care. J Med Syst 2014;38:1-7.
32. Washburn AL, Luchansky MS, Bowman AL, Bailey RC. Quantitative, label-free detection of five protein biomarkers using multiplexed arrays of silicon photonic microring resonators. Analytical Chemistry 2010;82:69-72.
33. Luchansky MS, Bailey RC. Rapid, multiparameter profiling of cellular secretion using silicon photonic microring resonator arrays. Journal of the American Chemical Society 2011;133:20500-6.
34. Luchansky MS, Bailey RC. Silicon photonic microring resonators for quantitative cytokine detection and t-cell secretion analysis. Analytical Chemistry 2010;82:1975-81.
35. Luchansky MS, Washburn AL, McClellan MS, Bailey RC. Sensitive on-chip detection of a protein biomarker in human serum and plasma over an extended dynamic range using silicon photonic microring resonators and sub-micron beads. Lab on a Chip 2011;11:2042-4.
36. Kindt JT, Luchansky MS, Qavi AJ, Lee S-H, Bailey RC. Subpicogram per milliliter detection of interleukins using silicon photonic microring resonators and an enzymatic signal enhancement strategy. Analytical Chemistry 2013;85:10653-7.

Chapter 2:

Single Domain Antibodies for the Detection of Ricin using Silicon Photonic Microring Resonator Arrays

Acknowledgments

This chapter is adapted from "Single domain antibodies for the detection of ricin using silicon photonic microring resonator arrays" (Shia, W. W., Bailey, R. C., *Analytical* Chemistry, **2013**, 85 (2), 805-810). It has been reprinted here with permission from the American Chemical Society © 2015.

Single domain antibodies used for experiments in this chapter were graciously provided by Drs. George P. Anderson and Ellen R. Goldman from the US Naval Research Laboratory. We also thank Dr. Courtney Sloan for preparation of the ricin unknown sample. This research was supported by the NIH Director's New Innovator Award Program, part of the NIH Roadmap for Medical Research, through Grant number 1-DP2-OD002190-01 and the National Science Foundation through grant NSF CHE 12-14081.

2.1 Abstract

Ricin is a lethal protein toxin derived from the castor bean plant. Given its notorious history as a biowarfare agent and homicidal weapon, ricin has been classified as a category B bioterrorism agent. Current ricin detection methods based on immunoassays lack the required sensitivity and specificity for many homeland security surveillance applications. Importantly, many conventional antibody-based methodologies are unable to distinguish ricin from RCA 120, a non-toxic protein also found in the castor bean plant. Single domain antibodies (sdAbs), which are recombinantly derived from immunized llamas, are known to have high affinities for ricin A or B chains, and low cross-reactivity with RCA 120. Herein, we demonstrate the use of silicon photonic microring resonators for antibody affinity profiling and one-step ricin detection at concentrations down to 300 pM using a 15 minute, label-free assay format. These sdAbs were also simultaneously compared with a commercial anti-RCA IgG antibody in a multicapture agent, single target immunoassay using arrays of microrings, which allowed direct comparisons of sensitivity and specificity. A selected sdAb was also found to exhibit outstanding specificity against another biotoxin, saporin, which has mechanism of action similar to ricin. Given the rapidity, scalability, and multiplexing capability of this silicon-based technology, this work represents a step toward using microring resonator arrays for the sensitive and specific detection of biowarfare agents.

2.2 Introduction

Since ancient times, biological agents have been used as weapons by both militaries and terrorist organizations.(1) The use of ricin was considered by both the US and British militaries in both the First and Second World Wars, and was also employed in the infamous 1978 poisoned umbrella assassination of Bulgarian dissident Georgi Markov.(1, 2) More recently, the anthrax-containing letters sent to media outlets and two U.S. Senators in 2001 in the aftermath of 9/11 attacks, and similar attacks in 2003 and 2004, brought bioterrorism surveillance to the forefront of homeland security efforts.(1) Accordingly, there are pressing needs to develop robust analytical tools for the detection of ricin, and other potential biowarfare agents.

Ricin is a ~60 kDa proteinaceous toxin derived from the seeds of the castor bean plant, *Ricinus communis*.(3) The castor bean plant is grown worldwide and is the main raw material for production of castor oil, which has a broad range of industrial and medical applications.(2) As a byproduct of oil production, ricin is easily obtainable in large quantities,(2, 4) fueling fears that this agent could easily fall into the hands of terrorist organizations. A type 2 ribosome inactivating protein (RIP), ricin's structure consists of an A chain and B chain linked by disulfide bonds.(3, 5, 6) The B chain is a lectin that binds to the galactose residues of glycoproteins and glycolipids on the cell surface, which facilitates ricin entry into the cytosol.(6) The chains are cleaved apart, and the A chain depurinates an adenine residue from the 28S rRNA of ribosomes at a rate of ~1500 ribosomes/min, which leads to inhibition of protein synthesis and eventually causes cell death.(3)

The lethal dose of ricin varies dramatically depending upon the route of exposure, but inhalation represents the most dangerous mode, with a median lethal dose (LD_{50}) of 3-5 μg/kg for inhalation versus 20 mg/kg via ingestion. This high lethality, ease of extraction, and high accessibility of ricin led to its classification as a category B bioterrorism agent by the Centers of Diseases Control and Prevention (CDC).(7)

At present, common approaches for ricin detection includes polymerase chain reaction (PCR),(8-10) assays measuring the catalytic activity of ricin,(11-13) , and immunoassays.(14-20) Both PCR and catalytic activity assays are indirect methods for detecting ricin. PCR only detects nucleic materials from the plant origin of the toxin, and therefore is not applicable to detect purified ricin,(21, 22) while catalytic activity assays lack specificity towards ricin, since the catalytic activity of all RIPs is similar.(21, 23) Because of these limitations, most studies in the literature have utilized immunoassays for ricin detection. Immunoassays generally rely upon antibody recognition elements and can be used in a variety of formats, including radioimmunoassays,(14) enzyme-linked immunosorbent assays (ELISA),(15) electroluminescence,(16) fluorescent-based flow cytometry,(17) optical waveguide sensors,(18) surface plasmon resonance (SPR),(19) and colorimetric hand-held assays,(20) Importantly, the broad reliance upon immunoaffinity methods has generated strong interest in developing stable and robust antibodies that are specific for ricin.(23-25)

One limitation to ricin immunoassay development is that polyclonal immunoglobulin G (IgG) antibodies often do not have high specificity for ricin, and although monoclonal antibodies have improved specificity, they also have limited stability.(26) An alternative to conventional IgG antibodies is a class of recombinant antibodies known as single-domain antibodies (sdAb). sdAbs are derived from a special class of heavy-chain antibodies, which are found in animals of the *Camelidae* family, and also in sharks.(27-31) Unlike IgG antibodies, which consist of two heavy chains and two light chains linked by disulfide bonds, sdAbs do not have light chains, thus only a variable domain (VHH) on the heavy chain is responsible for antigen binding.(28, 29) This VHH region can be cloned and expressed as a recombinant sdAb,(27) with ten times lower molecular weight (~15 kDa),(27, 30) as compared to a standard IgG. Importantly, sdAbs are robust to heat and chemical treatment as they can refold to maintain their antigen affinity after denaturation.(29,32) These properties make sdAbs attractive capture agents for immunoassays of various formats. Anderson *et al*.(27) have recently developed a series of anti-ricin sdAbs and demonstrated their high affinity, specificity, and robustness in ELISA and bead-based immunoassay formats. These sdAbs were selected from a phage display library constructed by extraction of the mRNA of heavy chain antibodies in lymphocytes of immunized llamas, followed by PCR amplification to clone resulting sdAb genes into a phage display vector, and transformed to *E. coli* cells for antibody production.

In this paper, we demonstrate the applicability of anti-ricin sdAbs for agent detection on a label-free microring array detection platform. Silicon photonic microring resonators are an emerging class of chip-integrated sensors that have been used to detect a range of biomolecular targets: including protein and nucleic acid biomarkers,(33-40) and viruses.(41) Microring resonators are refractive index-based sensors that are sensitive to the local environment near the microring surface. When the surface is modified with capture agents, such as antibodies, the binding of the target antigen is readily detected as a shift in the resonance wavelength supported by the microcavity. These changes are monitored as a function of time and used to quantify the amount of analyte in solution, or alternatively used to interrogate the kinetics of binding interactions. In addition to the high surface sensitivity and analytical versatility, advantages of this silicon photonic sensing technology come from its genesis in well-established semiconductor fabrication methodologies, which make the sensors highly scalable, inherently multiplexable, and cost-effective. Herein, we demonstrate the applicability of this technology for the relatively

rapid and quantitative detection of ricin using sdAbs down to a concentration of 300 pM in a label-free assay format. Furthermore, we verify that the sdAbs are significantly more specific than a standard IgG antibody when challenged with the molecularly similar, but non-toxic ricin analogue RCA 120. Importantly, we feel this work establishes this silicon photonic as a useful platform for detection biowarfare agents, since the multiplexing capability and cost effective nature of the technology would lend itself well to network surveillance efforts in which large numbers of sensor arrays could be distributed as a network for autonomous environmental monitoring.

2.3 Experimental section

2.3.1 Materials

Unless specified, all chemicals were purchased from Sigma-Aldrich (St. Louis, MO) and used as received. 3-N-((6-(N′-isopropylidenehydrazino))nicotinamide)propyltriethoxysilane (HyNic Silane) and succinimidyl 4-formyl benzoate (S-4FB) were purchased from Solulink (San Diego, CA). *Ricinus communis* agglutinin II (ricin), *Ricinus communis* agglutinin I (RCA 120) and a polyclonal goat anti-RCA antibody were purchased from Vector Laboratories, Inc. (Burlingame, CA). Polyclonal Chicken anti-saporin was purchased from Advanced Targeting Systems (San Diego, CA). Single domain antibodies (sdAb) C8 and B4 used in the experiments were a generous donation from Drs. George Anderson and Ellen Goldman at the Naval Research Laboratory. Aniline and glycine were purchased from ACROS Organics (Geel, Belgium). Zeba spin desalting columns were purchased from Thermo Fisher Scientific (Rockford, IL).

All buffers were made from purified water (ELGA PURELAB filtration system; Lane End, UK) and the pH was adjusted with 1 M HCl or 1M NaOH. Phosphate buffered saline (PBS) was reconstituted from Dulbecco's phosphate buffered saline packets purchased from Sigma-Aldrich (St. Louis, MO). The low pH glycine buffer consisted of 10 mM glycine and 160 mM NaCl adjusted below pH 3.0. PBST-BSA buffer consisted of 0.1mg/ml bovine serum albumin (BSA) and 0.05% (v/v) Tween 20 in 10 mM PBS at pH 7.4. The sensor chip blocking buffer consisted of 2% (w/v) BSA and 0.01% (w/v) sodium azide in 10 mM PBS at pH 7.4.

2.3.2 Sensor chip layout and instrumentation

The microring resonator instrument and sensor chips were acquired from Genalyte, Inc. (San Diego, CA). Instrumentation and sensor chips designs have been previously described in detail.(33, 42) Briefly, the sensor chips are 6 mm×6 mm in size, and fabricated from silicon-on-insulator wafers. Each chip consists of 32 microrings adjacent to linear waveguides. The entire chip is spin-coated with a perfluoropolymer cladding, with annular openings etched to expose 24 rings to be used as sensors exposed to solution, while the remaining 8 rings are left under the cladding to serve as thermal control rings to correct for temperature drift. Light from a tunable external cavity laser in the instrument (wavelength centered at 1560 nm) interrogates each individual microring via grating couplers placed at the edge of the chip. The scan speed of the system is ~250 ms/ring with the entire array interrogated every ~9 seconds.

2.3.3 Antibody immobilization on sensor chip surface

Sensor chips were batch-functionalized by the following procedures: The chips are first cleaned for 30 s in piranha solution (3:1 ratio of concentrated sulfuric acid to 30% hydrogen peroxide), then rinsed with copious amount of distilled water and dried under a stream of nitrogen *(Caution! Piranha solutions are extremely dangerous, reacting explosively with trace quantities of organics.).* A 20 μL drop of a 1 mg/ml HyNic silane solution in 95% ethanol and 5% N,N-dimethylformamide (DMF) was spotted on the surface of each sensor chip for 30 min, after which the chips were rinsed in 100% ethanol and dried under nitrogen to remove the excess HyNic Silane.

Separately, antibodies were conjugated with S-4FB molecules by first buffer exchanging the antibodies into 100 mM pH 6.0 PBS using Zeba spin desalting columns. The resulting concentration of antibodies in PBS was measured using the NanoDrop spectrophotometer (Thermo Fisher Scientific, Wilmington, DE). After the concentration was determined, a five-fold molar excess of S-4FB (0.1 mg/ml in DMF) was added and allowed to incubate at room temperature for 2 hrs. Unreacted S-4FB was then removed by buffer exchanging antibodies into 100 mM pH 7.4 PBS using the Zeba spin columns. The final concentration of the S-4FB-modified antibodies was again determined by the NanoDrop spectrophotometer and adjusted to 50 μg/ml.

Immediately before attachment to sensor chip surface, 4FB-modified antibodies were diluted to 25 µg/ml in PBS containing 100 mM aniline.(43) Approximately 1 µl aliquots of 4FB-modified antibodies were deposited on specific microrings on the sensor chip surface with the aid of a stereo microscope to direct spotting positions, while a selected set of rings were blocked with 2% w/v BSA (unexposed to any antibodies) to serve as control rings. The antibody solution-coated chips were then placed in a saturated humidity chamber overnight at room temperature. Afterwards, the sensor chips are immersed in chip blocking buffer overnight to block the chips surfaces prior to performing binding or detection experiments.

2.3.4 Assay procedures

Saporin, ricin and RCA 120 standard solutions were made via serial dilution of stock solutions in PBST-BSA. For each assay, a chip was placed in a holder with a two-channel microfluidic set-up defined by a Mylar gasket sandwiched between the holder and a Teflon lid. A syringe pump was used to control solution flow across 12 active sensor rings in each of two flow channels, the schematic of which was described in a previous publication.(33) Assays were conducted at 30 µl/min flow rate. Before each assay run, glycine buffer was flowed across the chip surface for 2 min to remove excess blocking BSA, before establishing a stable baseline by flowing PBST-BSA running buffer for at least 4 min. The analyte solution is then flowed across the chip for 10 min, followed by a 5 min PBST-BSA rinse. Each sensor chip is used only once without regeneration.

2.3.5 Data analysis

All microring responses were corrected for baseline thermal drift using the microrings occluded by the cladding layer as references. Each active microring signal was also corrected by setting the response of one blank control ring unmodified with antibodies as the “zero” reference to the response of antibody-modified rings. The initial slopes for all the sensograms of ricin standards and unknown samples were determined by a linear regression fit of the first five minutes upon binding of ricin to the sdAb immobilized on the microrings, after which the resulting slopes were averaged among the replicated measurements of each sdAb-modified ring exposed to the same sample. OriginPro 8.5.1 (OriginLab Corporation, Northampton, MA) was used to fit a linear regression plot to correlate the initial slopes with concentration of the ricin

standards in the calibration curve, while the concentration of the unknown sample was quantified by interpolating its corresponding initial slope on the calibration curve.

2.4 Results and discussion

As specificity towards ricin is of great importance when developing assays for this target our initial efforts focused on evaluating the reactivity and cross-reactivity of sdAbs towards ricin and RCA 120, respectively. The molecular weight of ricin is ~60 kDa and it sometimes referred to as RCA 60. Meanwhile, as its name suggests, RCA 120 is twice the mass of ricin, having a tetrameric structure that is >80% homologous to ricin, yet is much less toxic.(44) A commercially available goat anti-RCA IgG was arrayed next to the sdABs B4 and C8, as well as the BSA blocked control rings. All of the microrings were then simultaneously exposed to 10 nM RCA 120. In a separate experiment, an identically arrayed sensor chip was exposed to 10 nM ricin. Figure 2.1 shows the responses of the arrays to both RCA 120 and ricin. All of the ricin and RCA-specific capture agents show strong responses to ricin; however, the anti-RCA IgG shows a much larger response to RCA 120 as compared to the sdAbs, verifying the enhanced specificity of the sdAb capture agents.

In addition to specificity for ricin over RCA 120, we also investigated the cross-reactivity of the C8 sdAb against saporin, another RIP found in nature. Initially, we tested saporin against an anti-saporin antibody to confirm binding affinity of the molecule (Figure 2.2). Using a chip with all rings immobilized with C8 sdAbs, we consecutively exposed the rings to 30 nM saporin follow by 30 nM ricin. As shown in Figure 2.3, responses from the C8 immobilized microrings further demonstrate the specificity of this sdAb towards ricin over another RIP.

These cross-reactivity and detection results further support previous work by Anderson *et al.,* indicating that among sdAbs C8 and B4, C8 has the highest binding response to ricin while B4 have the lowest non-specific binding to RCA 120.(27, 30) Having established that sdAb C8 offered good specificity and sensitivity, we sought to demonstrating quantitative detection capabilities of ricin on our sensor platform. We flowed a set of standard ricin solutions, prepared in PBST-BSA to concentrations of 10 nM, 3 nM, 1 nM, 0.3 nM and 0 nM, across an array of microrings functionalized with sdAb C8. The binding responses to each concentration of ricin interacting with eight microrings per sensor chip were then recorded and corrected using the BSA-blocked rings, as shown in Figure 2.4. Response for four representative microrings are

shown in Figure 2.4 for the sake of clarity; however the average initial slopes and standard deviations for all eight sensors are provided in Table 2.1.

We previously showed the ability to perform rapid, label-free quantitation based upon the initial slope of binding response upon introduction of the antigen-containing solution.(33) Using the data from Figure 2.4, but including fits to all eight binding curves recorded at each concentration of ricin, we created a calibration plot that could be used for determination of an unknown. Figure 2.5 shows the resulting calibration curve. We then utilized this calibration curve to determine the concentration of a solution having an unknown ricin concentration prepared in PBST-BSA. Comparison of the sensor response with the calibration curve allowed us to determine the unknown concentration to be 4.20±0.43 nM. This value and error, determined as the 95% confidence interval for the n=8 measurement, was in good agreement with the "as prepared" value of 4.5 nM.

Finally, we determined the limit of detection for label-free ricin detection by analyzing the noise present in the measurement. Specifically, we determined assay "slope noise" (σ) of the running buffer baseline, which is a measure of how precisely we can determine the initial slope of the sensor binding response. Using the determined value of 0.09 pm/min for this system, we then determine the limit of detection as 3σ (~0.27 pm/min). Evaluation of this noise level against the ricin standard binding curve points to an overall limit of detection of 200 pM. Furthermore, it is worth noting that we have previously shown that assay sensitivity, and specificity, can be further increased by using a secondary capture agent and tertiary binding events.(34-36)

For applications in biodefense, a rapid, real-time ricin detection system is needed to ensure a prompt and efficient response capacity. Herein, we demonstrate a label-free detection methodology that achieves a relevant limit of detection within a rapid (<15 min) assay format. Admittedly, the matrix described in this manuscript is quite proteinaceous, but relatively well-controlled compared to that encountered in many analytical matrices. However, the detection of airborne agents is a rather unique potential application area, as samples collected using air filtration are typically resuspended in a convenient buffer of choice. As mentioned above, ricin and many other biowarfare agents pose very high inhalation threats, and therefore air and surface sampling, both of which often involve suspension in a neat buffer solution, are commonly

utilized for these agents.(8, 45, 46) This practical operation procedure adds support to the utility of this rapid and label-free, buffer-based assay for ricin and its potential for future deployment as sensor networks for biowarfare agent surveillance.

2.5 Conclusions

In this work, we demonstrated that silicon photonic microring resonator arrays are a powerful and promising tool for detecting biowarfare agents such as ricin. Our evaluation of anti-ricin sdAbs on the microring arrays platform is consistent with the previous reports that show sdAbs to have selective affinity towards ricin, yet minimal cross-reactivity with the non-toxic analogue RCA 120. We further established specificity for the sdAb C8 againts saporin, another potential biotoxin that acts through a similar catalytic mechanism. Using the sdAb C8 as a capture agent, we also illustrated a rapid, real-time, one-step quantitative approach of ricin detection, detecting a concentration of 300 pM in a 15 minute, label-free assay format. Future efforts will focus on further improving assay performance in terms of specificity and sensitivity, as well as the creation of multiplexed detection panels towards the goal of surveillance for multiple agents within environmental matrixes.

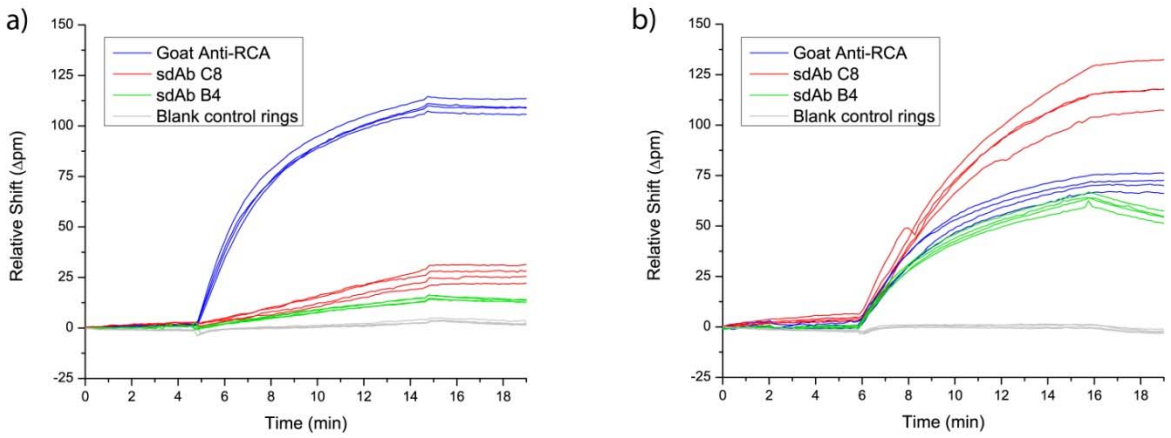

Figure 2.1 Responses of a 3-capture agent sensor array exposed to 10 nM of **a)** RCA 120 and **b)** ricin. sdAb clones C8 and B4 both show greater selectivity for ricin compared to the goat anti-RCA IgG, which shows the largest response to RCA 120. Both sdAb clones show a significantly reduced response to RCA 120 while displaying good binding responses to ricin. In both sensing experiments, blank control rings show insignificant levels of non-specific binding.

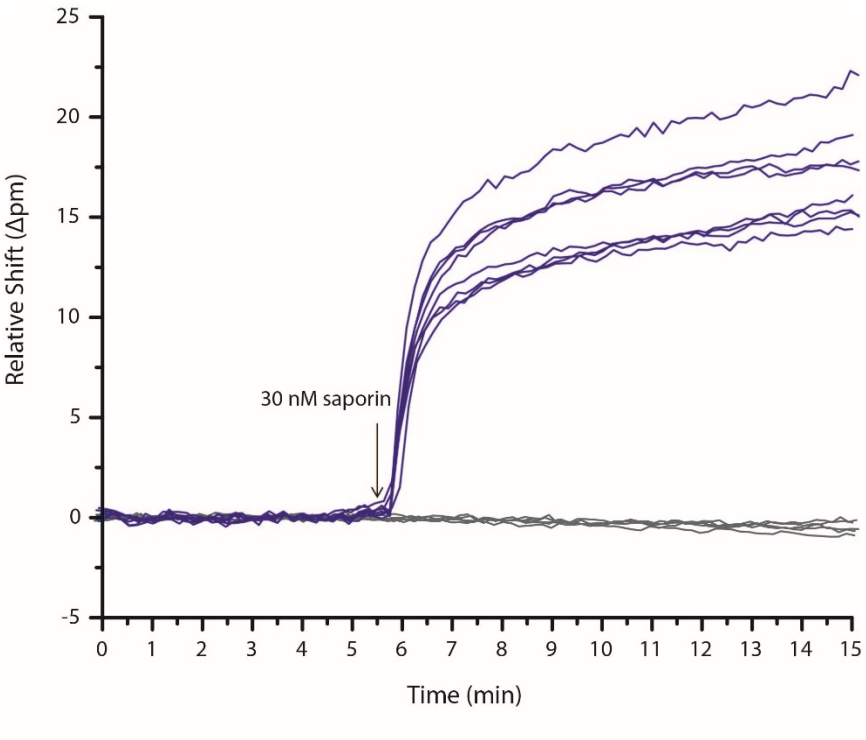

Figure 2.2 Response of microring arrays immobilized with polyclonal chicken anti-saporin antibodies (blue lines) upon addition of 30 nM saporin. Dark grey lines indicate thermal control rings.

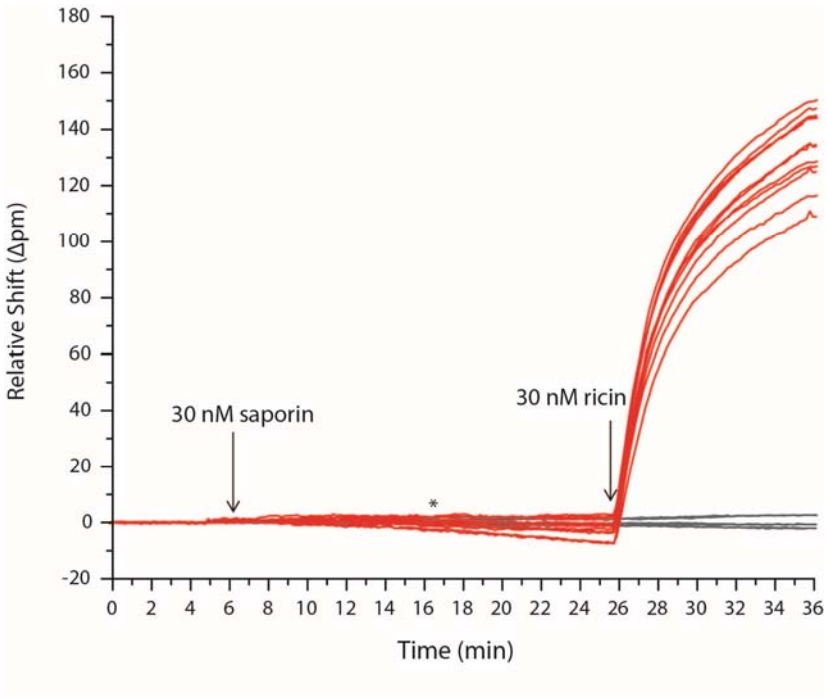

Figure 2.3 Response of sdAb C8 upon addition of 30 nM saporin, follow by addition of 30 nM ricin (Red lines). Arrows indicate injection of solutions, while the asterisk indicate a PBST-BSA buffer rinse step. Dark gray lines indicate thermal control rings.

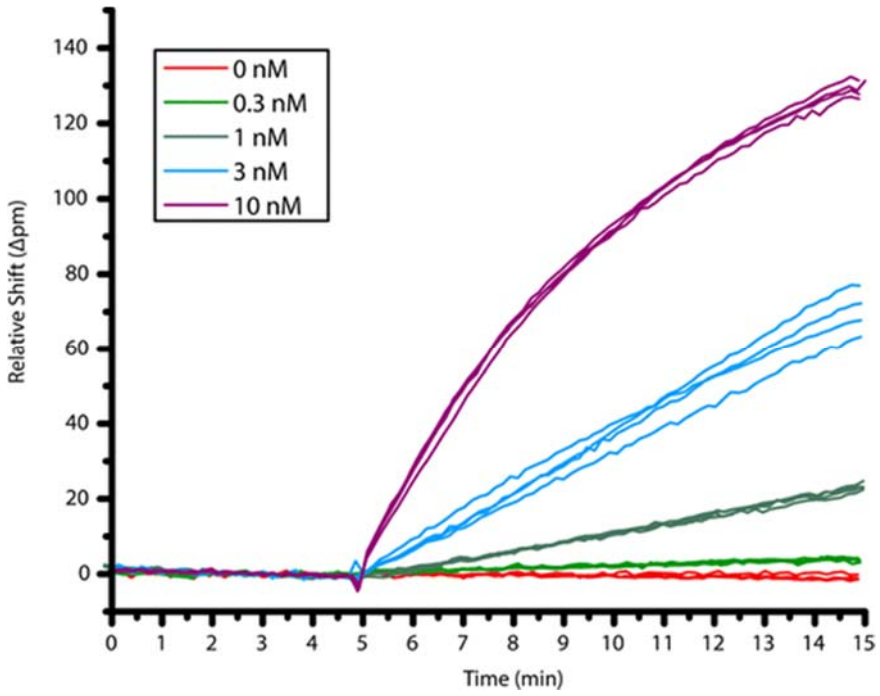

Figure 2.4 Concentration-dependent binding response of ricin as a function of target concentration. Each measurement was made eight times redundantly on the same sensor chip, functionalized identically with sdAb C8. Following the establishment of an initial baseline by equilibrating with PBST-BSA running buffer, ricin-containing solutions were flowed across the array (staring at t = 5 min) and persisted for a total of 10 minutes.

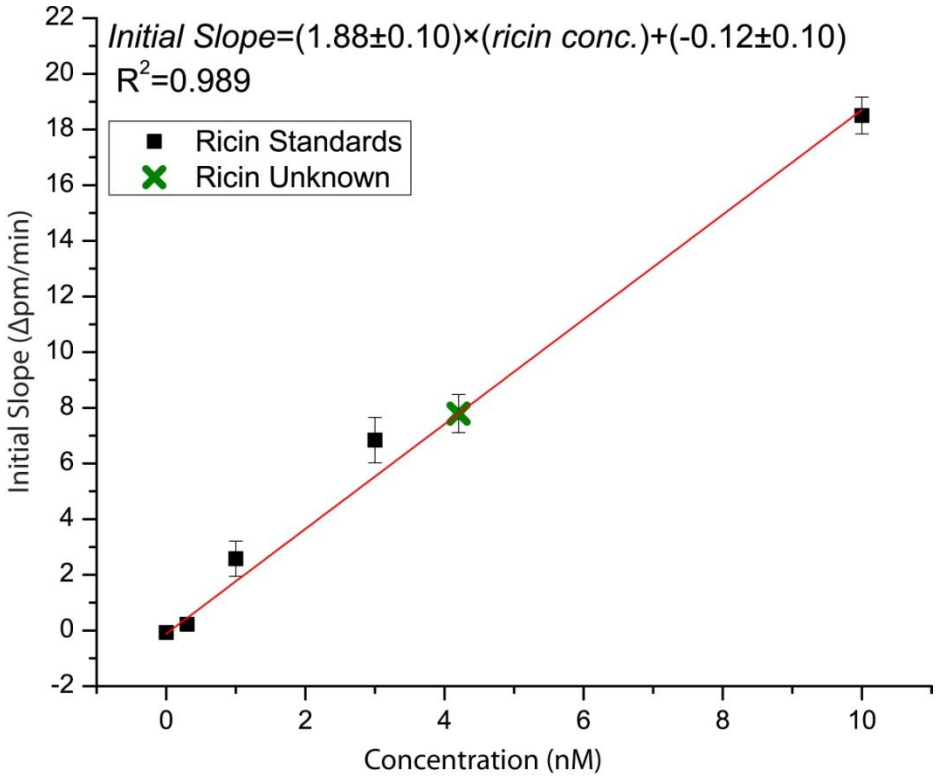

Figure 2.5 Calibration curve illustrating the concentration-dependent response of sdAb C8 functionalized microrings to solutions of various concentrations. Real-time binding curves were obtained (as in Figure 2.4) for samples prior to the analysis of a prepared solution containing an unknown amount of ricin. The sensor response for the unknown solution was then compared against the standard calibration curve, allowing for quantitative detection. Error bars represent the 95% confidence interval from n=8 measurements.

Ricin concentration (nM)	Average initial slope for n=8 rings (Δpm/min)	Standard deviation for n=8 rings (±Δpm/min)	95% Confidence interval (±Δpm/min)
0	-0.07	0.09	0.08
0.3	0.2	0.2	0.14
1	2.6	0.8	0.63
3	6.8	1.0	0.81
10	18.5	0.7	0.66

Table 2.1 Average initial slopes, standard deviations and initial slopes at 95% confidence interval for n=8 rings between 0-10 nM concentrations of ricin.

2.6 References

1. Bhalla DK, Warheit DB. Biological agents with potential for misuse: A historical perspective and defensive measures. Toxicology and Applied Pharmacology 2004;199:71-84.
2. Olsnes S. The history of ricin, abrin and related toxins. Toxicon 2004;44:361-70.
3. Audi J, Belson M, Patel M, Schier J, Osterloh J. Ricin poisoning. JAMA: The Journal of the American Medical Association 2005;294:2342-51.
4. Ler SG, Lee FK, Gopalakrishnakone P. Trends in detection of warfare agents: Detection methods for ricin, staphylococcal enterotoxin b and t-2 toxin. Journal of Chromatography A 2006;1133:1-12.
5. Leshin J, Danielsen M, Credle JJ, Weeks A, O'Connell KP, Dretchen K. Characterization of ricin toxin family members from ricinus communis. Toxicon 2009;55:658-61.
6. Sandvig K, Torgersen ML, Engedal N, Skotland T, Iversen T-G. Protein toxins from plants and bacteria: Probes for intracellular transport and tools in medicine. FEBS letters 2010;584:2626-34.
7. Rai AJ. Biomarkers in translational research: Focus on discovery, development and translation of protein biomarkers to clinical immunoassays. Expert Review of Molecular Diagnostics 2007;7:545+.
8. Schieltz DM, McGrath SC, McWilliams LG, Rees J, Bowen MD, Kools JJ, et al. Analysis of active ricin and castor bean proteins in a ricin preparation, castor bean extract, and surface swabs from a public health investigation. Forensic Science International 2011;209:70-9.
9. Melchior Jr WB, Tolleson WH. A functional quantitative polymerase chain reaction assay for ricin, shiga toxin, and related ribosome-inactivating proteins. Analytical Biochemistry 2010;396:204-11.
10. He X, Carter JM, Brandon DL, Cheng LW, McKeon TA. Application of a real time polymerase chain reaction method to detect castor toxin contamination in fluid milk and eggs. Journal of Agricultural and Food Chemistry 2007;55:6897-902.
11. Hale ML. Microtiter-based assay for evaluating the biological activity of ribosome-inactivating proteins. Pharmacology & Toxicology 2001;88:255-60.
12. Keener WK, Rivera VR, Young CC, Poli MA. An activity-dependent assay for ricin and related rna n-glycosidases based on electrochemiluminescence. Analytical Biochemistry 2006;357:200-7.
13. Sturm MB, Schramm VL. Detecting ricin: Sensitive luminescent assay for ricin a-chain ribosome depurination kinetics. Analytical Chemistry 2009;81:2847-53.
14. Godal A, Olsnes S, Pihl A. Radioimmunoassays of abrin and ricin in blood. Journal of Toxicology and Environmental Health 1981;8:409-17.
15. Poli MA, Rivera VR, Hewetson JF, Merrill GA. Detection of ricin by colorimetric and chemiluminescence elisa. Toxicon 1994;32:1371-7.
16. Brandon DL. Detection of ricin contamination in ground beef by electrochemiluminescence immunosorbent assay. Toxins 2011;3:398-408.
17. Kim JS, Anderson GP, Erickson JS, Golden JP, Nasir M, Ligler FS. Multiplexed detection of bacteria and toxins using a microflow cytometer. Analytical Chemistry 2009;81:5426-32.

18. Bhatta D, Michel AA, Marti Villalba M, Emmerson GD, Sparrow IJG, Perkins EA, et al. Optical microchip array biosensor for multiplexed detection of bio-hazardous agents. Biosensors and Bioelectronics 2011;30:78-86.
19. Feltis BN, Sexton BA, Glenn FL, Best MJ, Wilkins M, Davis TJ. A hand-held surface plasmon resonance biosensor for the detection of ricin and other biological agents. Biosensors and Bioelectronics 2008;23:1131-6.
20. Wade MM, Biggs TD, Insalaco JM, Neuendorff LK, Bevilacqua VLH, Schenning AM, et al. Evaluation of handheld assays for the detection of ricin and staphylococcal enterotoxin b in disinfected waters. International Journal of Microbiology 2011;2011.
21. Griffiths GD. Understanding ricin from a defensive viewpoint. Toxins 2011;3:1373-92.
22. Bogomolova A. Sensing of biowarfare agents. Sensors for chemical and biological applications, Vol.: CRC Press, 2010:333-51.
23. Ezan E, Duriez E, Fenaille F, Becher F. Functional assays for ricin detection
detection of biological agents for the prevention of bioterrorism. In: Banoub J, ed., Vol.: Springer Netherlands, 2011:131-47.
24. He L, Deen B, Rodda T, Ronningen I, Blasius T, Haynes C, et al. Rapid detection of ricin in milk using immunomagnetic separation combined with surface-enhanced raman spectroscopy. Journal of Food Science 2011;76:N49-N53.
25. Kalb SR, Barr JR. Mass spectrometric detection of ricin and its activity in food and clinical samples. Analytical Chemistry 2009;81:2037-42.
26. Vermeer AWP, Norde W. The thermal stability of immunoglobulin: Unfolding and aggregation of a multi-domain protein. Biophysical Journal 2000;78:394-404.
27. Anderson GP, Liu JL, Hale ML, Bernstein RD, Moore M, Swain MD, Goldman ER. Development of antiricin single domain antibodies toward detection and therapeutic reagents. Analytical Chemistry 2008;80:9604-11.
28. Wesolowski J, Alzogaray V, Reyelt J, Unger M, Juarez K, Urrutia M, et al. Single domain antibodies: Promising experimental and therapeutic tools in infection and immunity. Medical Microbiology and Immunology 2009;198:157-74.
29. Liu JL, Anderson GP, Hayhurst A, Goldman ER. Single-domain antibodies: Rugged recognition elements for tomorrow's biosensors. In: Frances SL, Chris Rowe T, eds. Optical biosensors (second edition), Vol. Amsterdam: Elsevier, 2008:469-92.
30. Anderson GP, Bernstein RD, Swain MD, Zabetakis D, Goldman ER. Binding kinetics of antiricin single domain antibodies and improved detection using a b chain specific binder. Analytical Chemistry 2010;82:7202-7.
31. Flajnik MF, Deschacht N, Muyldermans S. A case of convergence: Why did a simple alternative to canonical antibodies arise in sharks and camels? PLoS Biol 2011;9:e1001120.
32. Dumoulin M, Conrath K, Van Meirhaeghe A, Meersman F, Heremans K, Frenken LGJ, et al. Single-domain antibody fragments with high conformational stability. Protein Science 2002;11:500-15.
33. Washburn AL, Gunn LC, Bailey RC. Label-free quantitation of a cancer biomarker in complex media using silicon photonic microring resonators. Analytical Chemistry 2009;81:9499-506.
34. Luchansky MS, Washburn AL, McClellan MS, Bailey RC. Sensitive on-chip detection of a protein biomarker in human serum and plasma over an extended dynamic range using

silicon photonic microring resonators and sub-micron beads. Lab on a Chip 2011;11:2042-4.
35. Luchansky MS, Bailey RC. Silicon photonic microring resonators for quantitative cytokine detection and t-cell secretion analysis. Analytical Chemistry 2010;82:1975-81.
36. Luchansky MS, Bailey RC. Rapid, multiparameter profiling of cellular secretion using silicon photonic microring resonator arrays. Journal of the American Chemical Society 2011;133:20500-6.
37. Qavi A, Kindt J, Bailey R. Sizing up the future of microrna analysis. Analytical and Bioanalytical Chemistry 2010:1-15.
38. Qavi AJ, Kindt JT, Gleeson MA, Bailey RC. Anti-DNA:Rna antibodies and silicon photonic microring resonators: Increased sensitivity for multiplexed microrna detection. Analytical Chemistry 2011:5949-56.
39. Kindt JT, Bailey RC. Chaperone probes and bead-based enhancement to improve the direct detection of mrna using silicon photonic sensor arrays. Analytical Chemistry 2012;84:8067-74.
40. Scheler O, Kindt JT, Qavi AJ, Kaplinski L, Glynn B, Barry T, et al. Label-free, multiplexed detection of bacterial tmrna using silicon photonic microring resonators. Biosensors and Bioelectronics 2012;36:56-61.
41. McClellan MS, Domier LL, Bailey RC. Label-free virus detection using silicon photonic microring resonators. Biosensors and Bioelectronics 2012;31:388-92.
42. Iqbal M, Gleeson MA, Spaugh B, Tybor F, Gunn WG, Hochberg M, et al. Label-free biosensor arrays based on silicon ring resonators and high-speed optical scanning instrumentation. Selected Topics in Quantum Electronics, IEEE Journal of 2010;16:654-61.
43. Byeon J-Y, Limpoco FT, Bailey RC. Efficient bioconjugation of protein capture agents to biosensor surfaces using aniline-catalyzed hydrazone ligation. Langmuir 2010;26:15430-5.
44. Roberts LM, Lamb FI, Pappin DJ, Lord JM. The primary sequence of ricinus communis agglutinin. Comparison with ricin. Journal of Biological Chemistry 1985;260:15682-6.
45. Edmonds J. Surface sampling of a dry aerosol deposited ricin. Applied Sciences 2012;2:13.
46. Shea DA, Lister SA. The biowatch program: Detection of bioterrorism. Congressional Research Service Report Vol., 2003.
47. Goldman E, Liu J, Bernstein R, Swain M, Mitchell S, Anderson G. Ricin detection using phage displayed single domain antibodies. Sensors 2009;9:542-55.

Chapter 3:

Multiplexed Cancer Biomarker Detection Using Chip-Integrated Silicon Photonic Sensor Arrays

Acknowledgments

This chapter is adapted from "Multiplexed Cancer Biomarker Detection Using Chip-Integrated Silicon Photonic Sensor Arrays" (Washburn, A. L., Shia, W. W., Lenkeit, K. A., Lee, S.-H., Bailey, R. C. Submitted, **2016**)

Dr. Adam Washburn is acknowledged for his joint assistance in this project, especially in the initial version figures of this paper. Undergraduate assistants Kimberly Lenkeit and So-Hyun Lee are acknowledged for their assistance in data collection, and Prof. Ryan Bailey is acknowledged for initiating this project.

This work in this chapter was funded by the NIH Director's New Innovator Award Program, part of the NIH Roadmap for Medical Research, through grant number 1-DP2-OD002190-01, and National Science Foundation grant CHE 12-14081. ALW was supported via a National Science Foundation Graduate Research Fellowship as well as a Division of Analytical Chemistry Summer Graduate Research Fellowship sponsored by the Society for Analytical Chemists of Pittsburgh. WWS was supported by American Heart Association Predoctoral Fellowship. KAL was supported by a REU program run by the University of Illinois' Department of Chemistry and sponsored by 3M.

3.1 Abstract

The analysis of disease-specific biomarker panels holds promise for the early detection of a range of diseases, including cancer. Blood-based biomarkers, in particular, are attractive targets for minimally-invasive disease diagnosis. Specifically, a panel of organ-specific biomarkers could find utility as a general disease surveillance tool enabling earlier detection or prognostic monitoring. Using arrays of chip-integrated silicon photonic sensors, we describe the simultaneous detection of eight cancer biomarkers in serum in a relatively rapid (1 hour) and fully automated antibody-based sandwich assay. Biomarkers were chosen for their applicability to a range of organ-specific cancers, including disease of the pancreas, liver, ovary, breast, lung, colorectum, and prostate. Importantly, we demonstrate that selected patient samples reveal biomarker "fingerprints" that may be useful for a personalized cancer diagnosis. More generally, we show that the silicon photonic technology is capable of measuring multiplexed panels of protein biomarkers that may have broad utility in clinical diagnostics.

3.2 Introduction

The development of targeted protein-based diagnostics promises to increase the degree of biomolecular detail that can be gleaned into the state of disease. For example, biomarker panels have been investigated as a means to provide more personalized and effective treatment for cancer.(1, 2) Although much work has been accomplished to discover putative biomarkers and biomarker panels, validation and clinical deployment of diagnostic biomarker panels remains to be achieved.(3-5) Typically, clinical assays for protein biomarkers rely on immunoassays such as the enzyme-linked immunosorbent assay (ELISA), which is traditionally designed to measure one biomarker at a time. However, given the diagnostic potential of multiplexed analyses, there is an increasing emphasis on the development of technologies capable of simultaneously detecting multiple protein targets from within a single sample, with the bead-based Luminex platform being the most commercially successful. Many emerging technologies leverage advances micro- and nanoscale fabrication technologies to create small footprint sensors that can be configured into multiplexed sensor arrays.(6-9)

To this end, our own group has been developing a scalable silicon photonic technology detection platform that can be readily configured into multiplexed detection arrays for to create multiplex sensors that can measure multiple proteins from a given sample.(10, 11) Silicon photonic microring resonators belong to a larger class of refractive index-responsive "whispering gallery resonators" (12) and this chip-integrated geometry leverages robust semiconductor fabrication methods to create multiplexable sensor arrays. Light is coupled into microring resonators from adjacent linear waveguides only under conditions of optical resonance, as described by:

$$m\lambda = 2\pi r n_{eff}$$

where m is an integer, λ is the wavelength of light, r is the radius of the ring, and n_{eff} is the effective refractive index of the waveguide mode. When functionalized with target-specific capture agents, binding induced changes in the local refractive index at the sensor surface can be used to sensitively quantitate the presence of a range of analytes.

The scalability of silicon enables the facile creation of microsensor chips containing multiple sensors on a given chip. Experiments described in this paper were performed on sensor chips with 32 active microring sensors, with two additional sensors used to correct for thermal drift. Using these arrays, we create a microsensor chip that can detect eight different analytes, each measured in quadruplicate, as illustrated in Figure 3.1. As described in greater detail in the experimental methods section, antibodies were attached to the surface via the DNA-encoded antibody method,(13, 14) which provides a robust approach for creating on-demand antibody arrays. The following eight biomarkers were targeted on account of their previously reported correlation with organ-specific cancer: α-fetoprotein (AFP; liver and germ cell cancers(15)); activated leukocyte cell adhesion molecule (ALCAM; breast cancer(16)); cancer antigen 15-3 (CA15-3; breast cancer(15)); cancer antigen 19-9 (CA19-9; pancreatic, colorectal, and ovarian cancers(15, 17)); cancer antigen-125 (CA-125; ovarian cancer(15, 18)); carcinoembryonic antigen (CEA; colorectal and pancreatic cancers(19-21)); osteopontin (ovarian and liver cancers(18, 22)); and prostate specific antigen (PSA; prostate cancer(23)). Within our selected 8-plex panel, five biomarkers are FDA-approved biomarkers (AFP, CA15-3, CA-125, CEA, PSA).(24) These

biomarkers were also convenient targets because they have broad relevance across diverse organ-specific cancers and also have a good selection of commercially available antibodies.

It is important to note that many of these biomarkers have been observed in other types of cancer and even within a single organ-type of cancer their elevation is not ubiquitous, which reflects underlying heterogeneities in disease mechanism. In fact, patient heterogeneity often complicates the universal diagnostic utility of any single biomarker. Moreover, the validation of any biomarker(s) requires the analysis of many diverse patient samples, which underscores the need for robust and automated biomarker screening tools. In this manuscript our focus is not on the biological relevance of specific biomarkers, but rather the demonstration that the silicon photonic detection technology can be used for analyse panels of protein biomarkers from within clinically-relevant samples.

3.3 Results and discussion

In contrast to most other immunoassay technologies which only offer endpoint readout, microring resonators offer a unique real-time monitoring capacity that is extremely enabling in the assay development process. Specifically, every step of the assay, including antigen-capture antibody and tracer antibody binding, and the entirety of the signal enhancement process can be followed in real time as each of these steps causes a shift in resonance wavelength. We have previously demonstrated that this breadth of measurement capability can enable an extended dynamic range of detection, an important consideration when measuring multiple analytes each with a particular concentration range of interest.(25) Additionally, observation of direct binding of antigens and capture antibodies tremendously expedites the screening and identification of capture agents with the required binding affinity and specificity. While not a major focus of this manuscript, this complete assay development capability offers a significant advantage in that the same technology can be utilized throughout the entire assay design, validation, and (eventually) deployment process.

Figure 3.2 shows how microring resonator arrays can be used to construct a multiplexed biomarker detection panel, including the ability to reveal antibody cross reactivity. Figures 3.2a and 3.2b represent eight separate experiments showing primary and

tracer recognition, respectively, of single biomarkers in buffer. In Figure 3.2a, each antigen was added individually in order and the primary binding was observed. Most of the capture antibodies show a specific response for only the specified target; however, noticeable cross reactivity was observed for the analytes CA19-9 and CA15-3. Upon the introduction of 1 kU/mL CA19-9, the appropriate anti-CA19-9-functionalized rings (cyan) respond, but the anti-CEA-functionalized rings (orange) also show a resonance shift, indicating non-specific target binding to this capture antibody. Similarly, addition of 1 kU/mL of CA15-3 generated resonance shifts from not only the anti-CA15-3-functionalized sensors (purple), but also from the anti-CEA- (orange) and anti-CA19-9-functionalized (cyan) sensors.

In a continuation of these single biomarker studies, we then tested tracer antibodies, which can form a highly selective sandwich immunocomplex specific for the targeted biomolecule. Figure 3.2b shows the sensor responses upon the sequential addition of 1 μg/mL of each tracer antibody, which followed the introduction of a single biomarker for the primary binding step (Figure 3.2a). Interestingly, the addition of every tracer antibody shows a selective response, indicating on-target recognition, with one exception. The anti-CA 15-3 tracer was also observed to bind to anti-CA 19-9-functionalized rings, which had also showed an apparently non-specific response to CA 15-3. In a separate experiment (not shown) we flowed the anti-CA 15-3 tracer antibody alone (no antigen) over the array of capture antibodies, suggesting that the response is a function of the biomarker sample itself. Upon consulting the product literature provided by the vendor, CA 19-9 is a known contaminant in the CA 15-3 sample, which explains this response and provides confidence in the overall fidelity of our 8-plex biomarker detection panel. Moreover, arrays of silicon photonic sensors and the real-time analysis capability provide significant benefits in terms of assay development, optimization, and troubleshooting that will likely be helpful for reagent screening and assay validation even if they are to be used with alternative detection methodologies.

After determining that the 8-plex assay had sufficient specificity, we proceeded to make measurements of biomarkers in human serum samples. In order to obtain a detection of limit at the clinically relevant levels, we employed a multilayer antibody signal enhancement method similar to what our group(26) and Gauglitz et al.(27) have used for

creating protein multilayers on a surface. Except for a limited use by Anderson et al.,(28) this technique has not been previously applied to enhance the signal of an immunoassay in the literature.

Figure 3.2c illustrates this methodology on the microring resonator silicon surface. Following the binding of the primary antigen and biotinylated tracer antibody, a solution of PE-labelled anti-biotin antibodies is introduced and a binding response is only measured on microrings that have the fully assembled sandwich immunocomplex (capture antibody-antigen-tracer antibody). Biotinylated anti-PE antibodies are then introduced, which bind to the PE labels of the anti-biotin antibody. This process can be repeated with cycling between separate solutions containing either PE-labelled anti-biotin or biotinylated anti-PE antibodies giving an enhanced shift in the resonance wavelength shift that correlated with the initial concentration of antigen in solution. It is worth noting that the Maverick M1 instrumentation utilized in these experiments features completely automated fluid handling, which facilitated this multi-step signal enhancement strategy. For our assays, we used a maximum of six steps (3 multilayer cycles), though some biomarkers could be detected with fewer. Notably, negative control experiments revealed that the signal enhancement strategy in the absence of target did not contribute any non-specific sensor response (Figure 3.3). Furthermore, by quantitating in buffer, as opposed to sensor matrix, this sandwich assay format was immune to the sample matrix effects seen in the primary binding response.

Figure 3.2d shows the real-time shifts in resonance wavelength during an entire representative 8-plex biomarker assay from a representative human serum sample. The diluted serum sample was flowed across a pre-functionalized microring resonator array for a total of 30 minutes to allow primary antigen binding. After 30 minutes, the flow is switched to running buffer and the surface rinsed for 20 minutes. Note that there is a large bulk refractive index shift that is observed upon introduction of serum, which is confirmed by its reversal upon switching running buffer. A cocktail of all eight tracer antibodies were then flowed across the surface for 15 minutes, followed by a 5 minute rinse with running buffer. The multilayered signal enhancement scheme was then invoked with 2 minute cycles in the PE-labelled anti-biotin and biotinylated anti-PE antibodies.

After assay development and validation of specificity, we then created standard curves to be used for biomarker quantitation. Solutions containing known concentrations of biomarker standards were prepared and analysed using the 8-plex microring array. The total relative shift during the secondary enhancement is plotted as a function of concentration, with a calibration curve for each antigen presented in Figure 3.4. Further details about the calibration analysis and fitting parameters is given in the Experimental Methods section.

Following the generation of calibration curves, we next moved to quantitate the 8-plex biomarker panel in a handful of representative human serum samples. Specifically, we analysed commercially-available samples from patients generically diagnosed with pancreatic, liver, ovarian, breast, lung, colorectal, and prostate cancer, as well as a sample from a healthy patient. Figure 3.5 shows the real-time resonance shifts for each of the entire 8-plex assays. The resonance shift during the secondary, protein multi-layer enhancement regime was measured and compared against the calibration curves to determine the serum concentrations of each of the respective antigens (Table 3.1).

For the sake of comparison, the sensor responses of each biomarker determined from the cancer patient samples were divided by the response of the same biomarker measured in the healthy sample to generate a relative index of expression. That is to say that a relative index of 15 means that the biomarker level is elevated 15-fold over the healthy sample. This mechanism of data presentation is helpful as some biomarkers, such as ALCAM, have uniformly higher concentrations in all samples and therefore the importance in absolute concentrations is highly variable across this set of biomarkers. This indexing approach seems reasonable given that these markers are known to be elevated in the case of organ-specific cancer.

In Figure 3.6 we plotted relative indices across the 8-plex panel for each patient that revealed organ-specific biomarker “fingerprints” for these seven samples. For example, the known pancreatic cancer biomarker CA 19-9 shows the greatest level of elevation in the pancreatic cancer sample. Similarly, CA 15-3 and PSA show the largest elevations in breast and prostate cancer, respectively. For the liver cancer sample, AFP and osteopontin, both

known to be elevated in some liver malignancies, showed elevated levels. However, we also see examples where biomarkers are not elevated as have been reported in the literature. CA-125, a putative ovarian cancer biomarker, is not elevated in the ovarian cancer sample. Also, both CEA, a colorectal cancer marker, and ALCAM, a breast cancer marker, have relatively stable levels across all of the patient samples and are not elevated in breast or colorectal samples.

Importantly, we are not making any claims about the diagnostic of any of these markers. Rather we are reporting on the development of a silicon photonic technology that has the capability to robustly perform analyses of multiplexed panels of serum biomarkers. From a biological perspective, though, there are many reasons why the diagnostic utility of specific biomarkers might not strictly be observed in these (and other) serum samples. The patient-to-patient heterogeneity of cancers is well-documented and genetic and phenotypic differences can lead to wide disparities in secreted biomarker signatures. Perhaps the best instance of underling disease heterogeneity compromising the value of single biomarker-based diagnostics is the example of PSA, of which an overreliance on this assay for screening purposes can lead to over diagnosis and overly aggressive treatment.(29) Moreover, the limited specificity of many single disease biomarkers greatly restricts their independent diagnostic utility,(30) but rather suggest defined roles in screening and monitoring. Though taken together, panels of mildly specific serum biomarkers might, if recorded longitudinally using cost effective, multiplexed technologies, be very effective in the early detection of malignancies that could then be localized via more highly specific clinical means.

3.4 Experimental methods

3.4.1 Materials

Succinimidyl 4-formylbenzoate (S-4FB), succinimidyl 6-hydrazinonicotinamide acetone hydrazone (S-HyNic), and 3-N-((6-(N'-Isopropylidene-hydrazino))nicotinamide)-propyltriethyoxysilane (HyNic Silane) were purchased from SoluLink (San Diego, CA). Custom DNA oligonucleotides were synthesized by Integrated DNA Technologies (Coralville, IA). A list of all antigens and antibodies (capture and detection) purchased and

used for eight-plex experiments are listed in Table 3.2. NHS-PEG$_4$-Biotin, Zeba spin filters, and Starting Block were purchased from Pierce (Rockford, IL). NHS-PEG$_4$-Biotin was dissolved in *N,N*-dimethylformamide (DMF) to make a 20 mM stock solution. Vivaspin molecular weight cutoff filters (50,000 and 5,000 Da MWCO), were obtained from GE Healthcare (Waukesha, WI). Anti-biotin antibody conjugated to phycoerythrin (anti-biotin PE) and biotinylated anti-phycoerythrin (anti-PE biotin) were obtained from eBioscience (San Diego, CA). Phosphate buffered saline (PBS), with a standard 10 mM phosphate ion concentration, was reconstituted from Dulbecco's phosphate buffered saline packets purchased from Sigma-Aldrich (St. Louis, MO). All other chemicals were obtained from Sigma-Aldrich and used as received. Human serum samples from cancer patients were purchased from Innovative Research, Inc. (Novi, MI) and Asterand, Inc. (Detroit, MI).

Buffers were made with purified water (ELGA PURELAB filtration system; Lane End, UK), and the pH adjusted as necessary with 1 M HCl or 1 M NaOH. For NHS-ester chemistry, A high phosphate PBS buffer with 100 mM phosphate (100 mM PBS) was made to be 150 mM NaCl, 22.5 mM monobasic sodium phosphate, and 77.7 mM dibasic sodium phosphate and then pH-adjusted to either pH 7.4 or pH 6.0. PBS with 0.05% Tween-20 (PBST) was made by adding Tween-20 to standard PBS buffer (Dulbecco's formulation). PBST with Starting Block (PBST-SB) was made by adding 1% Starting Block to PBST buffer and then adding 0.01% sodium azide as a preservative. All solutions were degassed under vacuum with concurrent sonication before being flowed across the sensor surface.

3.4.2 Instrumental setup and microchip design

The instrument, sensor chips, and microring resonator measurement system was acquired from Genalyte, Inc. (San Diego, CA). The M1 version of the instrument offered optical detection performance equivalent to the previous version,(31) but with the enabling addition of full automation of fluidic flow with programming to allow sipping from a 96-well plate. The chips used in these experiments are 4 × 6 mm microchips with 34 microring sensors—32 active sensor rings and 2 thermal controls, which are rings covered by a polymeric cladding that allowed real-time correction of resonance shifts resulting only from temperature fluctuation. All measurements for these experiments were made with the

sensor chips loaded into a custom cell with microfluidic flow channels defined by a 0.007-inch thick Mylar gasket with a U-shaped channel 400 μm wide. Solution was drawn from pre-loaded 96-well plates via the automated fluid handling system in the instrument.

3.4.3 Surface functionalization with DNA

Microring array substrates were first cleaned with piranha solution (3:1 H_2SO_4:30% H_2O_2) for 30 seconds followed by rinsing with water and drying under a stream of N_2. To introduce reactive functional groups, substrates were covered with 20 μL of a 1 mg/mL solution of HyNic Silane (20 mg/mL HyNic Silane in DMF stock solution diluted to 1 mg/mL with ethanol) for ~30 minutes, followed by rinsing with ethanol and then sonicating in ethanol for ~30 minutes. Chips were then dried with N_2. Notably, the polymeric cladding layer confined surface functionalization to the annular openings surrounding microring sensors.

Antibodies were attached to the sensor surfaces via DNA-DNA hybridization, as is described below. For this purpose, individual microring sensors were modified with specific single-stranded DNA oligonucleotides, the sequences of which were previously designed to ensure minimal cross-reactivity.(32) The sequences of all surface attached oligonucleotides (B, C, D, F, J, K, L, and M), are provided in Table 3.3. Single-strand oligonucleotides were synthesized with a 5′ amino terminal group to facilitate surface attachment via standard bioconjugate reactions. Oligonucleotides were first functionalized with S-4FB according to manufacturer (SoluLink) instructions, with an initial buffer exchange to 100 mM PBS pH 7.4 using 5 kDa MWCO filters and then subsequent reaction with a 20-fold molar excess of S-4FB in DMF. Solutions were allowed to react overnight at room temperature and were then buffer exchanged into 100 mM PBS pH 6.0 using 5 kDa MWCO filters to remove excess S-4FB reagent.

Eight-plex chips were created by microspotting 4FB-functionalized DNA strands onto HyNic-functionalized microring resonator chips. Each chip had four microrings spotted with a unique DNA sequence (B, C, D, F, J, K, L, and M). Spotting was accomplished with a Nano eNabler spotting system from BioForce Nanosciences (Ames, IA). The 4-FB-modified DNA was diluted to a concentration of ~100 μM in 100 mM PBS

buffer pH 6.0 and mixed in a 1:1 ratio with dimethyl sulfoxide (DMSO). After spotting, the drops evaporated on a hot plate (~80 °C) for five minutes and then incubated in a saturated humidity chamber overnight. The chips were then briefly rinsed in Starting Block, and then immediately in water. The chips were then again rinsed with fresh Starting Block and stored in PBST-SB until use.

3.4.4 DNA-Antibody conjugate synthesis and sensor array encoding via self-assembly

To create DNA-antibody conjugates, antibodies were functionalized with S-HyNic as previously demonstrated.(13) The sequences of oligonucleotides attached to antibodies (B′, C′, D′, F′, J′, K′, L′, and M′; with the prime denoting complementarity to the respective surface-attached sequence) are provided in Table 3.3. Again, each oligonucleotide had a 5′-NH_2 functionality. S-HyNic solutions, dissolved in DMF, was added in 20- to 30-fold molar excess to ~1 mg/mL antibody that had been buffer exchanged into 100 mM PBS pH 7.4 with a Zeba spin filter. This reaction was allowed to proceed for at least two hours at room temperature. The HyNic presenting antibodies were then exchanged into 100 mM PBS pH 6.0 with a Zeba spin filter to remove excess HyNic.

DNA modified with 4FB was then added in >10-fold molar excess to the HyNic-modified antibody and allowed to react overnight at 4 °C. The resulting DNA-antibody conjugates were then purified away from the excess 4FB-DNA using a Superdex 200 10/300 GL column on an AKTA FPLC, both from GE Healthcare (Waukesha, WI). The separation was performed at 4 °C with a PBS isocratic elution. Collected fractions were concentrated with 50 kDa MWCO filters to yield purified solutions of DNA-antibody conjugates. The final conjugate concentration was determined by measuring the differential absorption at 260 versus 280 nm, corresponding to the DNA and IgG, respectively, using a NanoDrop UV-Vis absorbance system (ThermoFisher Scientific, Wilmington, DE). The following conjugates were synthesized using the capture antibodies listed in Table 3.2, resulting in the following DNA-capture antibody combinations: B′-anti-AFP, C′-anti-ALCAM, D′-anti-CA19-9, F′-anti-osteopontin, J′-anti-CA15-3, K′-anti-CEA, L′-anti-CA-125, M′-anti-PSA.

To create multiplexed biomarker detection arrays, each of the DNA-antibody conjugates were combined into a single mixed with each conjugate at 5 μg/mL (except for L′-anti-CA-125, which was used at 1 μg/mL) in PBST. To each eight-plex, DNA-functionalized microchip, 10 μL of DNA-antibody conjugate mixture was added to the surface of each chip and the array allowed to self-assemble. Chips were incubated overnight to enable maximum binding of the DNA-antibody conjugates to the DNA capture probes on the surface. Following overnight binding, the chips were rinsed and stored immersed in PBST-SB.

3.4.5 Tracer antibody biotinylation

Each of tracer antibodies was biotinylated to facilitate the layer-by-layer signal enhancement scheme. The ALCAM tracer was purchased as a pre-biotinylated polyclonal antibody. Each of the other tracer antibodies were first buffer exchanged into 100 mM PBS pH 7.4 via a Zeba spin column. A 20-fold molar excess of 20 mM NHS-PEG_4-biotin was then added allowed to react for 2 h at room temperature. For the anti-AFP and anti-osteopontin tracer antibodies, it was empirically determined that 5-fold and 50-fold molar excesses, respectively, gave the best performance. Excess NHS-PEG_4-biotin was removed by buffer exchange using Zeba spin filter columns. Prior to use in the layer-by-layer signal enhancement scheme, the anti-PE biotin and anti-biotin PE antibodies were buffer exchanged into the PBST-SB.

3.4.6 Eight-plex antigen analysis

To generate calibration curves, all antigens were diluted in PBST-SB or 50% Starting Block/50% PBST-SB. Human serum samples were analysed after diluting to 33% in PBST-SB. The sensor array was placed into the fluidic cartridge and loaded into the M1 instrument. For all assay steps, except for sample and biotinylated tracer antibody introduction, the flow rate was 30 μL/min. When the sample and biotinylated tracer was introduced, the flow rate was reduced to 15 μL/min to reduce consumption. PBST-SB was used as the running buffer and was flowed over the surface for ~5 minutes to establish a stable baseline. The sample was introduced and flowed over the chip for a total of 30 minutes (200 μL of serum diluted 3-fold) before a 20 minute rinse with running buffer to

help remove non-specifically bound proteins for 20 minutes. A mixture of biotinylated tracer antibodies each at a concentration of 1 μg/mL was then flowed over the chip for 15 minutes followed by a 5 minute running buffer rinse. For the layer-by-layer signal enhancement step, the solution flowing across the chip was repeatedly switched between 1 μg/mL anti-biotin (PE) and 2 μg/mL anti-PE (biotin) for two minutes each, with a 15-second running buffer rinse between each step. This process was repeated up to 3 times (six steps), yielding an enhanced signal magnitude for biomarkers present in the sample. Importantly, each of these steps was completely automated and did not require any under intervention during the assay.

The difference in resonance wavelength shift before and after the signal enhancement step was determined and used for quantitation. Importantly, since the signals are measured only from this secondary step, resonance shifts from non-specific protein adsorption do not contribute to the analytical signal.

Calibration curves were made to cover a range of biomarker concentrations relevant for clinical serum specimens, as shown in Figure 3.4. To conserve analysis time while avoiding possible interferences between antigens, calibrations were obtained simultaneously for CEA, ALCAM, AFP, and PSA. CA19-9 and CA15-3 calibrations were obtained together, but apart from the other antigens. By running a few concentrations of CA15-3 with no CA19-9 and vice versa, it was possible to obtain corrections for how the stock antigen solutions interfered with each other. Similarly, osteopontin and CA-125 calibrations were run together, but apart from the other antigens. Each point on the calibration curve represents one measurement on one chip based on the net shift in resonance frequency (pm) obtained from the tertiary amplification step. Because the tertiary amplification step consisted of 6 mini-steps (anti-biotin, anti-PE, anti-biotin, anti-PE, anti-biotin, anti-PE), it was possible to use a different region of the tertiary amplification curve for each antigen. This was important because some of the antigens tended to generate higher signals and would saturate the tertiary signal faster than the antigens that generated lower signal. For example, the ALCAM calibration curve had the largest range of quantitation when the shift was measured after only one of the amplification mini-steps. At later steps of the amplification, the last two points on the calibration curve became indistinguishable from each other. In contrast, CA15-3 tended to display only small relative shifts, and thus using 6 amplification steps increased the

signal that could be observed. Incidentally, we have observed that amplification beyond about 6 steps tends to increase the signal, but the noise increases proportionally leading to a relatively constant signal to noise ratio. The number of amplification steps used for each antigen's calibration curve is given in Table 3.4.

The error bars shown on the calibration curves were derived based on the standard deviation of the ring-to-ring measurements on a given chip or the chip-to-chip, whichever was larger. Chip-to-chip variability was determined by performing the identical assay on multiple 8-plex chips, and this variability was calculated to have a coefficient of variation (CV) of 17%. This same error formula was applied to the relative signal index measurements used in Figure 3.6.

Calibration curves were based on unweighted fits with either a linear model or a dose-response model fit in OriginPro software package version 8.5. The dose-response equation used is given here:

$$y = A + \frac{(B - A)}{1 + 10^{(C-x)D}}$$

Calibration curves overlaid on data plots are shown in Figure 3.3. Calibration parameters are listed in Table 3.4. The units for AFP, ALCAM, Osteopontin, CEA, and PSA are given in ng/mL whereas CA19-9, CA15-3, and CA125 are given in units/mL (U/mL). These labels are based on the units given from the commercially obtained antigen solutions. Table 3.1 lists the results of the calibration analysis for individual tested serum samples with reference to the upper and lower quantitation limits for the calibration curves listed in Table 3.5. A "—" indicates a measurement that was below the range of quantitation used for the calibration curve. A result with a ">" indicates that the measurement fell higher than the quantitation range used for the calibration curve. CA-125 fell below the range of accurate quantitation in all samples, and so it is not listed on the table. A few of the samples still had measurable shifts even though the values fell below the range of quantitation. As a result, Figure 3.6 displays a relative index value for these antigens. This is a case of the limit of detection (LOD) being lower than the limit of quantitation (LOQ).

In Table 3.1. the errors shows for each measurement are extrapolated from the standard deviation of the measurement signal via the calibration curve. In other words, $y \pm y_{error}$ is converted to $x \pm x_{error}$, where y_{error} was determined using relative standard deviation, as described previously.

3.5 Conclusions

The emergence of a number of disease-related biomarkers place an impetus on the development of robust diagnostic technologies of cost-effective and relatively rapid measuring levels of multiple biomarkers from within single patient sample. Using a silicon photonic microring resonator platform we demonstrate the multiplexed detection of eight cancer serum biomarkers. The real-time analytical capabilities of the technology streamlined the assay development and optimization process, and an automated layer-by-layer signal enhancement scheme provided requisite analytical performance. Comparison of biomarkers levels across a narrow subset of samples suggest that panel-based disease "fingerprints" might have utility in the screening, early detection, or monitoring of disease on an individualized level. Obviously the next step for this technology involves the analysis of many more patient samples in concert with a more directed clinical applications and patient outcomes. However, we feel that this technological achievement is noteworthy in the context of analytical sensor development. Moreover, the cost effective and modularly multiplexable nature of the technology position it as an attractive platform for a wide number of biomarker-based diagnostic applications that are becoming increasingly valuable in the pursuit of personalized cancer diagnostics.

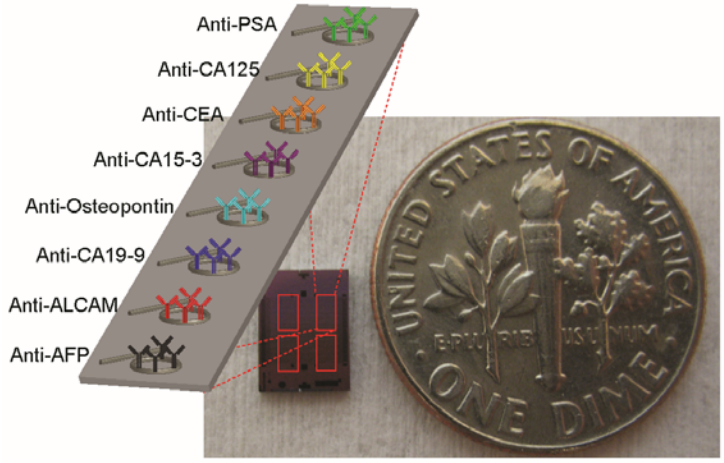

Figure 3.1 Photograph of silicon microchip overlaid with four red boxes indicating sub-array regions containing 8 microring resonators, each functionalized with an antibody specific for a different cancer biomarker antigen.

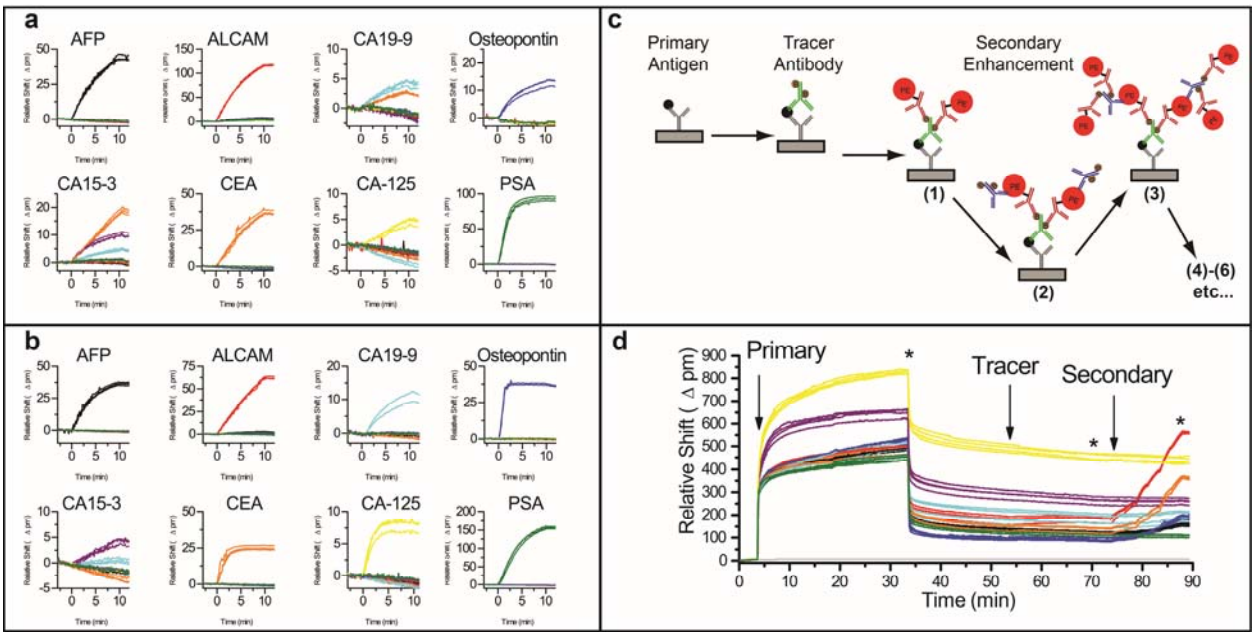

Figure 3.2 8-plex analysis for cross reactivity and 8-plex serum sensing. **a)** Response of 8-plex chip upon sequential addition of 1 µg/mL (or 1 kU/mL) of each antigen in buffer. Each plot shows the responses for the entire array of microring sensors, each functionalized with a different capture antibody, to a single biomarker. **b)** Response of the same 8-plex chip upon subsequent addition of 1 µg/mL of the capture antibody. Each plot shows the responses for the entire array exposed to the single listed analyte and corresponding tracer antibody. **c)** Schematic showing the layer-by-layer signal enhancement strategy. **d)** A real-time plot showing the resonance wavelength shifts through the entire assay analysing a representative human serum sample. Vertical arrows represent the start of the primary, tracer, and secondary enhancement steps, respectively. The * symbol indicates a buffer rinse. For panels, a, b, and d, responses are color-coded according to the capture antibody on each microring: anti-AFP = black, anti-ALCAM = red, anti-CA19-9 = cyan, anti-osteopontin = blue, anti-CA15-3 = purple, anti-CEA = orange, anti-CA125 = yellow, anti-PSA = green.

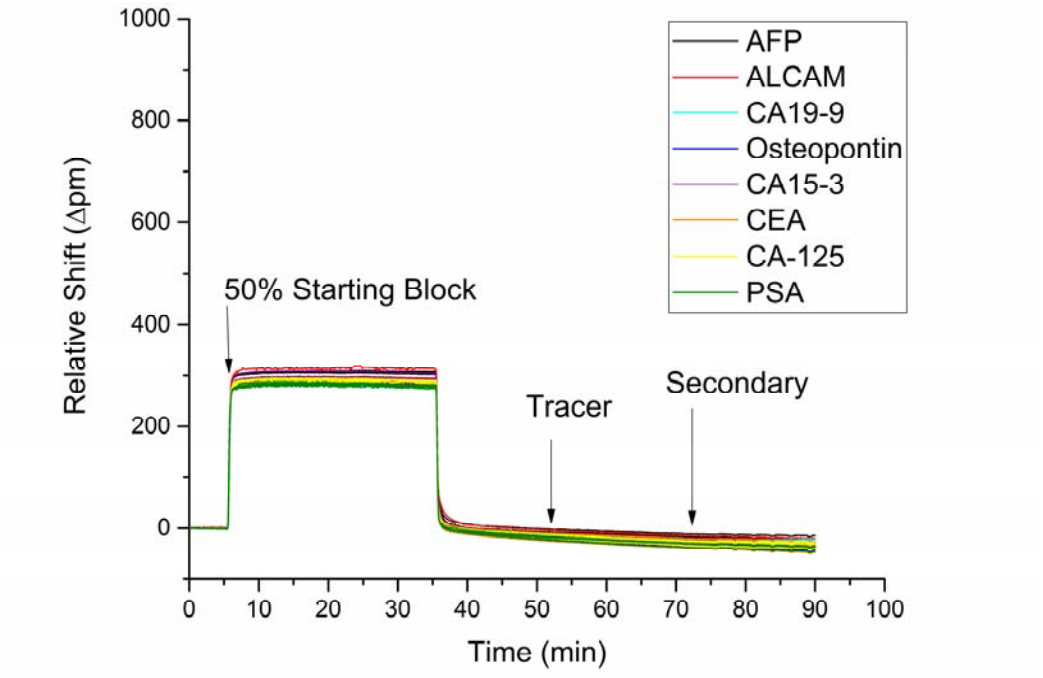

Figure 3.3 Negative control experiment where 50% Starting Block solution is flowed across the array in the primary binding step. The running buffer before primary binding is 1% starting block in PBS-Tween 20 buffer (PBST), which explains the large bulk refractive index step. The experiment demonstrates that the tracer and secondary signal enhancement steps do not lead to non-specific binding responses.

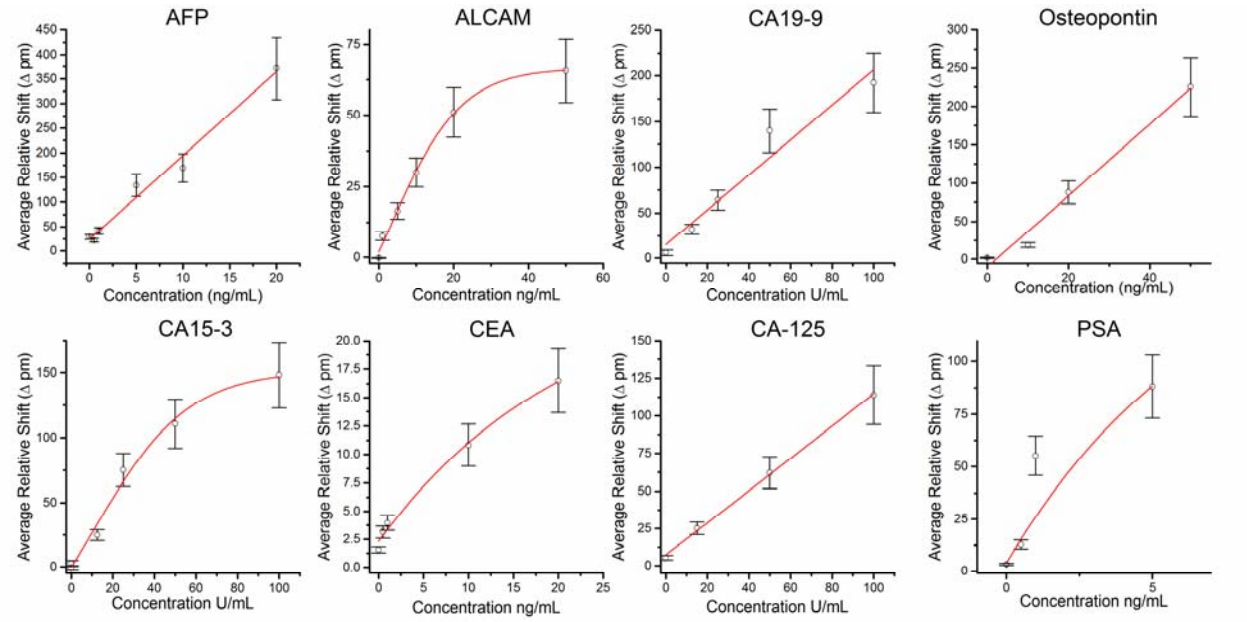

Figure 3.4 Calibration curves for each cancer biomarker. Each plot shows the dose-response relationship and fit for each of the targeted antigens as detected by the specific sandwich assay immunoassay. Error bars were calculated based on the chip-to-chip variation of 17% CV, or ring-to-ring standard deviation if larger than 17% CV.

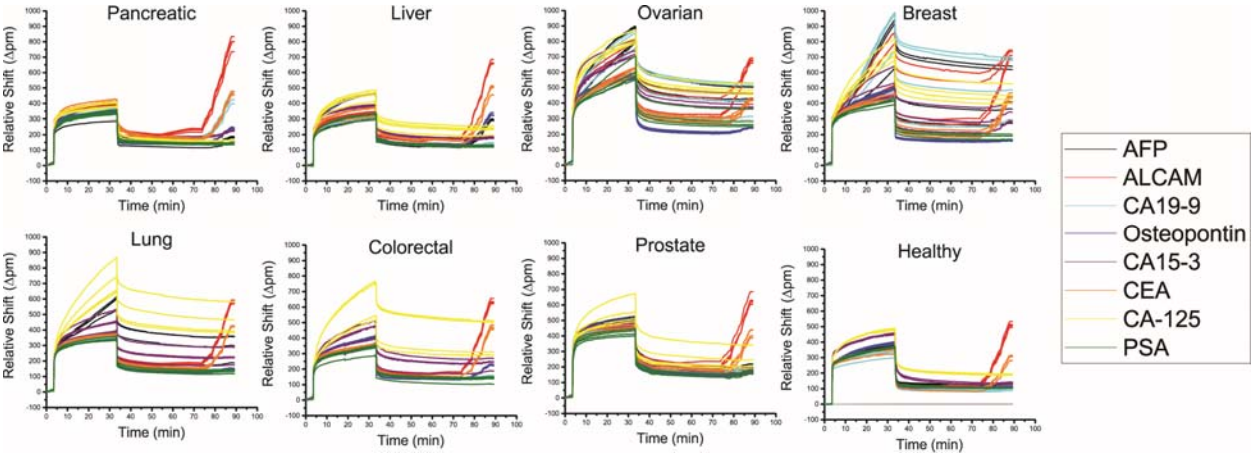

Figure 3.5 Real-time response of the 8-plex cancer biomarkers assay in eight evaluated serum samples from healthy patients as well as cancer patients. Each panel shows the real-time shift in resonance shift throughout the entire assay to detect the 8-plex biomarker panel from each commercial, organ-specific serum sample. Although clear differences are observed through the primary antigen binding response, quantification is achieved only from the layer-by-layer secondary enhancement component of the assay.

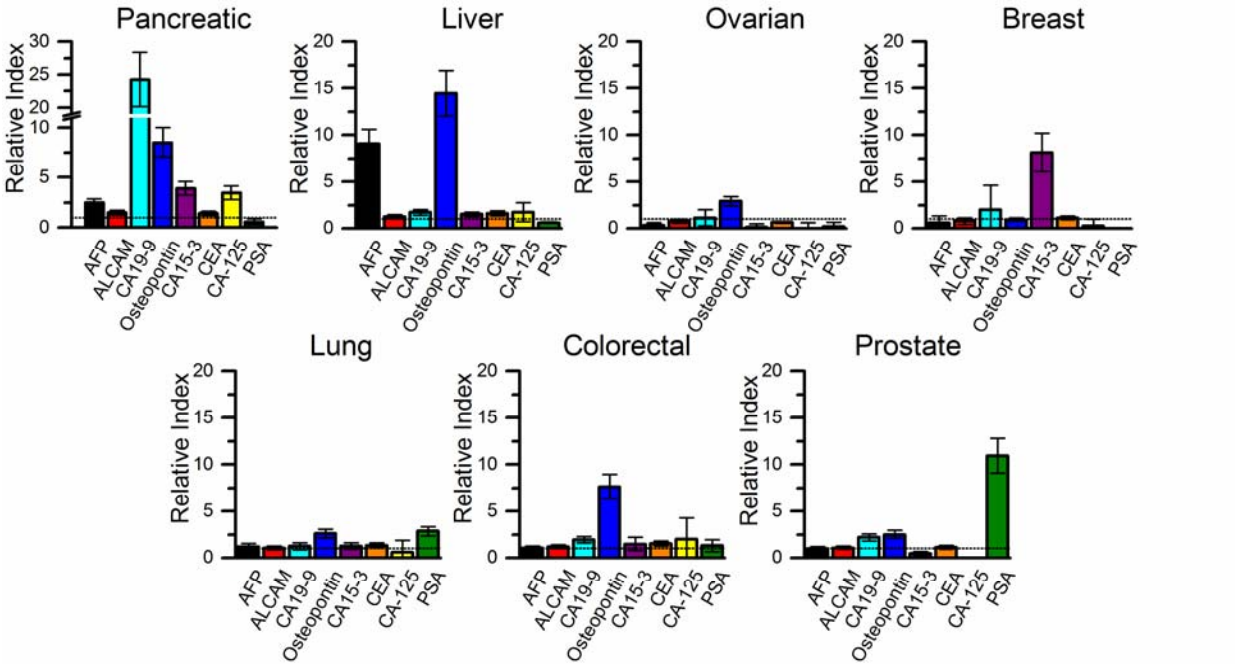

Figure 3.6 Relative biomarker "fingerprints" for selected cancer patient serum samples. This "fingerprint" was generated by dividing the sensor response for each biomarker in each cancer serum sample by the response measured in the healthy serum sample. Error bars indicate the relative standard deviation for the four technical replicate sensors on each chip used to measure each antigen. A relative index level of 1.0 indicates (horizontal dashed lines in each plot) that the biomarker was equivalent in both disease and normal sample, with indices greater than 1.0 representing organ-specific biomarker elevation.

	Pancreas		Prostate		Liver		Ovarian		Breast		Lung		CRC		Healthy	
	ng/mL	error	ng/mL	error	ng/mL	error	ng/mL	error	ng/mL	error	ng/mL	error	ng/mL	error	ng/mL	error
AFP	**1.3**	0.5	**—**	—	**8.8**	1.7	**—**	—	**—**	—	**—**	—	**—**	—	**—**	—
ALCAM	**>65**	—	**7.6**	1.5	**16.7**	4.4	**5.4**	2.8	**7.5**	5.8	**10.5**	2.2	**15.4**	3.8	**>65**	—
CA19-9	**>100**	—	**—**	—	**—**	—	**—**	—	**—**	—	**—**	—	**3.8**	2.0	**—**	—
Osteopontin	**14.6**	2.1	**—**	—	**21.3**	3.3	**6.1**	0.7	**—**	—	**6.5**	0.7	**13.3**	1.9	**5.1**	0.2
CA15-3	**12.8**	2.1	**3.6**	2.5	**5.1**	0.8	**—**	—	**27.2**	7.8	**4.3**	1.0	**5.1**	2.2	**3.5**	0.5
CEA	**>20**	7.1	**18.0**	5.8	**>20**	12.5	**3.9**	2.1	**12.0**	3.4	**19.9**	6.8	**>20**	—	**>20**	—
PSA	**—**	—	**0.14**	0.05	**—**	—	**—**	—	**—**	—	**—**	—	**—**	—	**—**	—

Table 3.1 Measured concentration values for each serum sample. Entries with ">" indicate values are over the limits of quantitation; entries with "—" indicate values below the limits of quantitation. Bold values indicate the concentration and non-bold entries to the right represent the error of the measurement.

Antibody / Antigen Type		Source*	Product Number	Antibody Clone
AFP	**Antigen**	Meridian	A81510H	
	Capture	Meridian	MAM01-301	057-11301
	Detection	Meridian	M01254M	B491M
ALCAM	**Antigen**	R&D Systems	656-AL	
	Capture	R&D Systems	MAB656	105901
	Detection	R&D Systems	BAF656	Polyclonal
CA 125	**Antigen**	Fitzgerald	30-AC21	
	Capture	Life Span	LS-C84288/ 28658	M002201
	Detection	Meridian	10-C02F	M002203
CA 15-3	**Antigen**	Meridian	A32000H	
	Capture	Fitzgerald	10-C03E	M002204
	Detection	Fitzgerald	10-C03F	M002208
CA 19-9	**Antigen**	Fitzgerald	30AC14	
	Capture	Fitzgerald	10C04C	M8073021
	Detection	Meridian	M37301M	241
CEA	**Antigen**	Fitzgerald	30-AC32	
	Capture	Meridian	MAM02-009	057-10009
	Detection	Meridian	MAM02-008	057-10008
Osteopontin	**Antigen**	Fitzgerald	30RA0008	
	Capture	Meridian	M66102M	2C5
	Detection	Meridian	H01278M	B697M
PSA	**Antigen**	Fitzgerald	30R-AP019	
	Capture	Meridian	M66279M	B731M
	Detection	Meridian	M86506M	5A6

*Full source information:

Meridian Life Science, Saco, ME

R&D Systems, Minneapolis, MN

Fitzgerald Industries International, Concord, MA

Life Span Biosciences, Seattle WA

Table 3.2 List of antigens and antibodies used for eight-plex experiments, company source, product number and antibody clone (for monoclonal antibodies)

Name	Sequence (5′ to 3′)
B	AAA AAA AAA AGC CTC ATT GAA TCA TGC CTA
B′	AAA AAA AAA ATA GGC ATG ATT CAA TGA GGC
C	AAA AAA AAA AGC ACT CGT CTA CTA TCG CTA
C′	AAA AAA AAA ATA GCG ATA GTA GAC GAG TGC
D	AAA AAA AAA AAT GGT CGA GAT GTC AGA GTA
D′	AAA AAA AAA ATA CTC TGA CAT CTC GAC CAT
F	AAA AAA AAA AAT CAG GTA AGG TTC ACG GTA
F′	AAA AAA AAA ATA CCG TGA ACC TTA CCT GAT
J	AAA AAA AAA ATC TTC TAG TTG TCG AGC AGG
J′	AAA AAA AAA ACC TGC TCG ACA ACT AGA AGA
K	AAA AAA AAA ATA ATC TAA TTC TGG TCG CGG
K′	AAA AAA AAA ACC GCG ACC AGA ATT AGA TTA
L	AAA AAA AAA AGT GAT TAA GTC TGC TTC GGC
L′	AAA AAA AAA AGC CGA AGC AGA CTT AAT CAC
M	AAA AAA AAA AGT CGA GGA TTC TGA ACC TGT
M′	AAA AAA AAA AAC AGG TTC AGA ATC CTC GAC

Table 3.3 List of DNA oligonucleotide sequences used. All sequences have a 5′ terminal amino group attached via a 6-carbon chain (5AmMC6 from IDT)

Dose-Response	**Antigen**	**# of Enhancement Steps**	**A**	**B**	**C**	**D**
	ALCAM	1	-45.85	66.50	2.85	0.046
	CA15-3	6	-98.22	151.91	10.09	0.019
	CEA	1	-4214.83	25.29	-109.06	0.021
	PSA	2	-37051.34	165.89	-36.65	0.064
Linear	**Antigen**	**Time Range (min)**	**Intercept**	**Slope**		
	AFP	6	24.4	17.01		
	CA19-9	6	15.2	1.91		
	Osteopontin	4	-9.9	4.67		
	CA125	6	7.4	1.07		

Table 3.4 Number of amplification steps used for the calibration curve, the upper and lower limits of quantitation used for these curves, and the fitting parameters for both the dose-response calibration curves as well as the linear calibration curves.

	MILLIPLEX® MAP Human Circulating Cancer Biomarker Magnetic Bead Panel- Cancer Multiplex Assay*	**8-plex Microring Resonator Cancer biomarker assay**
	Working ranges	
AFP (ng/mL)	0.0747-500	0.3-20.6
ALCAM	n/a	1.0-43.7
CA19-9 (U/mL)	0.3-625	2.5-96.6
Osteopontin (ng/mL)	0.2853-500	4.3-50.3
CA15-3 (U/mL)	0.03-625	2.0-91.5
CEA (ng/mL)	0.0052-500	0.2-20.2
CA-125 (U/mL)	0.2-625	2.4-95.6
PSA† (ng/mL)	0.0014-500	0.054-4.7

* Working range was assumed to span from the Minimum detectable concentration up to the upper limit of the reported dynamic range, which may be an overestimate of the upper end of the working range. Values taken from MILLIPLEX® MAP Human Circulating Cancer Biomarker Magnetic Bead Panel 1 Protocol.

† Reported free PSA value.

Table 3.5 Comparison of working ranges for the MILLIPLEX® MAP Human Circulating Cancer Biomarker Magnetic Bead Panel and the 8-plex microring resonator cancer biomarker assay described in this manuscript.

3.6 References

1. Etzioni R, Urban N, Ramsey S, McIntosh M, Schwartz S, Reid B, et al. Early detection: The case for early detection. Nature Reviews Cancer 2003;3:243.
2. Petricoin EF, Ardekani AM, Hitt BA, Levine PJ, Fusaro VA, Steinberg SM, et al. Use of proteomic patterns in serum to identify ovarian cancer. Lancet 2002;359:572-7.
3. Sawyers CL. The cancer biomarker problem. Nature 2008;452:548-52.
4. Arnaud CH. Biomarkers wanted. Chemical and Engineering News 2011 July 25, 2011:40-3.
5. Rusling JF. Multiplexed electrochemical protein detection and translation to personalized cancer diagnostics. Analytical Chemistry 2013;85:5304-10.
6. He B, Morrow TJ, Keating CD. Nanowire sensors for multiplexed detection of biomolecules. Current Opinion in Chemical Biology 2008;12:522-8.
7. Carregal-Romero S, Caballero-Díaz E, Beqa L, Abdelmonem AM, Ochs M, Hühn D, et al. Multiplexed sensing and imaging with colloidal nano- and microparticles. Annual Review of Analytical Chemistry 2013;6:53-81.
8. Muzyka K. Current trends in the development of the electrochemiluminescent immunosensors. Biosensors and Bioelectronics 2014;54:393-407.
9. Estevez MC, Otte MA, Sepulveda B, Lechuga LM. Trends and challenges of refractometric nanoplasmonic biosensors: A review. Analytica Chimica Acta 2014;806:55-73.
10. Luchansky MS, Bailey RC. Silicon photonic microring resonators for quantitative cytokine detection and t-cell secretion analysis. Analytical Chemistry 2010;82:1975-81.
11. Washburn AL, Luchansky MS, Bowman AL, Bailey RC. Quantitative, label-free detection of five protein biomarkers using multiplexed arrays of silicon photonic microring resonators. Analytical Chemistry 2010;82:69-72.
12. Foreman MR, Swaim JD, Vollmer F. Whispering gallery mode sensors. Adv Opt Photon 2015;7:168-240.
13. Washburn AL, Gomez J, Bailey RC. DNA-encoding to improve performance and allow parallel evaluation of the binding characteristics of multiple antibodies in a surface-bound immunoassay format. Analytical Chemistry 2011;83:3572-80.
14. Bailey RC, Kwong GA, Radu CG, Witte ON, Heath JR. DNA-encoded antibody libraries: A unified platform for multiplexed cell sorting and detection of genes and proteins. J Am Chem Soc 2007;129:1959-67.
15. Sturgeon C. Practice guidelines for tumor marker use in the clinic. Clinical Chemistry 2002;48:1151-9.
16. Kulasingam V, Zheng Y, Soosaipillai A, Leon AE, Gion M, Diamandis EP. Activated leukocyte cell adhesion molecule: A novel biomarker for breast cancer. International Journal of Cancer 2009;125:9-14.
17. Berger AC, Meszoely IM, Ross EA, Watson JC, Hoffman JP. Undetectable preoperative levels of serum ca 19-9 correlate with improved survival for patients with resectable pancreatic adenocarcinoma. Annals of Surgical Oncology 2004;11:644-9.
18. Mor G, Visintin I, Lai Y, Zhao H, Schwartz P, Rutherford T, et al. Serum protein markers for early detection of ovarian cancer. Proceedings of the National Academy of Sciences of the United States of America 2005;102:7677-82.
19. Schiemann U, Günther S, Gross M, Henke G, Müller-Koch Y, König A, et al. Preoperative serum levels of the carcinoembryonic antigen in hereditary non-polyposis colorectal cancer

compared to levels in sporadic colorectal cancer. Cancer Detection and Prevention 2005;29:356-60.
20. Szymendera J, Nowacki M, Szawlowski A, Kamińska J. Predictive value of plasma cea levels: Preoperative prognosis and postoperative monitoring of patients with colorectal carcinoma. Diseases of the Colon and Rectum 1982;25:46-52.
21. Wang JY, Tang RP, Chiang JM. Value of carcinoembryonic antigen in the management of colorectal-cancer. Diseases of the Colon & Rectum 1994;37:272-7.
22. Cao D-X, Li Z-J, Jiang X-O, Lum YL, Khin E, Lee NP, et al. Osteopontin as potential biomarker and therapeutic target in gastric and liver cancers. World Journal of Gastroenterology : WJG 2012;18:3923-30.
23. Andriole GL, Crawford ED, Grubb RL, III, Buys SS, Chia D, Church TR, et al. Mortality results from a randomized prostate-cancer screening trial. New England Journal of Medicine 2009;360:1310-9.
24. Rhea JM, Molinaro RJ. Cancer biomarkers: Surviving the journey from bench to bedside. MLO: Medical Laboratory Observer 2011;43:10-8.
25. Luchansky MS, Washburn AL, McClellan MS, Bailey RC. Sensitive on-chip detection of a protein biomarker in human serum and plasma over an extended dynamic range using silicon photonic microring resonators and sub-micron beads. Lab on a Chip 2011;11:2042-4.
26. Luchansky MS, Washburn AL, Martin TA, Iqbal M, Gunn LC, Bailey RC. Characterization of the evanescent field profile and bound mass sensitivity of a label-free silicon photonic microring resonator biosensing platform. Biosensors and Bioelectronics 2010;26:1283-91.
27. Spaeth K, Brecht A, Gauglitz G. Studies on the biotin-avidin multilayer adsorption by spectroscopic ellipsometry. Journal of Colloid and Interface Science 1997;196:128-35.
28. Anderson GP, Taitt CR. Suspension microarray immunoassay signal amplification using multilayer formation. Sensor Letters 2008;6:213-8.
29. Carter HB, Albertsen PC, Barry MJ, Etzioni R, Freedland SJ, Greene KL, et al. Early detection of prostate cancer: Aua guideline. The Journal of Urology;190:419-26.
30. Sturgeon CM, Lai LC, Duffy MJ. Serum tumour markers: How to order and interpret them. BMJ 2009;339.
31. Iqbal M, Gleeson MA, Spaugh B, Tybor F, Gunn WG, Hochberg M, et al. Label-free biosensor arrays based on silicon ring resonators and high-speed optical scanning instrumentation. IEEE Journal of Selected Topics in Quantum Electronics 2010;16:654-61.
32. Fan R, Vermesh O, Srivastava A, Yen BKH, Qin L, Ahmad H, et al. Integrated barcode chips for rapid, multiplexed analysis of proteins in microliter quantities of blood. Nature Biotechnology 2008;26:1373-8.

Chapter 4:

Development and Validation of an Immunosensor for Monocyte Chemotactic Protein 1 using a Silicon Photonic Microring Resonator Biosensing Platform

Acknowledgments

This chapter was reproduced from "Development and validation of an immunosensor for monocyte chemotactic protein 1 using a silicon photonic microring resonator biosensing platform". (Valera, E. V., Shia, W. W., Bailey, R. C. *Clinical Biochemistry*. **2016**, *49*, 121-126).

This work is done in collaboration with Dr. Enrique Valera, especially for his efforts in data collection and putting together the final version of the manuscript. Prof. Ryan Bailey is acknowledged for initiating this project.

We gratefully acknowledge financial support from the National Science Foundation (CHE 12-14081) and National Cancer Institute (R33-CA177462-01). WWS was supported by an American Heart Association Predoctoral Fellowship.

4.1 Abstract

a) Objectives:

We report the development of an optical immunosensor for the detection of monocyte chemotactic protein 1 (MCP-1) in serum samples. MCP-1 is a cytokine that is an emerging biomarker for several diseases/disorders, including ischemic cardiomyopathy, fibromyalgia, and some cancers.

b) Design and Methods:

The detection of MCP-1 was achieved by performing a sandwich immunoassay on a silicon photonic microring resonator sensor platform. The resonance wavelengths supported by microring sensors are responsive to local changes in the environment accompanying biomarker binding. This technology offers a modularly multiplexable approach to detecting analyte localization in an antibody-antigen complex at the sensor surface.

c) Results:

The immunosensor allowed the rapid detection of MCP-1 in buffer and spiked human serum samples. A 2.5 order of magnitude linear range was observed, between 84.3 and 1582.1 pg/mL and the limits of blank and detection were 0.3 and 0.5 pg/mL, respectively. The platform's ability to analyze MCP-1 concentrations across a clinically-relevant concentration range was demonstrated.

d) Conclusions:

A silicon photonic immunosensor technology was applied to the detection of clinically-relevant concentrations of MCP-1. The performance of the sensor was robustly validated through a broad dynamic range and across a number of suggested clinical cut-off values. Importantly, the intrinsic scalability and rapidity of the technology makes it readily amenable to the simultaneous detection of multiplexed biomarker panels, which is particularly needed for the clinical realization of inflammatory diagnostics.

4.2 Introduction

Major advances in the field of biomolecular detection have recently led to improvements in the sensitivity and specificity achievable for the detection of a myriad of biomarker targets. Many of these technologies have been applied to clinical diagnostics, where the analysis of biomarker signatures can be utilized to identify and monitor a wide spectrum of human diseases and disorders (1-5). Due to their important roles in modulating the immune response and inflammation, cytokines are attracting increasing attention for clinical diagnostics (6-8). Cytokines, a broadly defined category of small (~5–20 kDa) proteins that include chemokines, interleukins, interferons, lymphokines, and tumor necrosis factors, regulate many types of cellular interactions in response to both self- and non-self antigens. Not surprisingly, alterations of cytokine levels can be diagnostic for a wide variety of maladies, including autoimmune disorders, cancer, and pathogenic infections. Importantly, the low basal concentrations and overlapping functions of cytokines, coupled with the acute nature of many inflammatory conditions conspire to demand high analytical specifications for cytokine-based clinical diagnostics. To fully realize the promise of cytokine-based diagnostics, new technologies that deliver robust and cost effective performance with high sensitivity (pg/mL), specificity, and rapid time-to-result are needed.

Of particular relevance to this manuscript is monocyte chemotactic protein 1 (MCP-1, also known as CCL2). MCP-1 is a low molecular weight (~13 kDa), 76-amino acid protein, that belongs to the CC chemokine family. MCP-1 is implicated in pathogeneses of several diseases such as ischemic cardiomyopathy (9), fibromyalgia syndrome (10), or systemic lupus erythematosus (11). It is also related to the rare neurological disorder Miller Fisher syndrome (12), and proposed as a biomarker for ovarian cancer (13). The concentrations of clinical interest of this cytokine vary considerably depending on its clinical application; however, studies have defined MCP-1 cut-off values of 130 pg/mL for fibromyalgia syndrome (10), 187 pg/mL in neonates with hypoxic-ischemic encephalopathy (14), and 718 pg/mL for prognosing ovarian cancer (13).

As an alternative to plate- and bead-based immunoassays, our group has investigated a silicon photonic microring resonator technology that leverages robust and cost effective semiconductor fabrication techniques to create a sensitive and modularly multiplexable

biomolecular detection platform. Microring resonators are chip-integrated optical microcavities that support the propagation of optical modes that are extremely sensitive to the local refractive index environment. Specifically, photons of a particular wavelength will only propagate in the microring under a tightly held resonance condition.

$$m\lambda = 2\pi r n_{eff} \quad (1)$$

In Equation 1, m is a non-zero integer, λ is the wavelength of light, r is the radius of the resonator, and n_{eff} is the effective refractive index sampled by the optical mode. Importantly, biomolecular binding events at the microring surface lead to a local change in refractive index, which in turn leads to a shift in the resonance wavelengths supported by the device. The shifts in particular resonance wavelengths can then be tracked for individual sensors and utilized to quantitate unknown amounts of biomolecular targets. Our group has previously demonstrated the applicability of this technology to detect a several different classes of biologically-relevant targets, including proteins, nucleic acids, viruses, and biotoxins (15-18). We have also demonstrated several different signal enhancement strategies on the silicon photonic platform (19-21) that deliver limits of detection comparable with many commercial immunoassays.

In this manuscript we describe the development of a robust and high-performing silicon photonic immunosensor for MCP-1. Using an enzymatically-enhanced, sandwich immunoassay, we were able to sensitively detect this representative cytokine at sub-pg/mL levels with a relatively rapid (71 min) time-to-result. We demonstrate the ability to quantitate MCP-1 over a 2.5 order of magnitude linear range in both buffer and human serum samples. We find minimal matrix effects when detecting in serum with full signal recovery achieved by a simple 10-fold dilution of the sample. Importantly, we demonstrate the ability to clearly detect MCP-1 concentrations at the previously defined, clinically-relevant cut-off values for the biomarker. The robust performance metrics of this technology, coupled with the capability to perform multiplexed detection, position this technology as an attractive platform for inflammatory cytokine-based clinical diagnostics.

4.3 Materials and methods

4.3.1 Instrumentation

Resonance wavelength shifts were monitored using the Maverick Detection System (Genalyte, Inc., San Diego, CA). The pH of all buffers and solutions were measured with an Orion 3-star benchtop pH meter (Thermo Scientific). Data analysis was performed using OriginPro 9.1.0 (OriginLab Corporation, Northampton, MA) and calibration curves were fit with a four-parameter logistic equation using GraphPad Prism 5 for Windows (GraphPad Software, San Diego, CA). Data presented corresponds to the average of at least 16 on-chip technical replicates per concentration of MCP-1.

4.3.2 Chemical and biochemical reagents

Dulbecco's phosphate buffered saline packets were purchased from Sigma-Aldrich (St. Louis, MO). 3-aminopropyltriethoxysilane (APTES) (cat. num. 80370), bis[sulfosuccinimidyl] suberate (BS3, cat. num. 21585), streptavidin-HRP conjugate (cat. num. 21130), 1-step 4-chloro-1-naphthol (4-CN) solution, and StartingBlock (PBS) blocking buffer (cat. num. 37538) were purchased from Thermo Scientific. DryCoat assay stabilization reagent was purchased from Virusys (cat. num. AG066-1) and glycerol (cat. num. BP229-1) from Fisher BioReagents. The capture antibody (anti-Human MCP-1 (CCL2), cat. num. 14-7099), detection antibody (biotinylated anti-MCP-1 (CCL2), cat. num. 13-7096), and the target analyte (recombinant human protein MCP-1 (CCL2), cat. num. 14-8398) were purchased from eBioscience (San Diego, CA). The non-specific adsorption control antibody (Mouse IgG, cat. num. ab37355) was purchased from Abcam (Cambridge, MA).

4.3.3 Buffers and solutions

PBS buffer (10 mM) was reconstituted from Dulbecco's phosphate buffered saline packets and the pH was adjusted to 7.4. The MCP-1 capture antibody was buffer exchanged to 10 mM PBS, followed by addition of glycerol to a final 5% (v/v) glycerol in PBS. The assay running buffer was 0.5% BSA in 10 mM PBS. All buffer solutions were prepared with purified water (ELGA PURELAB filtration system; Lane End, UK).

4.3.4 Human serum samples

Certified pooled normal human serum was obtained from Innovative research (Novi, MI). The test material was aliquotted upon receipt and stored at – 20°C until to use.

4.3.5 Silicon photonic microring resonators: Sensor substrates and read-out instrumentation

The Maverick M1 optical scanning instrumentation utilized to measure shifts in microring resonance wavelengths and sensor substrates were obtained from Genalyte, Inc. The fabrication of the sensor chip and scanning instrumentation operation used has been described previously (22, 23). The 4 mm x 6 mm silicon-on-insulator chips each contain 128 individually-addressable microrings. Four additional microrings rings in the fluidic channel, but covered by a fluoropolymer cladding layer, serve as controls to correct for thermal drift. An additional 4 exposed microrings (no cladding layer) lie outside the fluidic channel and serve as leak sensors.

Each individual microring is located next to an adjacent linear waveguide, such that interference between photons circulating the microring and passing down the linear waveguide create a resonant microcavity that supports optical modes only at specific wavelengths (23). The configuration of the fabricated chip allows for division of the 128 microrings in two fluidically-addressable flow channels, as defined a laser cut Mylar gasket that is sandwiched between the chip and Teflon lid. This fluidic design allows two unique samples to be assayed simultaneously.

To measure the resonance wavelength shift associated with the steps of the immunoassay, a tunable external cavity diode laser centered at 1550 nm serially probes each microring individually as a function of time. Resonances were determined as dips in the intensity of light propagating down the linear waveguide past the microring as the laser wavelength is scanned across a suitable spectral window. Relative shifts in resonance wavelength were recorded as a function of time during each of the immunoassay steps. The data acquisition software enables real-time control subtraction and averaging of active sensor responses.

4.3.6 Surface functionalization

Before functionalization, sensor chips were briefly rinsed with acetone to remove a protective photoresist coating. Sensor chips were immersed into a 5 % (v/v) solution of APTES

(2 mL in acetone, 4 min, with stirring) and then sequentially rinsed in acetone (2 min), isopropanol (2 min), and water. Silanized chips were gently dried under with N_2, reacted with a 5 mM solution of the BS3 crosslinker (20 µL, 2 mg in 700 µL 2 mM acetic acid) for 3 min, and again dried with N_2.

Solutions of capture and control antibodies (0.3 mg/mL, in 10 mM PBS with 5% glycerol) were immobilized onto specific regions in both channels of the chip via microspotting (0.2 µL per drop). Antibody solutions were reacted for 1 h at RT. The chips were then immersed in the blocking solution (600 µL, StartingBlock) for 1 h at RT. After blocking, the chips were dip-coated with DryCoat (600 µL; 30 dips). After this procedure, the chips were stored in a desiccator at 4°C until use.

4.3.7 Immunosensor measurement procedure

Before each measurement, the chips were loaded into a base cartridge holder and then sandwiched between a 0.007" laser cut Mylar gasket, and a Teflon cartridge top. Solutions were delivered to the cartridge assembly via a 0.01" ID Teflon tubing screwed directly into the cartridge top. The reagents in the assay were diluted in degassed running buffer, and loaded into a 96-well plate.

The Maverick system control software enables fully programmable reagent delivery. For all steps in the assay, the flow rate was 30 µL/min. Before starting the scan, the flow across the system was checked by a pre-buffer rinse step (< 4 min, running buffer). Solutions were flowed across both channels of the chip in the following order: 1) running buffer (2 min); 2) sample (20 min); 3) running buffer (2 min); 4) biotinylated detection antibody (10 min, 4 µg/mL); 5) running buffer (2 min); 6) streptavidin-HRP conjugate (10 min, 4 µg/mL); 7) running buffer (3 min); 8) 4-CN (15 min, 4 µg/mL); 9) running buffer (7 min). The total assay time was 71 minutes.

4.3.8 Data analysis and processing

The resonance wavelength shifts, related to the MCP-1 concentration, were calculated using the OriginPro 9.1.0 software, after subtracting responses from thermal and leak rings. Standard curves were constructed using GraphPad Prism 5 for Windows by plotting the resonance shift as a function of MCP-1 concentration and fitting to a logistic four-parameter equation:

$$Y = (A - B) / [1 + (x/C)^D] + B$$

where A is the shift measured for the highest concentration of target, B is the shift measured for the lowest concentration of target, C is the concentration producing 50% of the maximum response, and D is the slope at the inflection point of the sigmoid curve. The limit of blank (LoB) was estimated as the concentration providing the average of the blank plus 3 time the standard deviation of the blank. The limit of detection (LoD) was defined as the lowest value that has a 95% confidence to exceed the LoB (24). Thus, the LoD was estimated as:

$$LoB + (c_\beta \, x \, SD_S)$$

where SD_S is the analytical standard deviation of a sample with the lowest measured concentration (0.2 pg/mL), and c_β is the standard normal deviate (approximately 1.65). The working range was determined to be in the interval between 20% and 80% of the A value.

4.4 Results

The objective of this work was to robustly validate the ability of the silicon photonic microring resonator platform to measure MCP-1 in buffer and human serum samples, and to establish quantitative detection metrics. The sensor array was first created by covalently immobilizing capture and control antibodies onto discrete sensor elements (Figure. 4.1a). Chips were assembled into a fluidic cartridge (Figure. 4.1b) and loaded into the Maverick detection system for analysis.

A pair of commercial antibodies against MCP-1 (capture and detection) was identified and utilized in a sandwich immunoassay, each step of which was monitored in real time using the silicon photonic detection platform (Figure. 4.1c). After functionalization and establishing baseline in running buffer (t = 0 min, and between subsequent reagent steps throughout assay), standard solutions of MCP-1 (between 0 and 50000 pg/mL, prepared in running buffer) were flowed across the chip surface (t = 2 min). Biotinylated detection antibodies were then introduced (t = 24 min), followed by a streptavidin−HRP conjugate (t = 36 min). The 4-CN solution was then introduced (t = 49 min) and the catalytic conversion of 4-CN to the insoluble 4-CNP was measured by subtracting the net resonance wavelength shift from running buffer steps immediately before and after the 4-CN/4-CNP step. The magnitude of resonance

wavelength shift from the 4-CNP step was related to the concentration of MCP-1 concentration in each standard solution.

The shift in resonance wavelength observed for different concentrations of MCP-1 is shown in Figure. 4.2a. This same data is plotted as a dose-response curve in Figure. 4.2b (for detailed values see Table 4.1), and from this data the LoB and LoD were determined to be 0.3 and 0.5 pg/mL, respectively, and the linear range of the assay was between 84 and 1582 pg/mL. Responses for microrings functionalized with a control antibody were negligible.

Turning to the analysis of human serum samples, the effects of the sample matrix on sensor response was determined. To accomplish this, pooled human serum samples were spiked with a high concentration of MCP-1 (10000 pg/mL). At this concentration the response is very near the saturated region of the calibration curve, meaning that any small amount of MCP-1 natively present in the human sample would not significantly change the sensor response. This allows for the direct observation of matrix effects. Figure. 4.2c shows the observed resonance wavelength shifts recorded under different dilutions of the spiked serum sample, when compared to equivalent concentrations measured in running buffer, after correction for dilution. A 1:1 dilution showed a ~15% reduction in response. A 1:5 dilution reduced this matrix effect and a 1:10 dilution showed full response recovery. Further dilution (1:20) did not improve the response recovery.

Working at this optimized 1:10 dilution, we analyzed human serum samples spiked with concentrations of MCP-1 surrounding clinically-established cut-off values associated with specific diseases/disorders. Specifically, cut-offs at 130 and 710 pg/mL have been established for fibromyalgia syndrome (10) and ovarian cancer (13), respectively. After 1:10 dilution, serum samples were spiked with 13, 30, 71.8 and 100 pg/mL of MCP-1. A non-spiked serum sample was used as reference. The measured resonance wavelength shifts for each of the spiked samples ($n \geq 23$ microring sensors for each sample) were interpolated to the buffer calibration curve, and the resulting MCP-1 concentrations determined are plotted in Figure. 4.3. The good agreement between the spiked values and those determined using the microring resonator technology is numerically illustrated in Table 4.2. Both of these representations illustrate that the microring immunosensor is capable robustly quantitating the concentration of MCP-1 in human serum

samples. This analysis also allowed determination of the concentration of MCP-1 natively present in the serum sample to be 56 ± 16 pg/mL.

4.5 Discussion

Silicon photonic microring resonators are an emerging optical sensing technology that is attractive for biomolecular diagnostic applications. This refractive-index sensitive technology can be operated in a label-free mode wherein the biomolecular target of interest does not have to be covalently modified with any chromogenic, fluorescent, or enzymatic tag. However, the use of multiple, high affinity, target-specific recognition elements (i.e. monoclonal antibodies) allows this technology to be deployed for the quantification of disease-relevant biomarkers within clinically-relevant matrices. In this manuscript, we utilize arrays of silicon photonic microring resonators in a sandwich immunoassay format for the detection of MCP-1, an inflammatory cytokine associated with a number of clinically-relevant diseases/disorders, robustly validate the sensor performance, and demonstrate many important analytical parameters.

The natively passivated silicon oxide present on the resonators makes it amenable to standard silane chemistries and bioconjugate techniques, analogous to those used in many conventional microrarrays. The sensors were first covalently modified with a monoclonal antibody specific for MCP-1. Importantly, the small size of the sensor minimizes reagent consumption such that < 1 μL (0.3 mg/mL) was needed to achieve a large number (n ≥ 23) of technical replicates on a single chip. After functionalization, MCP-1 standards or human serum samples were flowed across the antibody-functionalized sensor array. To ensure assay specificity within complex matrices, a biotinylated, monoclonal anti-MCP-1 monoclonal antibody targeting a different epitope was introduced as a tracer antibody. Though the resonance wavelength shift accompanying the binding of the tracer antibody is observable above the noise baseline at many concentrations, the signal can be greatly increased through an enzymatic enhancement step. Specifically, a streptavidin-HRP conjugate that recognizes the surface-localized, biotinylated tracer antibody is introduced. This enzyme can then catalytically convert a soluble 4-CN reagent into an insoluble 4-CNP product that is physically deposited on the microring surface (21), with the amount of precipitate

For the detection of MCP-1 on the silicon photonic microring resonator platform, the entire sandwich immunoassay took a total of 71 minutes and each step was monitored in real-time, as shown in Figure. 4.1c and Figure. 4.2a. By comparison, commercially available ELISA kits do not allow real-time visualization of each step and typically require much longer assays (R&D systems, 3.5 or 4.5 h (25); Thermo Scientific, 3h (26). The ability to watch each assay step in real time permits the observation of gross failures that might otherwise not be revealed until the final stage of assay read-out. The resonance wavelength shift from this final enzymatic enhancement step is measured and utilized to generate a standard curve and quantitate unknown levels of MCP-1 (Figure. 4.2b). Statistical analysis of the standard curve yielded LoD and LoB values of 0.5 and 0.3 pg/mL, respectively, and highlighted a broad 2.5-order of magnitude dynamic range up to ~1600 pg/mL (Table 4.1). Across this dynamic range, CVs were generally ≤ 10%. Importantly, these values compare well with both plate- and bead-based commercial assays for MCP-1,(25-27) which report sensitivities ranging from 0.47 - 10 pg/mL, similar working ranges, and CVs. Importantly, by requiring just over 1 h the microring immunosensor is considerably more rapid than these commercial immunoassays. Additionally, while not the focus of this report, antibodies specific for multiple targets can be simultaneously arrayed onto different microring sensor elements on a single chip allowing for high levels of multiplexing, similar to Luminex.(27) Therefore, the simultaneous quantitative analysis of multiple cytokine/chemokines should be readily achievable using the microring detection technology.

Essential to any clinically-relevant assay is the ability to assess and compensate for any matrix effects. To probe these effects, we spiked a known concentration of MCP-1 into human serum samples and found that only minor signal attenuation was observed (Figure. 4.2c) and that full response recovery could be achieved with only a 1:10 dilution of the serum samples into running buffer. Using this dilution, we then validated the ability to detect MCP-1 from within spiked serum at concentrations that corresponded to clinically-relevant cut-off values suggested for both fibromyalgia syndrome and ovarian cancer. The silicon photonic immunosensor was clearly able to distinguish baseline serum levels from these cut-off values with the measured shifts in resonance wavelength being quantitative through extrapolation to the standard calibration curve and with good response recovery through the linear working range (Table 4.2). Values for the lower spiked concentrations showed a reduced percent recovery; however, the absolute values are within 15 pg/mL of the spiked concentration.

Beyond the scope of this manuscript, it is worthwhile to mention that the current generation sensor chip has the capacity to be functionalized with up to 32 target-specific capture antibodies, which in principle would allow for high levels of multiplexing. Coupled with the rapidity and robust analytical performance metrics, we feel that this silicon photonic detection platform could be a valuable tool for translational applications of multiplexed cytokine and other biomarker-based diagnostics.

4.6 Conclusions

A silicon photonic immunosensor technology was applied to the detection of clinically-relevant concentrations of MCP-1. The performance of the sensor was robustly validated through a broad dynamic range and across a number of suggested clinical cut-off values. Performance metrics were comparable to commercial ELISA assays for this biomarker; however, the silicon photonic immunoassay was considerably more rapid. Importantly, the intrinsic scalability of the technology makes it readily amenable to the simultaneous detection of multiplexed biomarker panels, which is particularly needed for the clinical realization of inflammatory marker-based diagnostics.

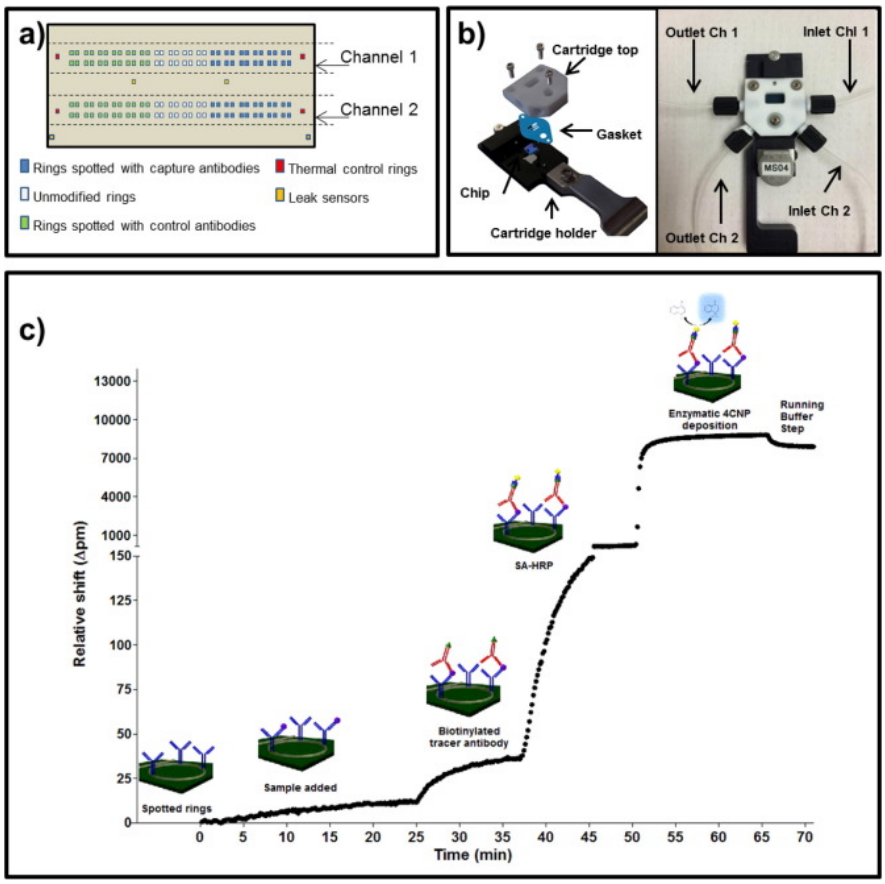

Figure 4.1 a) Schematic representation of the microring arrays on the sensor chip and the distribution of immobilized antibodies on chip. The antibodies were spotted in an identical formal over the two channels; b) Image of a chip assembled inside of the fluidic cartridge used; c) Overall strategy for the HRP-enhanced detection of MCP-1. MCP-1 concentration = 50000 pg/mL (buffer).

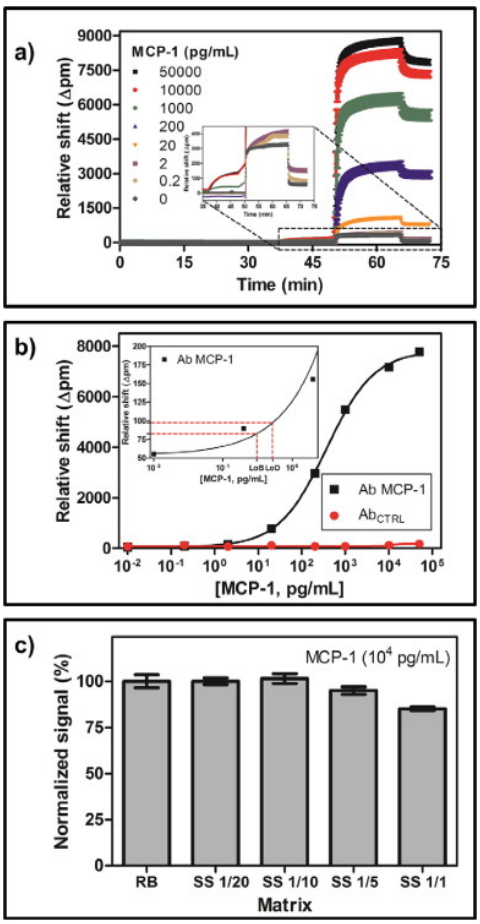

Figure 4.2 a) Data recorded with the developed immunosensor. MCP-1 standard solutions prepared in running buffer; b) Representative calibration curve (black curve, running buffer). See Table 4.1 for details. Each data point shown corresponds with the average of at least 23 replicates. The red curve corresponds to the signal of the control antibody; c) Matrix effect of pooled human serum.

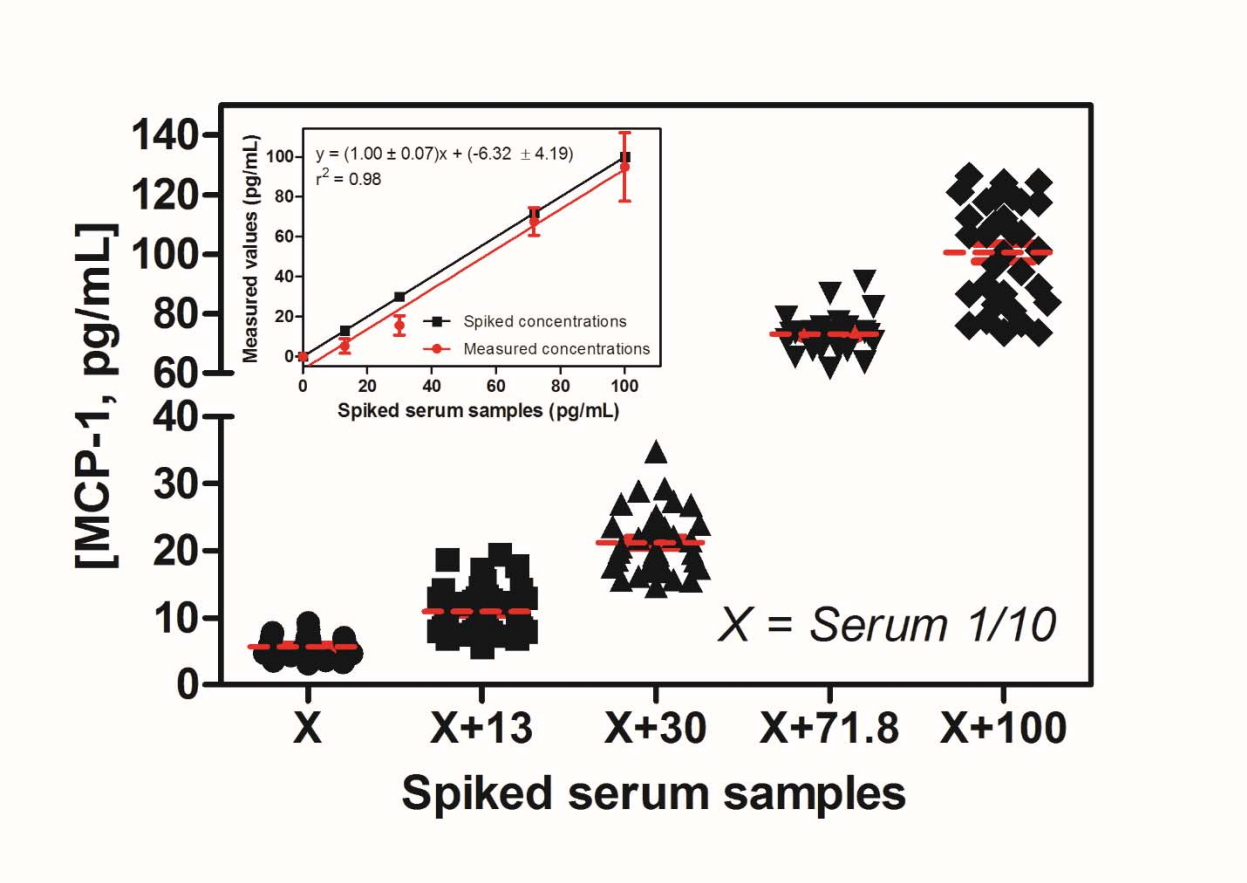

Figure 4.3 Concentrations around MCP-1 cut-offs values, 10-fold, were spiked (13, 30, 71.8 and 100 pg/mL) to the 10 times diluted serum samples. The signal obtained was converted to a MCP-1 concentration via the buffer calibration curve. Inset: correlation between the spiked samples and the measured values by the developed immunosensor. The error bars corresponded to the standard deviation of n≥23 replicated microring sensors measurements. The non-spike serum sample was used as reference.

	MCP-1 Immunosensor *
$Signal_{min}$	53.9 pm
$Signal_{max}$	7833 pm
Slope	0.79
LoB	0.3 pg/mL
LoD	0.5 pg/mL
Working range	84 – 1582 pg/mL
R^2	0.998

* S/N = 145. The standards were measured with the immunosensor following the procedure described in the experimental section. The parameters were extracted from the four-parameter equation used to fit the standard curve.

Table 4.1 Detailed values of the MCP-1 immunosensor calibration curve in running buffer

Human Serum Samples (1/10 dilution) *			
Spiked concentrations (pg/mL)	**Measured concentrations (pg/mL)**	**Recovery (%)**	**RSD (%)**
13	5 ± 4	41	28
30	16 ± 5	52	16
71.8	68 ± 7	94	10
100	91 ± 17	91	17

* The non-spike serum sample was used as reference.

The parameters were extracted from the four-parameter equation used to fit the standard curve.

Table 4.2 Analysis of spiked human serum samples using the MCP-1 immunosensor. The reported concentrations were calculated based on the average of interpolated concentrations from n≥23 replicated measured microring response based on the calibration curve of the assay, along with the associated standard deviation of each interpolated concentration.

4.7 References

1. Liotta L, Petricoin E. Molecular profiling of human cancer. Nature Reviews Genetics 2000;1:48-56.
2. Zhang X, Li L, Wei D, Yap Y, Chen F. Moving cancer diagnostics from bench to bedside. Trends in Biotechnology 2007;25:166-73.
3. Tothill IE. Biosensors for cancer markers diagnosis. Seminars in Cell & Developmental Biology 2009;20:55-62.
4. Teles FSRR. Biosensors and rapid diagnostic tests on the frontier between analytical and clinical chemistry for biomolecular diagnosis of dengue disease: A review. Analytica Chimica Acta 2011;687:28-42.
5. McNerney R, Daley P. Towards a point-of-care test for active tuberculosis: Obstacles and opportunities. Nature Reviews Microbiology 2011;9:204-13.
6. Kajikawa O, Goodman RB, II MCJ, Kiyoshi K, Martin TR. Sensitive and specific immunoassays to detect rabbit il-8 and mcp-1: Cytokines that mediate leukocyte recruitment to the lungs. Journal of Immunological Methods 1996;197:19-29.
7. Freer G, Rindi L. Intracellular cytokine detection by fluorescence-activated flow cytometry: Basic principles and recent advances. Methods 2013;61:30–8.
8. Jager Wd, Velthuis Ht, Prakken BJ, Kuis W, Rijkers GT. Simultaneous detection of 15 human cytokines in a single sample of stimulated peripheral blood mononuclear cells. Clinical and Diagnostoc Laboratory Immunology 2003;10:133-9.
9. Frangogiannis NG, Dewald O, Xia Y, Ren G, Haudek S, Leucker T, et al. Critical role of monocyte chemoattractant protein-1/cc chemokine ligand 2 in the pathogenesis of ischemic cardiomyopathy. Circulation 2007;115:584-92.
10. Blanco I, Janciauskiene S, Nita I, Fernández-Bustillo E, Cárcaba V, Gallo C, et al. Low plasma levels of monocyte chemoattractant protein-1 (mcp-1), tumor necrosis factor-alpha (tnfα), and vascular endothelial growth factor (vegf) in patients with alpha1-antitrypsin deficiency-related fibromyalgia. Clinical Rheumatology 2010;29:189–97.
11. Barbado J, Martin D, Vega L, Almansa R, Gonçalves L, Nocito M, et al. Mcp-1 in urine as biomarker of disease activity in systemic lupus erythematosus. Cytokine 2012;60:583-6.
12. Sato S, Suzuki K, Nagao R, Kashiwagi Y, Kawashima H, Tsuyuki K, Hoshika A. Detection of mcp-1 and il-8 in the serum and cerebrospinal fluid of a child with miller fisher syndrome. Journal of Clinical Neuroscience 2009;16:1698–9.
13. Hefler L, Tempfer C, Heinze G, Mayerhofer K, Breitenecker G, Leodolter S, et al. Monocyte chemoattractant protein-1 serum levels in ovarian cancer patients. British Journal of Cancer 1999;81:855–9.
14. Jenkins DD, Rollins LG, Perkel JK, Wagner CL, Katikaneni LP, Bass WT, et al. Serum cytokines in a clinical trial of hypothermia for neonatal hypoxic-ischemi c encephalopathy. Journal of Cerebral Blood Flow & Metabolism 2012;32:1888–96.
15. Washburn AL, Luchansky MS, Bowman AL, Bailey RC. Quantitative, label-free detection of five protein biomarkers using multiplexed arrays of silicon photonic microring resonators. Analytical Chemistry 2010;82:69-72.
16. Qavi AJ, Bailey RC. Multiplexed detection and label-free quantitation of micrornas using arrays of silicon photonic microring resonators. Angewandte Chemie International Edition 2010;49:4608-11.

17. McClellan MS, Domier LL, Bailey RC. Label-free virus detection using silicon photonic microring resonators. Biosensors and Bioelectronics 2012;31:388–92.
18. Shia WW, Bailey RC. Single domain antibodies for the detection of ricin using silicon photonic microring resonator arrays. Analytical Chemistry 2013;85:805-10.
19. Luchansky MS, Bailey RC. Silicon photonic microring resonators for quantitative cytokine detection and t-cell secretion analysis. Analytical Chemistry 2010;82:1975-81.
20. Luchansky MS, Washburn AL, McClellan MS, Bailey RC. Sensitive on-chip detection of a protein biomarker in human serum and plasma over an extended dynamic range using silicon photonic microring resonators and sub-micron beads. Lab on a Chip 2011;11:2042-4.
21. Kindt JT, Luchansky MS, Qavi AJ, Lee S-H, Bailey RC. Subpicogram per milliliter detection of interleukins using silicon photonic microring resonators and an enzymatic signal enhancement strategy. Analytical Chemistry 2013;85:10653−7.
22. Iqbal M, Gleeson MA, Bradley Spaugh, Tybor F, Gunn WG, Hochberg M, et al. Label-free biosensor arrays based on silicon ring resonators and high-speed optical scanning instrumentation. IEEE J Sel Topics Quantum Electron 2010;16:654-61.
23. Washburn AL, Gunn LC, Bailey RC. Label-free quantitation of a cancer biomarker in complex media using silicon photonic microring resonators. Analytical Chemistry 2009;81:9499–506.
24. Linnet K, Kondratovich M. Partly nonparametric approach for determining the limit of detection. Clinical Chemistry 2004;50:732–40.
25. R&Dsystems. Human ccl2/mcp-1 quantikine elisa kit. http://www.rndsystems.com/Products/dcp00 (Accessed August 01, 2015).
26. ThermoScientific. Human mcp-1 elisa kits. http://www.piercenet.com/product/human-mcp-1-elisa-kits (Accessed August 01, 2015).
27. R&Dsystems. Luminex performance human cytokine panel a. http://www.rndsystems.com/Products/luh000/ (Accessed August 01, 2015).

Chapter 5:

A Silicon Photonic Immunoassay for Cardiac Troponin I using a Microring Resonator Biosensing Platform

Acknowledgments

This chapter is adapted from "A Silicon Photonic Immunoassay for Cardiac Troponin I using a Microring Resonator Biosensing Platform" (Shia, W. W., Valera, E., Jaffe, A. S., Bailey, R. C. Submitted, **2016**).

Dr. Enrique Valera is acknowledged for his assistance in data collection of some of the serum samples, and Dr. Allan Jaffe is acknowledged for provision of patient samples from Mayo Clinic. Prof. Ryan Bailey is acknowledged for initiating this project.

This research was supported by the National Science Foundation Grant Awards CHE-12-14081 and CHE15-08656. WWS was supported by American Heart Association Predoctoral Fellowship. The authors also gratefully acknowledge Stacy Hartman for evaluating troponin ITC standards and patient samples on the Siemens ADVIA Centaur XP-TnI assay system.

5.1 Abstract

Cardiac troponins are highly selective markers for myocardial injury and therefore troponin assays hold potential for monitoring a broad spectrum of cardiovascular disorders, allowing timely intervention to improve patient outcome. Currently, there is a need for simultaneously rapid and sensitive troponin assays that could be used in in emergency care settings. An automated 54 minute cardiac troponin I (cTnI) sandwich immunoassay was developed on a microring resonator analysis platform. Serum matrix effects were evaluated for influences on assay sensitivity and selectivity. After assay optimization, cTnI levels from 11 cardiac disease patient serum samples were quantified and showed good correlation with values obtained using the Siemens ADVIA Centaur XP-TnI platform. This work describes initial efforts to apply a novel and highly automated silicon photonic detection technology to the detection of cardiac troponin. While further assay optimization will be required to lower the limit of detection, the good quantitative correlation with a standard laboratory-based assay demonstrates the potential of microring resonators for the measurement of clinically-relevant biomarkers.

5.2 Introduction

Cardiovascular diseases (CVDs) are the leading cause of death globally, claiming an estimated 17.5 million lives in 2012.(1) Reliable biomarkers that can differentially diagnose between acute and chronic cardiovascular diseases offer a powerful opportunity to make timely diagnoses and implement the most effective personalized treatments. Among the numerous biomarkers proposed for CVDs, cardiac troponins, and specifically the subunits I (cTnI) and T (cTnT), have nearly perfect specificity for myocardial injury. They also remain elevated in the blood stream for a longer time period compared with other cardiac biomarkers and are considered as gold standard markers to diagnose acute myocardial infarction (AMI).(2-4) Elevation of troponins levels continues to increase within an hour after the onset of cardiac injury, reaching peak levels (~100 ng/ml) at 16-32 hrs before degrading over the next 5-7 days.(5, 6) Technologies amenable to early and longitudinal monitoring of troponin levels would be a powerful tool in assessing patient status during acute cardiovascular events.

There currently is an unmet need for simultaneously rapid and highly sensitive troponin assays. Laboratory-based troponin assays have exceptional detection limits but have relatively long assay times that include transport to a central lab facility, whereas point-of-care assays can be conducted rapidly in emergency room settings but lack the analytical performance to monitor low enough levels to be clinically actionable on their own.(7-9)

Silicon photonic microring resonators are an emerging biomolecular detection technology that features attributes that may be useful for the detection of cardiac troponins. Specifically, relatively rapid and highly automated assays have been reported with limits of detection that reach levels of clinical utility.(10-13) Moreover, the robust fabrication of these silicon microdevices and integration with microfluidic fluid handling are well-suited for detection at the point-of-care. We have previously described the basic operation of these devices, as well as instrumentation developed to rapidly perform these measurements.(14, 15) Applied to biomarkers of potential clinical interest, we have demonstrated the ability to detect a number of inflammatory biomarkers, including C-reactive protein and cytokines,(10-12) as well as perform a multiplexed assay for phosphoproteins from tumor homogenate.(13) The detection of C-reactive protein is notable in the context of cardiovascular function as it has been speculated to play both and problematic roles in cardiovascular function, depending on the underlying pathophysiology.(16)

Herein, we report the application of this silicon photonic detection platform to cardiac troponin I. An antibody-based sandwich assay was developed and utilized for replicated analysis of 11 patient serum samples, with determined levels correlating well with those obtained using the commercial Siemens ADVIA Centaur XP-TnI system. While many improvements are still needed, this demonstration helps illustrate the future potential for this technology in the portfolio of clinical diagnostic tools.

5.3 Materials and methods

5.3.1 Reagents and buffers

Zeba Spin desalting columns (Cat. 89882), EZ-link NHS-PEG$_4$-Biotin (Cat.21329), 3-aminopropyltriethoxysilane (APTES, Cat. 80370), bis(sulfosuccinimidyl)suberate (BS3, Cat. 21585), 1-step chloronaphthol solution (1-step CN, Cat. 34012), StartingBlock blocking buffer

(Cat. 37538), glycerol (Cat. BP2291) and high sensitivity streptavidin-horseradish peroxidase conjugate (SA-HRP, Cat. 21130) were purchased from Thermo Fisher Scientific (Rockford, IL). DryCoat assay stabilizer (Cat. AG066-1) was from Virusys (Taneytown, MD). Nunc Maxisorp flat-bottom 96 well plates were purchased from eBioscience (San Diego, CA). Mouse IgG isotype control antibody (Cat. Ab37355) was purchased from Abcam (Cambridge, MA). Pooled normal human serum (Cat. IPLA-SER) was purchased from Innovative Research (Novi, MI). Monoclonal mouse anti-cardiac troponin I capture (Clones: M18, 560) and tracer (Clones 19C7, MF4) antibodies 2(Cat. 4T21), and human cardiac troponin ITC complex (Cat. 8T62) were purchased from HyTest (Turku, Finland). All other reagents were purchased from Sigma-Aldrich (St. Louis, MO).

A 10 mM PBS buffer was prepared by dissolving Dulbecco's phosphate buffered saline powder to distilled water, adjusted to pH 7.4 and filtered. The assay running buffer was prepared by dissolving 0.5% (w/v) BSA into 10 mM PBS.

5.3.2 Patient samples

Serum samples from patients admitted with acute cardiovascular disease and elevated values of cardiac troponin T were previously obtained and stored at -80 °C at Mayo Clinic (Rochester, MN). These samples were collected under consent according to an IRB-approved protocol during standard clinical treatment at the Emergency Department at Mayo Clinic and supplied to researchers at the University of Illinois in a de-identified format.

5.3.3 Biotinylation of tracer antibodies

cTnI tracer antibodies (Clones 19C7 and MF4, specific to residues 41-49 and 190-196 respectively) were first buffer exchanged to PBS buffer to remove sodium azide. NHS-PEG_4-Biotin (20 mM) was then added to each antibody in 20× molar excess and allowed to react at room temperature for 30 min. Excess biotinylation reagent was removed by spin filtration. The two cTnI tracer antibodies were then combined and diluted to 2 μg/ml final concentration of each antibody.

5.3.4 Surface chemistry, and spotting of capture antibodies

Similar to the tracer antibodies, the mouse IgG control and cTnI capture antibodies (Clones M18 and 560, specific to residues 18-28 and 83-93 resprctively) were buffer exchanged to remove sodium azide. Glycerol was then added and antibodies diluted to a concentration of 1 mg/ml in 5% (v/v) glycerol. The capture antibodies were combined together with each antibody clone having a final concentration of 0.5 mg/ml in 5% (v/v) glycerol in preparation for spotting on the sensor chips surface.

Microring resonator sensor chips were cleaned in piranha solution (3:1 H_2SO_4/30% H_2O_2, 10 s), followed by generous rinsing in distilled water and dried under N_2 (*Caution! Piranha solutions are extremely dangerous and react explosively with organics.*). The chips were immersed in acetone (2 min), 5% (v/v) APTES (in acetone, 4 min), fresh acetone (2 min), isopropanol (2 min), and rinsed distilled water (2 min), with gentle swirling during each step. After drying under N_2, a 5 mM BS3 linkers (20 µL, dissolved in 2 mM acetic acid) was spotted on the silanized chip surface to react with the free amine groups for 3 min. The linker solution was then removed and the capture and control antibodies were manually spotted, and allowed to incubate for 1 h. Chips were then immersed for 1 h in StartingBlock before a final rinse in DryCoat solution. Spotted chips were stored in a desiccator at 4°C until use.

5.3.5 Silicon photonic microring resonators instrumentation

Microring resonator sensor chips and Maverick optical scanning instrument were designed in collaboration with and acquired from Genalyte (San Diego, CA), as has been previously described.(17) Briefly, silicon photonic microring resonators support optical resonances at discrete wavelengths as described by:

$$m\lambda = 2\pi r n_{eff}$$

where m is an integer, λ is the wavelength of light, r is the microring radius, and n_{eff} is the refractive index of the local ring environment. Microrings can be modified with target-specific capture agents (e.g. antibodies) and analyte binding events at the sensor surface cause a change in the local refractive index, which in turn leads to a shift in the resonance wavelength ($\Delta\lambda$), which is measured

in units of Δpicometers (Δpm). The latest chip design includes an increase to a total of 128 active microring sensors on a 4 × 6 mm chip footprint. The latest instrumentation also features complete automation of fluid handling, via robotic sipping form 96- or 384-well plates.

5.3.6 Chip loading and assay details

Sensor chips pre-immobilized with capture and control antibodies were placed on to an aluminum chip holder, aligned to a 2-channel Mylar fluidic gasket and sandwiched against a Teflon lid that allowed connection of inlet and outlet tubing to direct assay reagent flow over the two active channels on the chip, before loading into the Maverick M1 system. Separately, assay reagents were loaded into a 96-well plate, also placed within the instrument. The instrument was then programmed to record resonance wavelength shifts while running the following pre-defined assay steps when optimizing the assay in 0.5% BSA running buffer: (1) Running buffer (3 min). (2) Introduction of sample/ITC calibrator solutions (15 min, samples 50% diluted in running buffer). (3) Rinse with running buffer (1 min). (4) Introduction of biotinylated tracer antibodies (4 min, 2 μg/mL each of clones 19C7 and MF4). (5) Running buffer rinse (1 min). (6) Introduction of SA-HRP solution (4 min, 4 μg/mL). (7) Running buffer rinse (2 min). (8) Introduction of 1-step CN (9 min). (9) Final running buffer rinse (3 min). The flow rate for all assay steps was set at 30 μL/min, except for analyte introduction (2), which was at 10 μL/min. The total time for this assay in buffer was 42 min. Later on when the assay was further optimized to test serum matrices, the steps of introducing tracer antibodies and SA-HRP were both increased to 10 min, thus increasing the total assay time to 54 min. The 1-step CN solution contains a stabilized mixture of 4-chloro-1-naphthol and H_2O_2, which in the presence of HRP, is converted to 4-chloro-1-naphthon—a precipitate that deposits on the microring surface giving a large signal enhancement.

5.3.7 Normalization of assay response in patients' serum samples

In order to account for daily fluctuations in assay response, two samples of 50% diluted pooled serum, one spiked with 625 μg/L troponin ITC (highest concentration in the assay calibration curve in Figure 3), and the other remaining un-spiked (0 μg/L ITC), were also measured on the same day of patients' samples measurements. The measured response of these two samples were set to 100% and 0% of the calibration curve response respectively, and assay response from each patient sample was re-expressed as a percentage response of the calibration curve for

normalization across the different days of measurements. In general, these correction factors were extremely minor; however, included as a precaution.

5.3.8 Data analysis

The net shifts in resonance wavelength were determined only before and after the 1-step CN signal enhancement. This avoid recording signal from non-specific adsorption that occurs in the presence of complex sample matrices. Specifically, the resonance shift at 43 min (Prior to addition of 1-step CN) was subtracted from that at 54 min (during buffer rinse). This response difference was normalized using the thermal control rings to correct for fluctuations in temperature during the assay run. Calibration plots obtained from the net shifts values on the microrings, as well as interpolation of serum sample responses, were analyzed using both OriginPro software and GraphPad Prism 5. The calibration plot was fitted by the following dose response equation:

$$y = A1 + \frac{A2 - A1}{1 + 10^{(\log x0 - x)p}}$$

Where *A1* is the bottom asymptote, *A2* is the upper asymptote, *x0* is the concentration at half response (EC50), and *p* is the hill slope of the fitted plot. The limit of blank (LOB) for described assays was defined as the interpolated concentrations generated by the mean blank measurement signal plus 1.645 standard deviations (1.645σ) of that measurement, based on the CLSI recommendations reported by Linnet *et. al.*(18) Similarly, the limit of detection (LOD) was calculated as follows:

$$LOD = LOB + 1.645\sigma$$

The working range was determined to be the analyte concentrations that generate instrumental response in the interval between 20% and 80% (EC20 to EC80) of the A2 value, which corresponds to the linear range of the calibration curve.

5.4 Results

Anti-cTnI capture and mouse IgG control antibodies were spotted in an identical layout for both channels on the microring array sensor chips (Figure 5.1a) allowing for two samples to be tested simultaneously. For the quantitative detection of cTnI, an enzymatically-enhanced sandwich

immunoassay was utilized (Figure 5.1b), which was previously utilized on this platform to achieve LODs for interleukins IL-2, IL-6, and IL-8 at and below the pg/mL level.(19) Standard solutions or patient samples flowed across the array allowing the binding of cTnI to the target-specific capture agents. Biotinylated anti-cTnI tracer antibodies were then flowed across the array, specifically binding to the analyte captured by the primary antibodies. Streptavidin-HRP conjugate was then introduced followed by the enzymatic enhancement using the 1-step CN reagent. The cTnI assay was optimized by spiking various concentrations of human troponin ITC complex into running buffer and observing the real-time shifts in resonance wavelength during the assay steps (Figure 5.2a). The resulting resonance shifts measured from the CN enhancement step (between 29 min and 40 min of the assay) were recorded and plotted as a function of cTnI concentration to obtain a calibration curve (Figure 5.2b). Responses were also recorded from IgG isotype control sensors, revealing minimal non-specific binding response. Table 5.1 summarizes the key analytical parameters, including a LOB and LOD for the assay in buffer of 0.010 ng/ml and 0.015 ng/ml, respectively, and working range of 0.5-9.4 ng/ml.

Moving to analyses in serum, the troponin ITC standard was spiked into 50% and 33% diluted serum. An initial analysis at 125 ng/ml of troponin ITC in these two matrices, compared to the assay performed in running buffer, showed a response reduction of ~1000 pm (Figure 5.3 Inset). This matrix effect was not reduced with further dilution and therefore 50% diluted serum was selected for further assay evaluation. Using diluted serum samples spiked with a range of troponin concentrations, a calibration curve was constructed (Figure 5.3). Table 5.2 summarizes key analytical parameters for the assay performed in 50% diluted serum, including a LOB and LOD of 0.001 ng/ml and 0.003 ng/ml, respectively, and working range of 1.9-179.5 ng/ml.

This sandwich immunoassay on the silicon photonic platform was then applied to the measurement of troponin levels from 11 patient samples (Patients A-K). Each blinded serum sample was diluted 50% prior to measurement and the resulting resonance shifts converted to a troponin concentration using the serum calibration described above. Since these measurements were performed on different days from the calibration curve, daily fluctuations in assay response were normalized as described in the Materials and Methods section. Eight of the samples had detectable troponin levels, while three yielded responses lower than the LOD of the assay. For comparison with a validated clinical assay, the same patient samples were also evaluated using the

Siemens ADVIA Centaur XP-TnI assay at Mayo Clinic. However, troponin concentrations from the Siemens assay gave consistently higher values compared with those obtained from the microring assay (Figure 5.4a). Interestingly, plotting the Siemens versus microring troponin levels (Figure 5.4b) showed a strong correlation (R^2=0.952) with a positive slope (m=3.40), which suggested a possible discrepancy between the calibrators used in the two assays. A series of troponin ITC standards used for the microring calibration were prepared in 50% serum and submitted for analysis on the Siemens assay platform and similar correlation was observed (Figure 5.5; R^2=0.995, m=3.16). Given the apparent inconsistency between the as prepared troponin standard values and the Siemens results, the microring resonator serum calibration curve was replotted using the Siemens cTnI concentrations as x-axis values. Using this corrected microring calibration, serum troponin values were re-evaluated and found to be in good agreement with those measured on the Siemens platform (Figure 5.6). Additionally, the three serum samples with undetectable troponin levels on the microring array platform (Patients I-K) were found via Siemens to have cTnI values ≤1 ng/ml. Considering this and the lowest quantitated patient sample (Patient H), the lowest detectable concentration for the microring assay was empirically estimated to be 2 ng/ml.

5.5 Discussion

The goal of this work was to develop a silicon photonic immunosensor for cardiac troponin using a recently developed microring resonator detection technology. This technology is attractive on account of its relatively rapid and cost effective analytical capabilities. As a target for assay development and validation, we utilized a commercially available troponin ITC complex, rather than the cTnI subunit alone. Importantly, the selection of standard calibrator materials and the impact on assay performance has been a point of considerable discussion.(20, 21) With consideration of literature precedent, the HyTest ITC standard was selected as it demonstrated consistent analytic response.(21-23) Capture and detection antibodies were also selected to target epitopes at the stable midfragment region and terminal ends of the cTnI subunit, in hopes to reduce interferences from troponin autoantibodies.(24, 25)

The immunoassay was developed first in buffer (Figure 5.2) and then in 50% diluted serum (Figure 5.3). When evaluating patient samples and comparing the microring immunoassay against

the Siemens ADVIA Centaur XP-TnI platform, the measured troponin values were correlated, but offset a factor of ~3.4, with the Siemens values being uniformly higher (Figure 5.4). Concerned that differences in the calibration standard might explain this discrepancy, a series of HyTest ITC complex standards used for microring measurements was analyzed on the Siemens platform and found to again give values ~3.2 times larger than the as prepared ITC concentrations (Figure 5.5). Having confirmed that the assay discrepancies could be corrected taking into account the offset in measured versus as prepared calibrator concentrations, the microring calibration curve was corrected and replotted using the Siemens cTnI values as the standard concentrations on the x-axis. Re-evaluating the patient samples with the corrected microring calibration curve, good agreement was found between the silicon photonic and Siemens measurement platforms (Figure 5.6). Notably, microring resonator measurements utilized an array of sensors that offered at least 10 technical replicates per analysis, allowing confidence intervals to be determined on the basis of technical assay variation. Historically, cTnI assays have been plagued by high assay-to-assay variation (21, 23, 26, 27), and therefore the correlation for this first generation silicon photonic assay with the Siemens platform is encouraging.

A sandwich immunoassay was developed and applied to the detection of troponin in patient serum samples, showing reasonably good correlation with an established clinical assay after calibrator normalization. While improvements remain to be achieved for the detection of cTnI on the silicon photonic platform—most notably in a need for a lower limit of detection—this initial demonstration is promising. Two potential routes to lower limits of detection include the selection of higher affinity capture agents and the integration of an on-chip sample pre-concentration module. This assay adheres within the ACC/AHA target of <1 hr,(28) with added advantage in the ability to perform multiplexed measurements.(11, 13, 29, 30) In this report, the array of microrings was functionalized only with anti-cTnI and isotype control antibodies; however, this array could also be functionalized with antibodies against specific troponin degradation products or phosphorylated epitopes in order to provide a more comprehensive analysis of circulating troponins that might correlate with unique cardio pathophysiologies and emerge as a powerful diagnostic tool to guide clinical intervention.(31-35)

5.6 Disclosures/Conflict of interest

RCB is a co-founder of Genalyte, Inc. and has a financial interest in the company. ASJ consults for or has consulted for most of the major diagnostic companies.

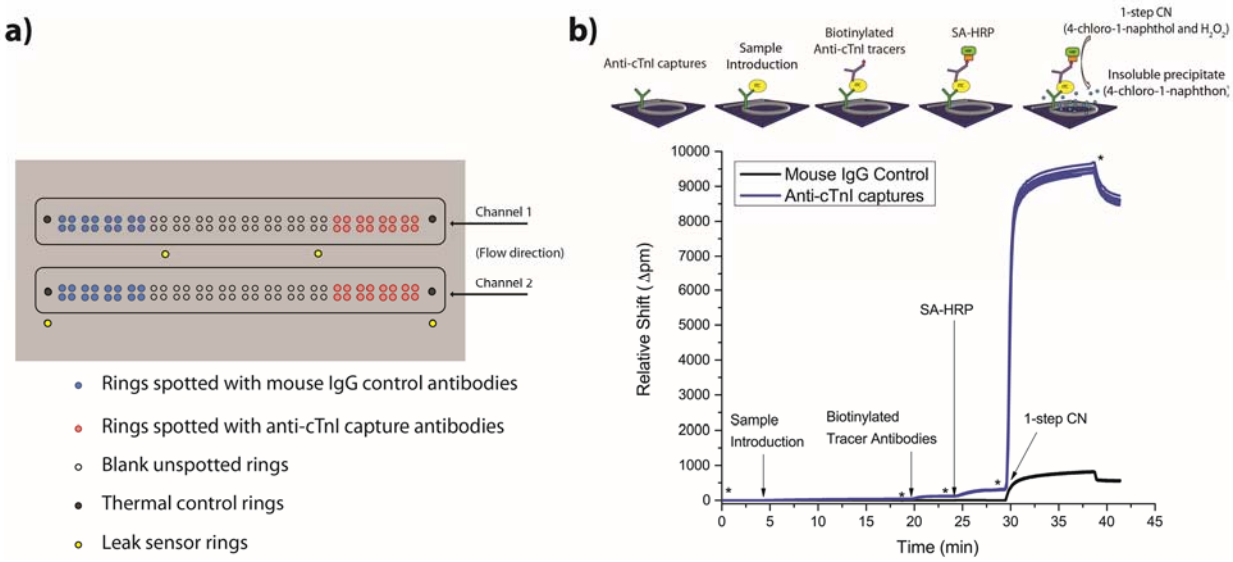

Figure 5.1 a) Layout of the microring arrays sensor chip indicating the position of antibodies spotted on microrings as well as thermal control rings and leak sensors. The chip is separated into two independent channels allowing analysis of two samples in parallel. **b)** Representative resonance shift from an enzymatically-enhanced sandwich assay detecting a 125 ng/ml ITC standard solution, starting from sample introduction at 3 min, addition of biotinylated tracer antibodies at 19 min, following by addition of SA-HRP at 24 min, and finally 1-step CN introduction at 29 min, with buffer rinse steps in between.

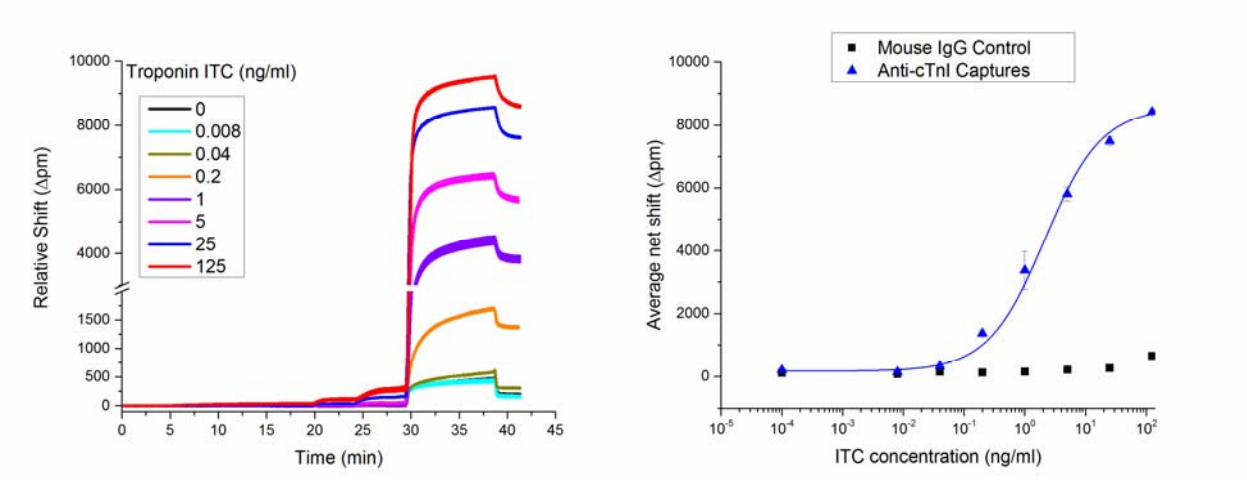

Figure 5.2 a) Instrumental response of various troponin ITC concentrations spiked in running buffer. The amplified signal upon addition of 1-step CN at 30 min can be clearly observed **b)** Corresponding calibration curve obtained based on fitting data points from net shift between 29-40 min of the assay. Error bars were calculated based on the standard deviation of n=16 replicated microring measurements.

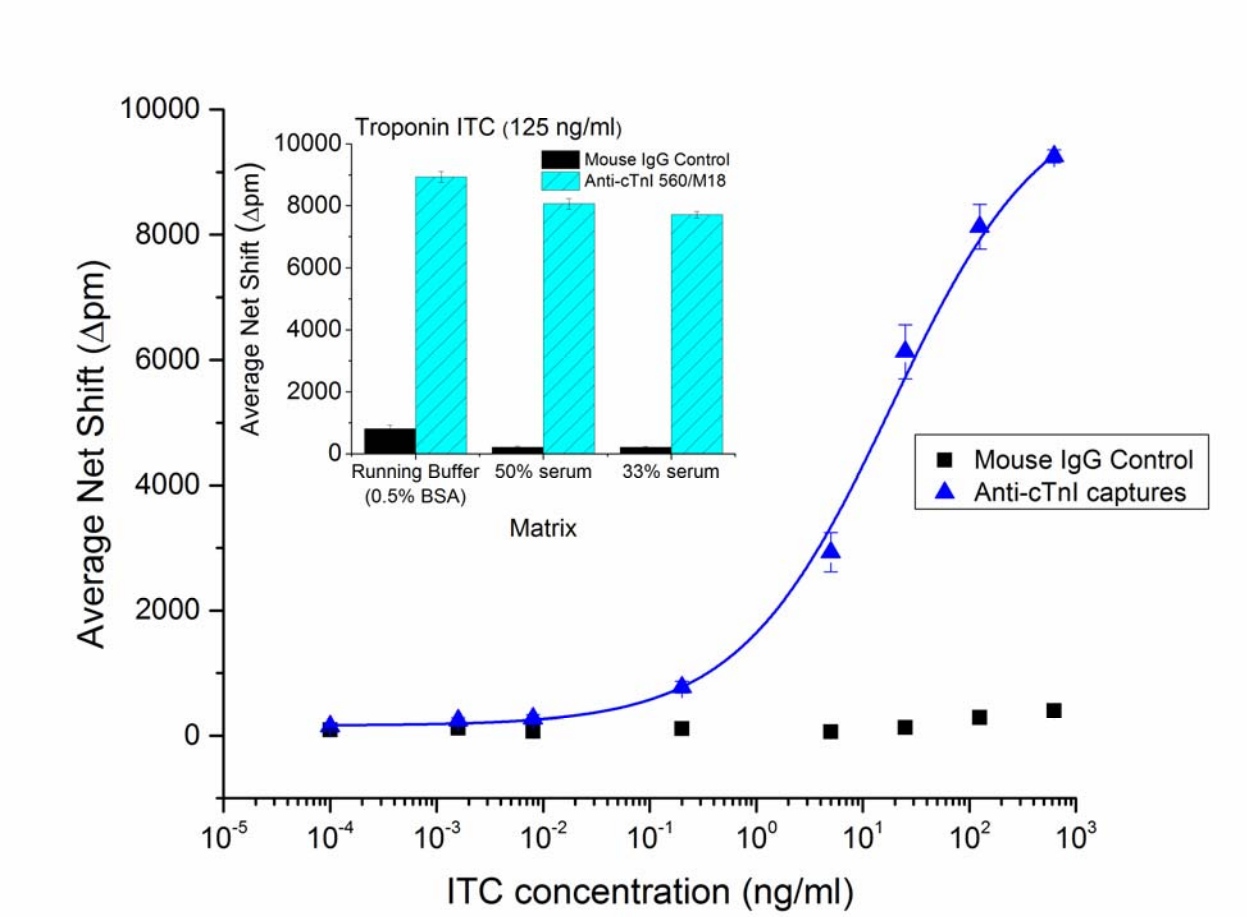

Figure 5.3 Calibration curve of troponin ITC concentrations spiked in 50% diluted serum. The inset graph illustrated serum matrix effects on the microring arrays assay, where a small amount of serum presented in the matrix can decrease the assay signal slightly. Error bars were calculated based on the standard deviation of n=16 replicated microring measurements.

a)

Patient Sample	Microring Array Platform (ng/ml)			Siemens ADVIA Centaur XP-TnI Platform (ng/ml)*
	Upper (95% CI)*	Lower (95% CI)*	Average*	
A	0.943	0.641	0.788	3.5
B	1.140	0.583	0.849	8.0
C	8.737	4.639	6.506	22.9
D	5.907	3.965	4.887	14.3
E	4.666	3.150	3.874	7.47
F	10.088	3.966	6.628	19.9
G	18.363	10.068	13.742	49.5
H	0.653	0.156	0.384	2.0
I	n/a	n/a	n/a	1.09
J	n/a	n/a	n/a	0.93
K	n/a	n/a	n/a	1.11

*Upper (95% CI) and Lower (95% CI): Upper and lower concentration ranges at 95% confidence interval. According to manufacturer information, the Siemens platform reports a 99th percentile concentration for a normal reference population as 0.04 ng/ml, and an imprecision of 0.03 ng/ml at 10% CV.

b)

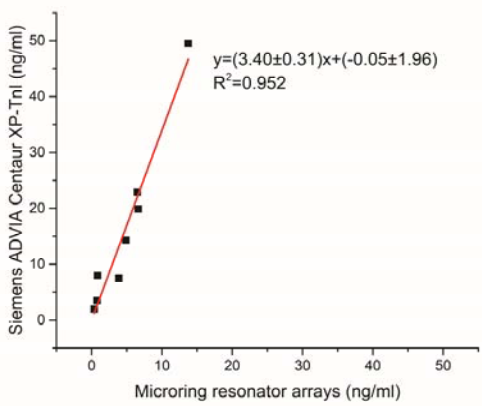

Figure 5.4 a) Table listing cTnI concentrations (ng/ml) for serum samples from Patients A-K, measured by the microring arrays platform (n≥10 replicates) compared to the Siemens ADVIA Centaur XP-TnI platform (n=1). **b)** Plot of the cTnI levels of the patient samples measure by the Siemens platform (y-axis) versus the microring arrays platform (x-axis), suggesting a correlation between the measurements and a discrepancy in the troponin ITC standard used for calibration.

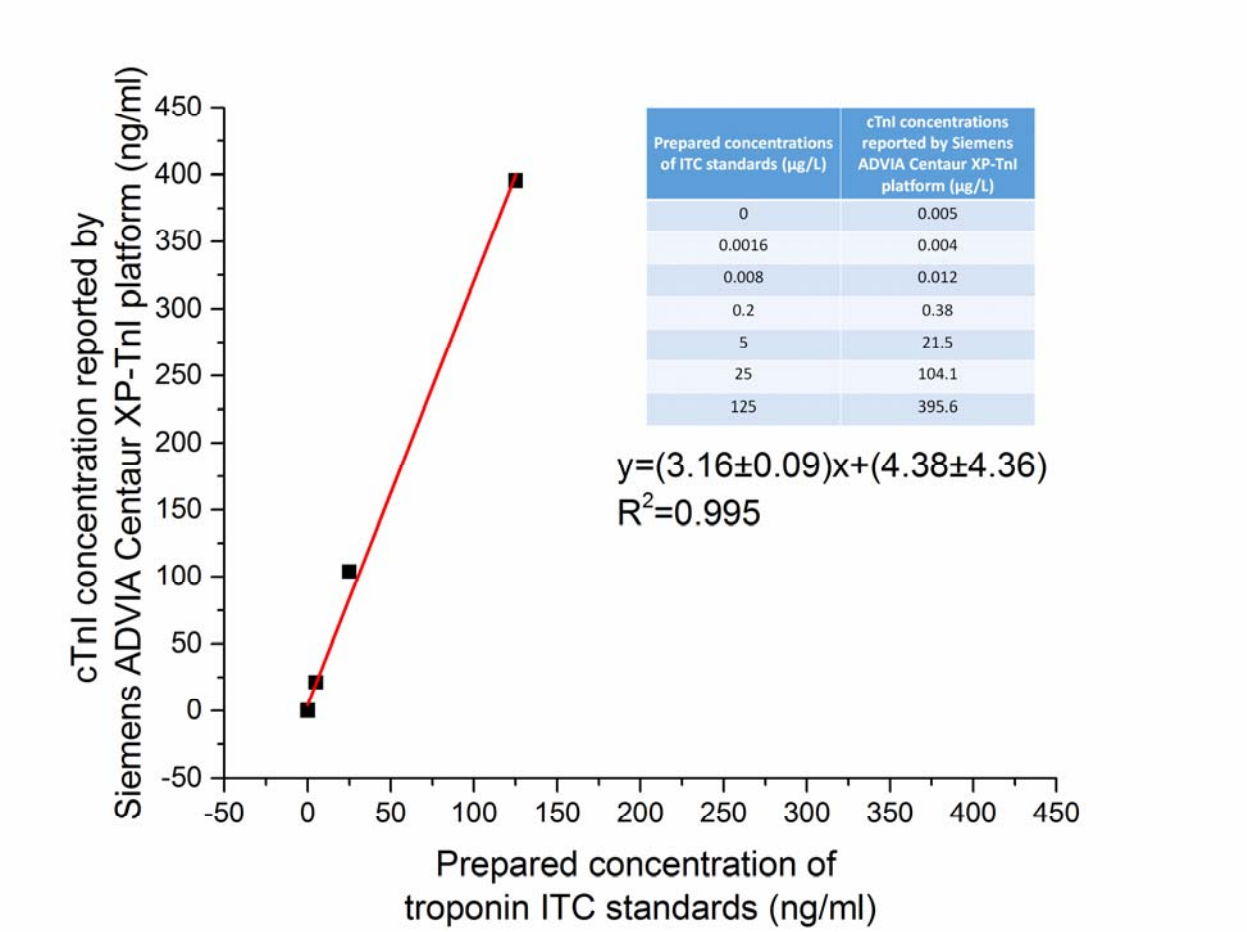

Prepared concentrations of ITC standards (µg/L)	cTnI concentrations reported by Siemens ADVIA Centaur XP-TnI platform (µg/L)
0	0.005
0.0016	0.004
0.008	0.012
0.2	0.38
5	21.5
25	104.1
125	395.6

Figure 5.5 Correlation between troponin ITC standards concentration in 50% diluted serum and measured cTnI concentrations in the Siemens ADVIA Centaur XP-TnI platform.

a)

Patient Sample	Microring Array Platform (ng/ml)			Siemens ADVIA Centaur XP-TnI Platform (ng/ml)*	% Recovery
	Upper (95% CI)*	Lower (95% CI)*	Average		
A	3.6	2.3	2.9	3.5	0.83
B	4.4	2.1	3.2	8.0	0.40
C	31.4	17.5	24.0	22.9	1.05
D	21.9	15.1	18.4	14.3	1.29
E	17.6	12.1	14.7	7.47	1.97
F	35.8	15.1	24.4	19.9	1.23
G	60.9	35.8	47.2	49.5	0.95
H	2.4	0.3	1.3	2.0	0.65
I	n/a	n/a	n/a	1.09	n/a
J	n/a	n/a	n/a	0.93	n/a
K	n/a	n/a	n/a	1.11	n/a

*Upper (95% CI) and Lower (95% CI): Upper and lower concentration ranges at 95% confidence interval. According to manufacturer information, the Siemens platform reports a 99th percentile concentration for a normal reference population as 0.04 µg/L, and an imprecision of 0.03 µg/L at 10% CV.

b)

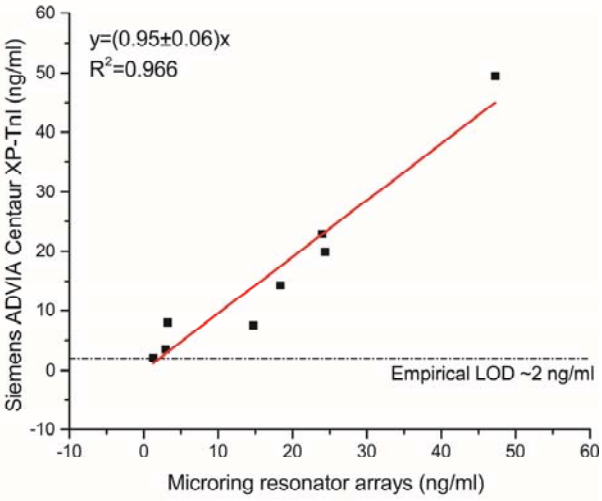

Figure 5.6 a) Table listing cTnI concentrations (ng/ml) of 11 patients' serum samples measured by the microring arrays platform (n≥10 replicates) after correction of troponin ITC standards concentration, and the respective comparison with measurements from the Siemens ADVIA Centaur XP-TnI platform (n=1 measurement). Also included is the percentage recovery of the patients' samples measured on the microring array platform compared to the Siemens assay platform. **b)** Plot illustrating the linearity of cTnI concentrations measured on the microring arrays platform (x-axis) and the Siemens platform (y-axis).

	cTnI assay (running buffer)
$Signal_{min}$	167 pm
$Signal_{max}$	8537 pm
Slope	0.931
LOB	0.010 ng/ml
LOD	0.015 ng/ml
EC50	2.1 ng/ml
Working range	0.5-9.4 ng/ml
R^2	0.995

Table 5.1 Analytical metrics from buffer calibration curve (Figure 5.2).

	cTnI assay in 50% serum
$Signal_{min}$	163 pm
$Signal_{max}$	10338 pm
Slope	0.608
LOB	0.001 ng/ml
LOD	0.003 ng/ml
EC50	18.4 ng/ml
Working range	1.9-178.5 ng/ml
R^2	0.999

Table 5.2 Analytical metrics from serum calibration curve (Figure 5.3).

5.7 References

1. World health organization cardiovascular diseases (CVDs) fact sheet no. 317. http://www.who.int/mediacentre/factsheets/fs317/en/ (Accessed April 21 2015).
2. Babuin L, Jaffe AS. Troponin: The biomarker of choice for the detection of cardiac injury. Canadian Medical Association Journal 2005;173:1191-202.
3. Thygesen K, Alpert JS, Jaffe AS, Simoons ML, Chaitman BR, White HD, et al. Third universal definition of myocardial infarction. European Heart Journal 2012;33:2551-67.
4. Gaze DC, Collinson PO. Multiple molecular forms of circulating cardiac troponin: Analytical and clinical significance. Annals of Clinical Biochemistry 2008;45:349-55.
5. Mahajan VS, Jarolim P. How to interpret elevated cardiac troponin levels. Circulation 2011;124:2350-4.
6. Wu AH, Christenson RH. Analytical and assay issues for use of cardiac troponin testing for risk stratification in primary care. Clin Biochem 2013;46:969-78.
7. Venge P, Öhberg C, Flodin M, Lindahl B. Early and late outcome prediction of death in the emergency room setting by point-of-care and laboratory assays of cardiac troponin i. American Heart Journal 2010;160:835-41.
8. Schneider HG, Ablitt P, Taylor J. Improved sensitivity of point of care troponin i values using reporting to below the 99 th percentile of normals. Clin Biochem 2013;46:979-82.
9. Hwang U, Baumlin K, Berman J, Chawla NK, Handel DA, Heard K, et al. Emergency department patient volume and troponin laboratory turnaround time. Academic Emergency Medicine 2010;17:501-7.
10. Luchansky MS, Washburn AL, McClellan MS, Bailey RC. Sensitive on-chip detection of a protein biomarker in human serum and plasma over an extended dynamic range using silicon photonic microring resonators and sub-micron beads. Lab Chip 2011;11:2042-4.
11. Kindt JT, Luchansky MS, Qavi AJ, Lee SH, Bailey RC. Subpicogram per milliliter detection of interleukins using silicon photonic microring resonators and an enzymatic signal enhancement strategy. Analytical Chemistry 2013;85:10653-7.
12. Valera E, Shia WW, Bailey RC. Development and validation of an immunosensor for monocyte chemotactic protein 1 using a silicon photonic microring resonator biosensing platform. Clin Biochem 2016;49:121-6.
13. Wade JH, Alsop AT, Vertin NR, Yang H, Johnson MD, Bailey RC. Rapid, multiplexed phosphoprotein profiling using silicon photonic sensor arrays. ACS Central Science 2015;1:374-82.
14. Washburn AL, Gunn LC, Bailey RC. Label-free quantitation of a cancer biomarker in complex media using silicon photonic microring resonators. Anal Chem 2009;81:9499-506.
15. Iqbal M, Gleeson MA, Spaugh B, Tybor F, Gunn WG, Hochberg M, et al. Label-free biosensor arrays based on silicon ring resonators and high-speed optical scanning instrumentation. IEEE J Sel Top Quantum Electron 2010;16:654-61.
16. Pepys MB, Hirschfield GM, Tennent GA, Ruth Gallimore J, Kahan MC, Bellotti V, et al. Targeting c-reactive protein for the treatment of cardiovascular disease. Nature 2006;440:1217-21.
17. Iqbal M, Gleeson MA, Spaugh B, Tybor F, Gunn WG, Hochberg M, et al. Label-free biosensor arrays based on silicon ring resonators and high-speed optical scanning instrumentation. Selected Topics in Quantum Electronics, IEEE Journal of 2010;16:654-61.

18. Linnet K, Kondratovich M. Partly nonparametric approach for determining the limit of detection. Clinical Chemistry 2004;50:732-40.
19. Kindt JT, Luchansky MS, Qavi AJ, Lee S-H, Bailey RC. Subpicogram per milliliter detection of interleukins using silicon photonic microring resonators and an enzymatic signal enhancement strategy. Analytical Chemistry 2013;85:10653-7.
20. Apple FS. Counterpoint: Standardization of cardiac troponin i assays will not occur in my lifetime. Clinical Chemistry 2012;58:169-71.
21. Christenson RH, Duh SH, Apple FS, Bodor GS, Bunk DM, Dalluge J, et al. Standardization of cardiac troponin i assays: Round robin of ten candidate reference materials. Clinical Chemistry 2001;47:431-7.
22. Christenson RH, Duh SH, Apple FS, Bodor GS, Bunk DM, Panteghini M, et al. Toward standardization of cardiac troponin i measurements part ii: Assessing commutability of candidate reference materials and harmonization of cardiac troponin i assays. Clinical Chemistry 2006;52:1685-92.
23. Christenson RH, Bunk DM, Schimmel H, Tate JR. Point: Put simply, standardization of cardiac troponin i is complicated. Clinical Chemistry 2012;58:165-8.
24. Savukoski T, Engstrom E, Engblom J, Ristiniemi N, Wittfooth S, Lindahl B, et al. Troponin-specific autoantibody interference in different cardiac troponin i assay configurations. Clin Chem 2012;58:1040-8.
25. Savukoski T, Twarda A, Hellberg S, Ristiniemi N, Wittfooth S, Sinisalo J, Pettersson K. Epitope specificity and igg subclass distribution of autoantibodies to cardiac troponin. Clinical Chemistry 2013.
26. Apple FS, Maturen AJ, Mullins RE, Painter PC, Pessin-Minsley MS, Webster RA, et al. Multicenter clinical and analytical evaluation of the axsym troponin-i immunoassay to assist in the diagnosis of myocardial infarction. Clinical Chemistry 1999;45:206-12.
27. Tate JR, Bunk DM, Christenson RH, Barth JH, Katrukha A, Noble JE, et al. Evaluation of standardization capability of current cardiac troponin i assays by a correlation study: Results of an ifcc pilot project. Clinical chemistry and laboratory medicine 2015;53:677-90.
28. Braunwald E, Antman EM, Beasley JW, Califf RM, Cheitlin MD, Hochman JS, et al. Acc/aha guidelines for the management of patients with unstable angina and non-st-segment elevation myocardial infarction: Executive summary and recommendations : A report of the american college of cardiology/american heart association task force on practice guidelines (committee on the management of patients with unstable angina). Circulation 2000;102:1193-209.
29. Washburn AL, Luchansky MS, Bowman AL, Bailey RC. Quantitative, label-free detection of five protein biomarkers using multiplexed arrays of silicon photonic microring resonators. Analytical Chemistry 2010;82:69-72.
30. Luchansky MS, Bailey RC. Rapid, multiparameter profiling of cellular secretion using silicon photonic microring resonator arrays. Journal of the American Chemical Society 2011;133:20500-6.
31. Jaffe AS, Eyk JE. Degradation of cardiac troponins
cardiovascular biomarkers. In: Morrow DA, ed., Vol.: Humana Press, 2006:161-74.
32. Jensen JK, Hallén J, Lund T, Madsen LH, Grieg Z, Januzzi JL, Atar D. Troponin i degradation in serum of patients with acute ischemic stroke. Scandinavian Journal of Clinical & Laboratory Investigation 2011;71:74-80.

33. Diris JHC, Hackeng CM, Kooman JP, Pinto YM, Hermens WT, van Dieijen-Visser MP. Impaired renal clearance explains elevated troponin t fragments in hemodialysis patients. Circulation 2004;109:23-5.
34. McDonough JL, Labugger R, Pickett W, Tse MY, MacKenzie S, Pang SC, et al. Cardiac troponin i is modified in the myocardium of bypass patients. Circulation 2001;103:58-64.
35. Bar-Or D, Thomas GW, Bar-Or R, Rael L, Winkler JV. Diagnostic potential of phosphorylated cardiac troponin i as a sensitive, cardiac-specific marker for early acute coronary syndrome: Preliminary report. Clinica Chimica Acta 2005;362:65-70.

Chapter 6:

Multiplex Monitoring of Immune System Biomarkers for Sepsis Diagnosis in a Hospital Intensive Care Unit

Acknowledgments

This work was funded by National Science Foundation Grant Award CHE 12-14081.W. W. S. was supported by the American Heart Association Predoctoral Fellowship.

The assistance of Dr. Enrique Valera, Heather Robison, and Shannon Wetzler in optimizing assay protocols was essential for development of this work. The generous support from Dr. Karen White at Carle Foundation Hospital for providing human plasma samples from septic patients of the hospital's intensive care unit is also gratefully acknowledged.

6.1 Abstract

A multiplexed assay was designed on a microring resonators platform for the detection of 14 inflammatory biomarkers associated with sepsis. Assay performance for each biomarker was characterized to illustrate the capability of the assay to detect the markers at plasma-relevant concentrations. Potential interferences among biomarkers in the assay panel were identified, and matrix effects of human plasma on the assay platform were also evaluated. Lastly, plasma samples collected from a hospital patient during a time course of sepsis were analyzed on the multiplexed assay panel, and the results provided a glimpse of pro- and anti-inflammatory markers trajectory over the time course of a sepsis episode

6.2 Introduction

Sepsis is a life-threatening condition that is among the most common cause of death for patients in the intensive care units of the hospital, with the mortality rates in the same range as deaths caused by myocardial infarctions.(1) With the improvement of healthcare, the fatality due to sepsis has overall decreased, but since sepsis mostly target the elderly, the growing age of the population also leads to a growing number of sepsis cases and results in an overall increase in the total number of deaths.(2-4) Subsequently, there is a huge financial burden for sepsis treatment, and it is estimated that the USA dedicates $20 billion spending towards hospital care for sepsis during 2011.(5)

Sepsis occurs due to host-response against systemic infection. In order to kill the invading pathogens, there is an acute release of multiple cell signaling molecules in the body to promote inflammation.(6) However, this high inflammatory response can lead to multiple organ failure that can be fatal. Currently, the criteria for sepsis diagnosis is based on monitoring clinical signs of systemic inflammatory response syndrome (SIRS), which is indicative of bodily trauma, and also in identifying the causative pathogen source that causes the infection.(7) For this latter point, the current gold standard for microbiological diagnosis is by using blood culture.(8) Unfortunately, there are limitations to this method, because the time required for blood culture is at 8-24 hours,(9) and upon a positive result in the culture, additional procedures such as gram-staining will be performed to further identify the pathogen.(10, 11) From a medical treatment standpoint, this long timeframe is undesirable, as physicians have to make immediate

treatment decisions before knowing the culture results, and consequently broad-spectrum antibiotics is liberally administered before clearly identifying the infectious pathogen source. Other than the long analysis time, there are additional drawbacks with this approach. Firstly, more than 50% of patients have negative blood culture results, despite their exhibition of sepsis-related signs and symptoms.(12) Secondly, the antibiotics administered might turn out to be ineffective to kill off the pathogen type identified by the blood culture, and this in turn promotes the increasing problem of antimicrobial resistance for bacteria.(11, 13)

At present, various molecular detection techniques are being investigated to improve upon the conventional blood culture method. Fluorescence *in situ* hybridization (FISH) is one such commercial method to identify the pathogen for a positive culture.(14, 15) Alternatively, DNA amplification strategies such has polymerase chain reaction (PCR) is also used.(16, 17) Another method that came up within the past 5-8 years is the use of mass spectrometry techniques to identify positive cultures.(18, 19) Nonetheless, these techniques do not work around the long timeframe required for blood cultures.(20) Thus, current research aims to perform analysis directly on the patient blood samples. The majority of direct blood sample analysis is based on DNA purification follow by multiplex PCR amplification strategies, yet preanalytical processing of the specimen is a big challenge since low levels of pathogens are found in blood,(21) and at present none of them are approved by the US Food and Drug Administration (FDA).(20)

Other than detecting the microbiological source of infection, there is increasing interest in monitoring biomarkers as early indicator for sepsis or predictors of sepsis outcome. As mentioned earlier, sepsis stems from systemic inflammatory response to an infection, and its fatality is not solely due to the pathogen causing damage to tissues and cells, but more directly related to the triggered host immune response that causes widespread organ dysfunction.(22) It is established that the course of sepsis can be divided into two phases: pro-inflammatory phase and compensatory anti-inflammatory phase.(23) As its name implies, during the initial pro-inflammatory phase large amounts of pro-inflammatory cytokines are released, and these cytokines are responsible for the hyper-inflammation that is characteristic of the initial phase of sepsis. Over time, if this condition is not resolved, this will progress to a compensatory phase where the immune system attempts to down-regulate the inflammation by producing anti-

inflammatory cytokines. At this stage, the septic patient might still recover if appropriate measures are administered, but often this results in death. Currently, there are very few studies in the literature that look into how these pro- and anti-inflammatory markers variate over the duration of a sepsis episode and the associate patient prognosis, thus monitoring these markers trends can potentially correlate with sepsis prognosis patterns among different patients. Ultimately, this can help with earlier diagnosis of sepsis and improvement in how it can be treated.

In this work, our goal is to develop an immunoassay panel for the multiplexed detection of 12 biomarkers based on sepsis literature. These biomarkers are: tumor necrosis factor-α (TNF-α), interleukin-1β (IL-1β), interleukin-6 (IL-6), interleukin-8 (IL-8), interleukin-10 (IL-10), interleukin-18 (IL-18), interleukin-1 receptor antagonist (IL-1ra), monocyte chemotactic protein-1 (MCP-1), procalcitonin (PCT), soluble tumor necrosis factor receptor-1 (sTNFRI), granulocyte colony-stimulating factor (G-CSF), and interferon-γ (IFN-γ). This panel consists of both pro-inflammatory markers (TNF-α, IL-1β, and IL-6, IL-8, IL-18, MCP-1, IFN-γ) and anti-inflammatory markers (sTNFRI, IL-1ra, IL-10), as well as other emergent markers that were reported to have correlation with sepsis in the literature.(24-29)

In collaboration with Carle Foundation Hospital (Urbana, IL), blood plasma samples from patients suspected to suffer from sepsis were collected at multiple time points over their course of stay in the intensive care units (ICU) of the hospital. We then used our multiplexed panel to detect the levels of the 12 biomarkers over the entire duration of the patients' stay in the ICU.

At the time of publishing, this work is only partially completed. In this chapter, we present initial work demonstrating this 12-plex biomarker panel performance, as well as an evaluation of plasma samples from ten ICU patients. In the near future, we aim to broaden our test to evaluate more patients' samples, as well as utilizing other physiological information collected about the patients for treatment purposes (E.g. Age, gender, body temperature, heart rate, blood count, blood pressure, medications, pre-existing conditions such family history etc.) to correlate our measured biomarker levels and the outcome of patients.

6.3 Materials and methods

6.3.1 Patients selection and sample collection

Patients recruited for the study were between 18-89 years of age, and admitted to the ICU of Carle Foundation Hospital in Urbana, IL with an admission diagnosis of sepsis. These patients were in poor state of health and required continuous monitoring and treatment, which included blood draws at regular time intervals for hospital laboratory tests. The blood samples were collected in lithium heparin-coated collection tubes to inhibit blood clotting, then centrifuged at 4500 g (6 min, 4°C) to obtain blood plasma. Leftover plasma samples from hospital laboratory analysis were then stored at -80°C and sent to researchers at University of Illinois for the 12-plex biomarker panel analysis.

6.3.2 Reagents and buffers

Zeba Spin desalting columns (Cat. 89882), EZ-link NHS-PEG$_4$-Biotin (Cat.21329), 1-step chloronaphthol solution (1-step CN, Cat. 34012), and high sensitivity streptavidin-horseradish peroxidase conjugate (SA-HRP, Cat. 21130) were purchased from Thermo Fisher Scientific (Rockford, IL). Pooled normal human plasma (Cat. IPLA-N) was purchased from Innovative Research (Novi, MI). DryCoat assay stabilizer (Cat. AG066-1) and DryCoat assay stabilizer with blocking protein (Cat: AG044-1) were purchased from Virusys (Taneytown, MD). Recombinant biomarker antigen standards, capture and tracer antibodies used for the biomarker panel were obtained from various companies listed in Table 6.1. All remaining reagents not listed in this section were purchased from Sigma-Aldrich (St. Louis, MO).

10 mM phosphate buffer saline (PBS) solution was prepared by dissolving Dulbecco's phosphate buffered saline powder to distilled water, filtered and adjusted to pH 7.4. Assay running buffer was prepared by dissolving 0.5% (w/v) bovine serum albumin (BSA) to 10 mM PBS.

6.3.3 Biotinylation of tracer antibodies

All of the tracer antibodies of the assay panel were purchased in biotinylated format, except for the tracer antibody for PCT, which was biotinylated in the laboratory. Procedures of biotinylation of this antibody was identical to that described in Chapter 5. Briefly, the antibody

was filtered through the desalting columns to remove excess sodium azide, and the antibody concentration was determined by NanoDrop spectrophotometer (Thermo Fisher Scientific, Wilmington, DE). Subsequently, 20 mM NHS-PEG$_4$-Biotin was added to the antibody at 20× molar excess to incubate at room temperature for 30 min. The biotinylated antibody was then filtered through the desalting columns to 10 mM PBS storage solution, and the final concentration was measured by the NanoDrop spectrophotometer again.

6.3.4 Capture antibodies immobilization on chips

In order to fit in a rather dense number of capture antibodies probes (12 biomarker antibodies plus mouse IgG control spotted in duplicates, 26 probes to spot in total) on a small sensor chip footprint (4 mm × 6 mm), assay capture antibodies were sent to Genalyte (San Diego, CA) to be spotted on microring sensor arrays using a piezoelectric spotter. The immobilization chemistry is identical to the APTES/BS3 method described in Chapter 5 except for the final blocking step, where each spotted antibody probe was spotted over again with a layer of DryCoat with blocking protein solution to reduce non-specific interactions during the immunoassay run.

6.3.5 Instrumentation

Microring resonator assay experiments were performed on the latest generation Maverick M24 instrument that was briefly mentioned in Chapter 1. Similar to the earlier Maverick M1 generation instrument described extensively in Chapters 4 and 5, the M24 system also has an integrated assay fluidic system to automate assay reagents flow. The major innovation in the M24 design is that the microring array sensor chips come pre-assembled in a disposable cartridge of 12 chips. As shown in Figure. 6.1, this cartridge consists of inlet sipper tubes to draw assay samples/reagents pre-loaded in standard 96-well plates, as well as a fluidic gasket sealed over each individual chip. This fluidic gasket has cut-outs that align over the two sample channels of sensor microrings of each chip, allowing solutions drawn by the inlet tube to flow across the microrings, as well as outlet holes that can be connected to the waste lines of the instrument to discard used reagents. The design of this cartridge enables performing successive assay runs on all 12 chips in the array without pauses, which greatly facilitates testing of multiple clinical samples of patients at various sample collection time points required by this project.

6.3.6 Microring resonator assay procedures

To perform microring resonator assays, a 96-well plate was first filled with assay reagents and samples/standards to be tested. This pre-filled well plate and the pre-assembled cartridge containing the antibody-spotted chips were then placed into the M24 instrument. A Maverick system control software was pre-programmed to control assay reagent delivery from the well plate to a single sensor chip in the cartridge, and two assays were performed simultaneously on this chip. After the assay runs on this chip were completed, the software automatically repeated the same procedures to the next chip in the cartridge. For each assay run, the total duration was 45.5 minutes. The assay was monitored in real-time in the following sequence: 1) assay running buffer rinse (3 min at 30 µl/min); 2) analyte standard/plasma sample (2 min at 40 µl/min, follow by 4.5 min at 20 µl/min); 3) assay buffer rinse (1 min, 40 µl/min); 4) biotinylated tracer antibodies cocktail (2 µg/ml for each antibody, 10 min at 30 µl/min); 5) assay buffer rinse (1 min at 40 µl/min); 6) SA-HRP (6 µg/ml, 10 min at 30 µl/min); 7) assay buffer rinse (2 min at 40 µl/min); 8) 1-step CN (9 min at 30 µl/min); 9) assay buffer rinse (3 min at 40 µl/min).

6.3.7 Data analysis

Data analysis was performed with OriginPro 2015 software. The net shift in resonance wavelength was determined by the difference in response between 34-45 min of the assay (before and after 1-step CN signal amplification step). Net shifts from analyte calibration standards were fit to the following dose response function:

$$y = A1 + \frac{A2 - A1}{1 + 10^{(\log x0 - x)p}}$$

where A1 is the bottom asymptote, A2 is the upper asymptote, x0 is the concentration at half response (EC50), and p is the hill slope of the fitted plot. In order to conform to guidelines for clinical diagnostic tests, the limit of blank (LOB) and limit of detection (LOD) were determined based on the EP17-A protocol published by Clinical and Laboratory Standards Institute (CLSI).(30, 31) Assuming a Gaussian distribution for instrumental response from blank samples, the LOB at 95th percentile of observed blank value is summarized as the following equation according to this protocol:

$$LOB = mean_{blank} + 1.645(SD_{blank})$$

Where $mean_{blank}$ is the mean instrumental response from free of analyte sample measurements and SD_{blank} is the corresponding standard deviation of those measurements.

For LOD determination, the equation is as follow:

$$LOD = LOB + 1.645(SD_{low\ concentration\ sample})$$

Here, $SD_{low\ concentration\ sample}$ refers to the standard deviation obtained from replicate measurements of a sample with known low analyte concentration. This sample selected should have an analyte concentration that generates an instrumental response between 1-4 times the response obtained from the LOB.

Another point to note is that this protocol recommended clinical diagnostic tests manufacturers to obtain 60 replicate measurements to establish the LOB/LOD values for a diagnostic test platform, but at the time of publishing this chapter, these assay performance metrics were evaluated based on 12 replicate measurements per concentration from microring sensor arrays to obtain an *estimate* of the assays performance. In the future, these performance metrics will need to be more rigorously determined, especially when this project reaches the stage to draw any clinical diagnostics conclusions from patients' samples.

6.4 Results and discussion

6.4.1 Dose-response calibration curves for 12-plex panel

Each chip on the 12-chip disposable cartridge was spotted with antibodies in clusters of four microrings, as illustrated by the layout in Figure. 6.2a. It is worthwhile to note from this figure that the antibodies were spotted in identical positions on both channels for each individual chip, which enables two assay experiments to run simultaneously for the chip. The real-time instrument response from each assay run is illustrated in Figure. 6.2b, which showed each binding step of the assay run, from analyte standards delivery (t=3-9.5 min), biotinylated tracer antibodies (t=10.5-20.5 min), streptavidin-HRP (t=21.5-31.5 min), and the final precipitated enzymatic substrate upon 1-step CN delivery (t=33.5-42.5 min), with buffer rinses between each step.

In order to identify the working range of each assay for the 12 biomarkers in the sepsis marker panel, standard solutions were made as a cocktail of the 12 biomarker standards spiked into the assay running buffer to measure the instrumental response after 1-step CN delivery, and this response was fitted with dose-response fitting function to generate calibration curves. This experiment was repeated on three different days to determine the reproducibility of this multiplexed assay, and Figure 6.3 illustrated the results of the fitted curves after optimization. It was discovered that for markers IL-1ra and G-CSF, their range for plotting a dose-response calibration curve is from 6.4 pg/ml to 800000 pg/ml of spiked markers analyte. For markers MCP-1, PCT, sTNFRI, IL-1β, IL-6, IL-8, IL-10, and IL-18, their dose-response curves shift down to ranging from 1.2 pg/ml to 150000 pg/ml. For TNF-α and IFN-γ, the dose-response range shifts down to an even lower range between 0.24 pg/ml to 30000 pg/ml. Table 6.2 lists out the metrics of the fitted curves from each assay of the panel based on the average of all measurements on the three different days, while the LOB and LOD values were reported based on the average LOB and LOD obtained over the three different days.. As stated in the "Data Analysis" subsection, the reported LOB and LOD values are meant to be estimates for each of the biomarker assays, since they were only calculated from 12 replicate microring measurements over three different days. Commercial assays manufacturers often set a threshold to report "zero" effective concentration for scenarios where the actual blank measurement has a lower instrumental response than the blank response obtained by the fitted calibration function.(31) Nevertheless, it is expected that if more replicate measurements of blank and low concentration standards are taken, there will be a more accurate estimation of the assay LOB and LOD values in the future. Another metric in Table 6.2 that puts some insight to the assay performance is the EC10 value reported for each assay. This value reports the concentration of the biomarker analyte that generates 10% of the maximum instrumental response for the assay. Overall, according to a literature report of evaluating the baseline concentration of 27 cytokines in healthy human subjects using a Luminex assay platform,(32) most of the biomarkers in the 12-plex microring arrays assay panel have comparable detection limits to detect baseline levels in healthy individuals.

6.4.2 Matrix effects of human plasma

After demonstrating assay quantitation for this 12-plex biomarker panel in assay running buffer, the next step in optimization is to apply this panel to evaluate biomarker levels in human plasma matrix. In our preliminary experiments, we spiked in saturating concentration of the 12 biomarkers that were determined from our dose response curves (800 ng/ml for IL-1ra and G-CSF, 30 ng/ml for TNF-α and IFN-γ, and 150 ng/ml for the remaining eight markers) to 0.5% BSA assay running buffer, 1:2 and 1:10 dilution of pooled healthy human plasma in assay running buffer. From the results illustrated in Figure. 6.4, most of the biomarkers showed equivalent response for the two plasma dilutions tested. Among the biomarkers that showed significant differences, TNF-α and PCT showed ~2000 pm reduction in response, while sTNR1, IL-6, IL-10, and IL-18 showed a slight increase in response in diluted plasma matrix. Non-specific binding to mouse IgG negative control rings was drastically reduced when the assay was ran in diluted plasma matrix. The results from this matrix effects analysis also suggested that when testing human plasma samples for the majority of biomarkers in the panel (e.g. IL-1β, MCP-1, IL-1ra, IFN-γ, and IL-8), it is reasonable to perform assays at 1:10 sample dilutions, providing that the sample dilution does not decrease the biomarker level to lower than the assay detection limit. For the remaining markers, it might be necessary to correct for the matrix effects from plasma when determining the marker concentration in the sample.

In a separate experiment illustrated in Figure. 6.5, a pooled healthy human plasma sample was diluted to 1:10 plasma concentration and assayed on the 12-plex biomarker panel. From the figure, it is low levels of sTNFRI were detectable in this healthy pooled plasma sample. The concentration of sTNFRI in this pooled human plasma sample was determined to be ~155 pg/ml based on interpolation from the sTNFRI calibration curve in Figure 6.3. This result is unsurprising, since for healthy human plasma there is still a baseline level of immunoregulatory biomarkers. In the future, it is worthwhile to repeat this evaluation at higher pooled plasma concentration to determine if the baseline levels of other biomarkers are detectable.

6.4.3 Plasma analysis from septic patients' samples

After investigating the matrix effects of human plasma, we proceeded to evaluate the performance of the 12-plex biomarker assay panel on ten septic patients' plasma samples. As shown in Figure 6.6, plasma samples were drawn from each patient at multiple time points

during his/her entire stay at the ICU of Carle Foundation Hospital. Each patient's physiological and clinical conditions (e.g. Basal temperature, plasma pro-calcitonin levels, white blood cell counts etc.) and the time intervals between plasma collections were all recorded by the hospital staff, but this information was withheld from our personnel at the University of Illinois at this preliminary study stage. Thus, for the purpose of reporting our measurements from the 12-plex biomarker panel, the time points were denoted as arbitrary time point units as shown in Figure. 6.6. The biomarker concentration for the evaluated time points for each patient was determined by interpolating the assay response to the calibration curves generated in Figure 6.3. Markers TNF-α, IL-1β, and IFN-γ had undetectable levels in all of the ten patients evaluated. Among the detectable markers PCT, sTNRI, and IL-6 levels mostly fall within the assay linear range for all the samples tested, and the interpolated concentrations are plotted in Figures 6.7-6.9. In general, PCT and IL-6 concentrations were the highest in the earlier time points and gradually decreased, and the IL-6 concentrations at certain time points for some patients were elevated beyond the linear range of the assay. In contrast, sTNFRI concentrations were rather consistently elevated over the assessed time points for all of the patients. Moreover, patients E, F, and G have lower concentrations of these three markers in comparison to the rest of the patients. At present, it is unclear how the trajectory of each of these biomarker levels correlate with one another, but it is interesting to note that both pro-inflammatory (PCT, IL-6) and anti-inflammatory (sTNFRI) markers among some of the patients' samples had elevated response on this 12-plex assay panel. Based on literature reports, pro-inflammatory markers are elevated initially in sepsis, and later on, anti-inflammatory markers levels will start increasing. It is speculated that some of these patients were admitted to the ICU after the pro-inflammatory phase of sepsis, thus high levels of anti-inflammatory markers were also observed.

6.5 Conclusions

In conclusion, this initial work has demonstrated the multiplexed capability of the microring resonators platform to detect 12 different biomarkers associated with sepsis. Calibration standards in buffer solutions were tested across this multiplexed panel, and the results were fitted with dose-response functions to characterize the performance of each assay in the panel and to determine assay reproducibility. Potential matrix effects from human plasma was also studied. Finally, plasma samples from ten sepsis patient were analyzed by the microring

resonators platform, and the results indicated both the elevation of pro-inflammatory markers (PCT, IL-6) and anti-inflammatory markers (sTNFRI) markers during sepsis. Overall, these initial results showed great promise in using microring resonators for clinical analysis of sepsis biomarkers in hospital patients, which can provide further insights to the correlation between immunoregulatory biomarkers and sepsis prognosis.

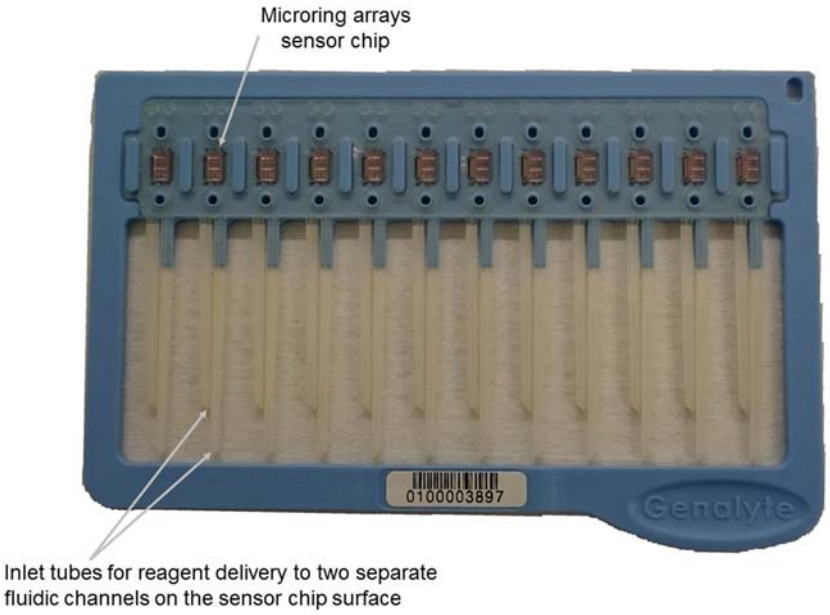

Figure 6.1 Photograph of the chips cartridge for the Maverick M24 instrument. A total of 12 sensor chips are placed into this cartridge, and each chip is connected to two inlet tubes that allow samples/assay reagents delivery to two channels with exposed microrings on the sensor chip surface.

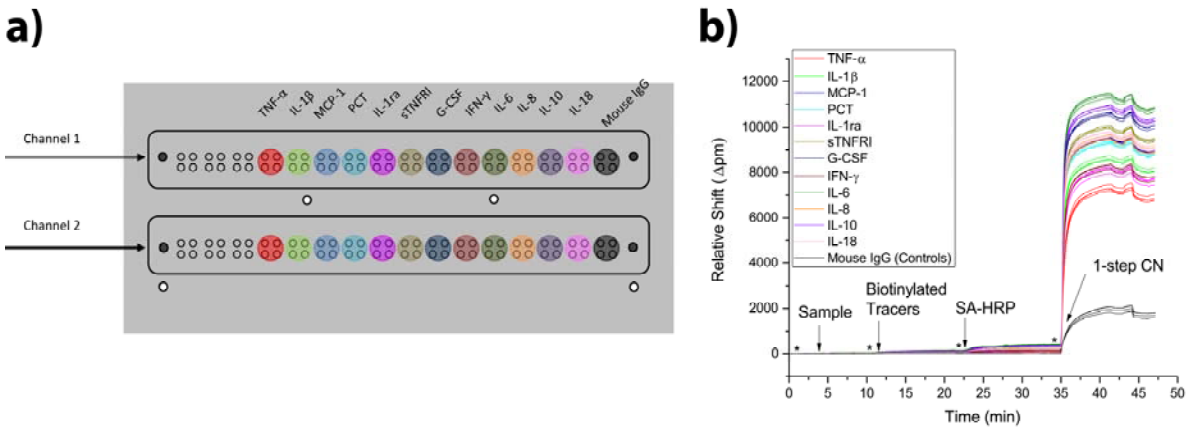

Figure 6.2 a) Diagram of the sensor chip layout and the relative position of each antibody spotted on the chip surface. Mouse IgG antibodies do not have specific affinity for any antigens, thus serving as negative controls for the assays. Each antibody in the array is spotted over a cluster of four microrings, and repeated over the two fluidic channels of the chip. The rings in black represent temperature control rings, while the rings in white represent leak sensor rings, since that are normally occluded by the fluidic gaskets and left unexposed to reagent delivery through the channels. The arrows represent the flow direction of sample/reagents during an assays run. **b)** Representative sensogram data from an individual assay run of all 12 biomarkers spiked at high concentrations in assay running buffer.

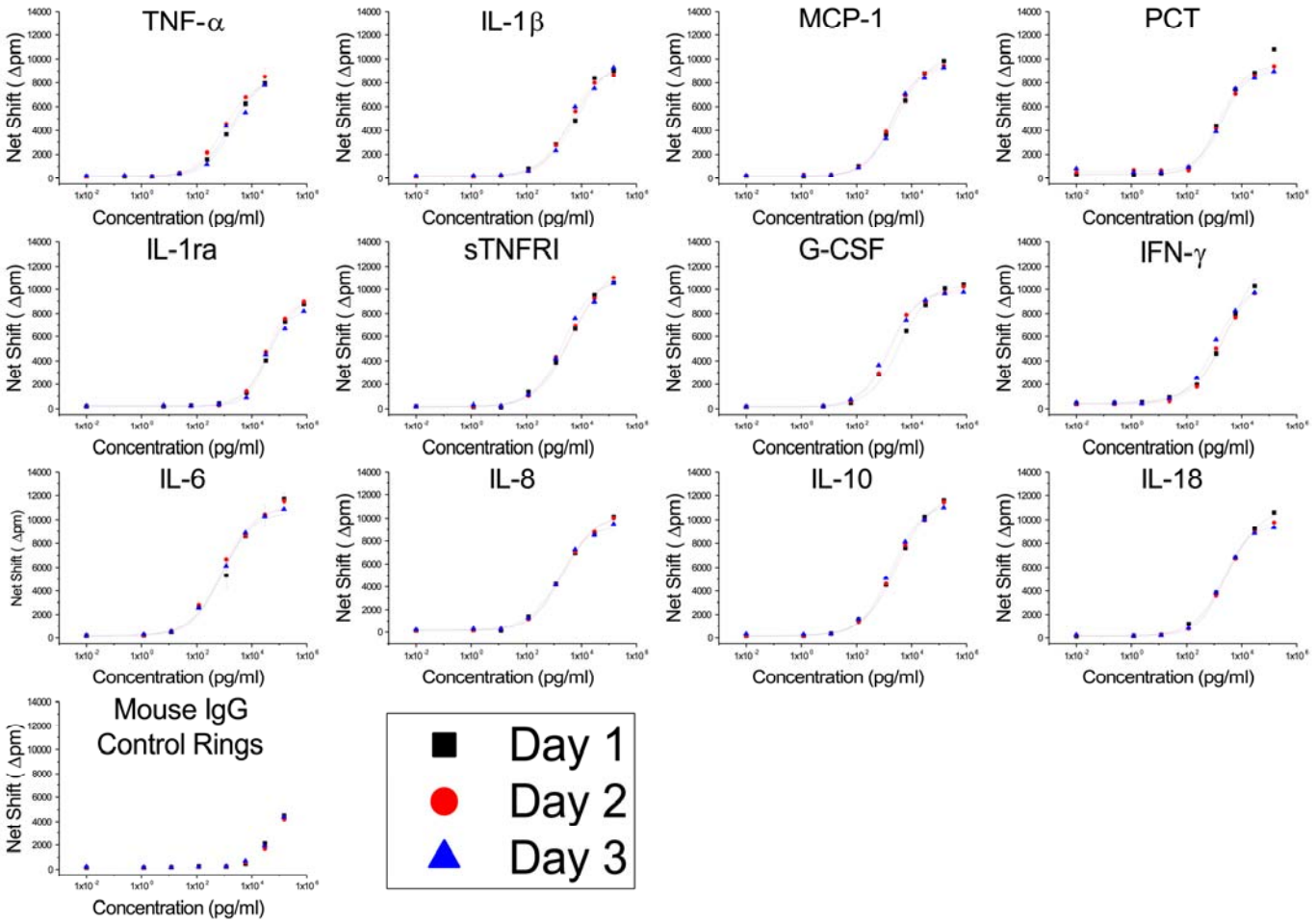

Figure 6.3 Dose-response curves for all 12 biomarkers along with a negative Mouse IgG control antibody in the microring arrays panel determined over three different days. Error bars on each curve represent standard deviation of n=4 replicated measurements on each individual day of the experiment.

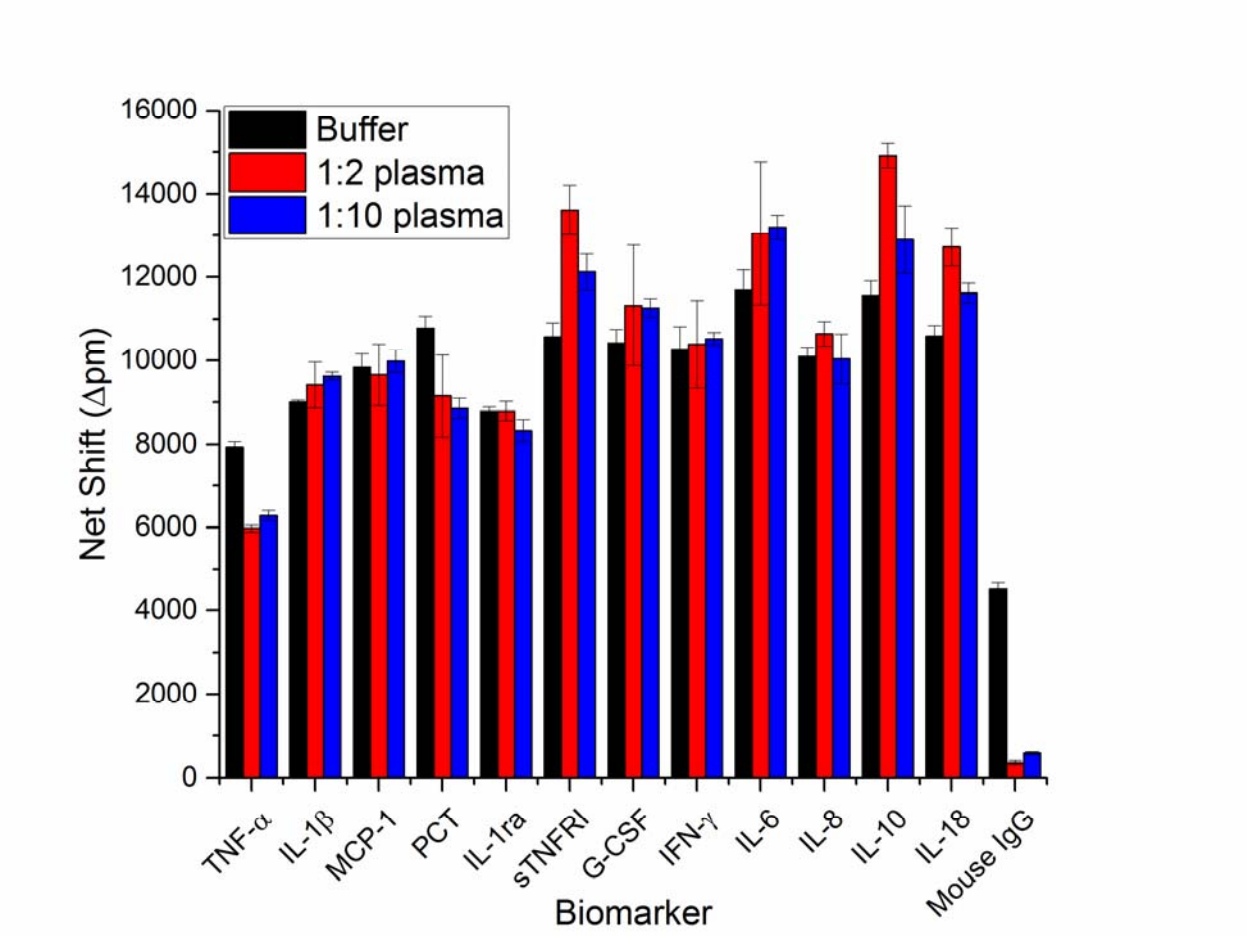

Figure 6.4 Matrix effects of pooled human plasma. The 12 biomarkers standards were spiked at saturating concentrations. Error bars represent the standard deviation of n=4 replicated measurements.

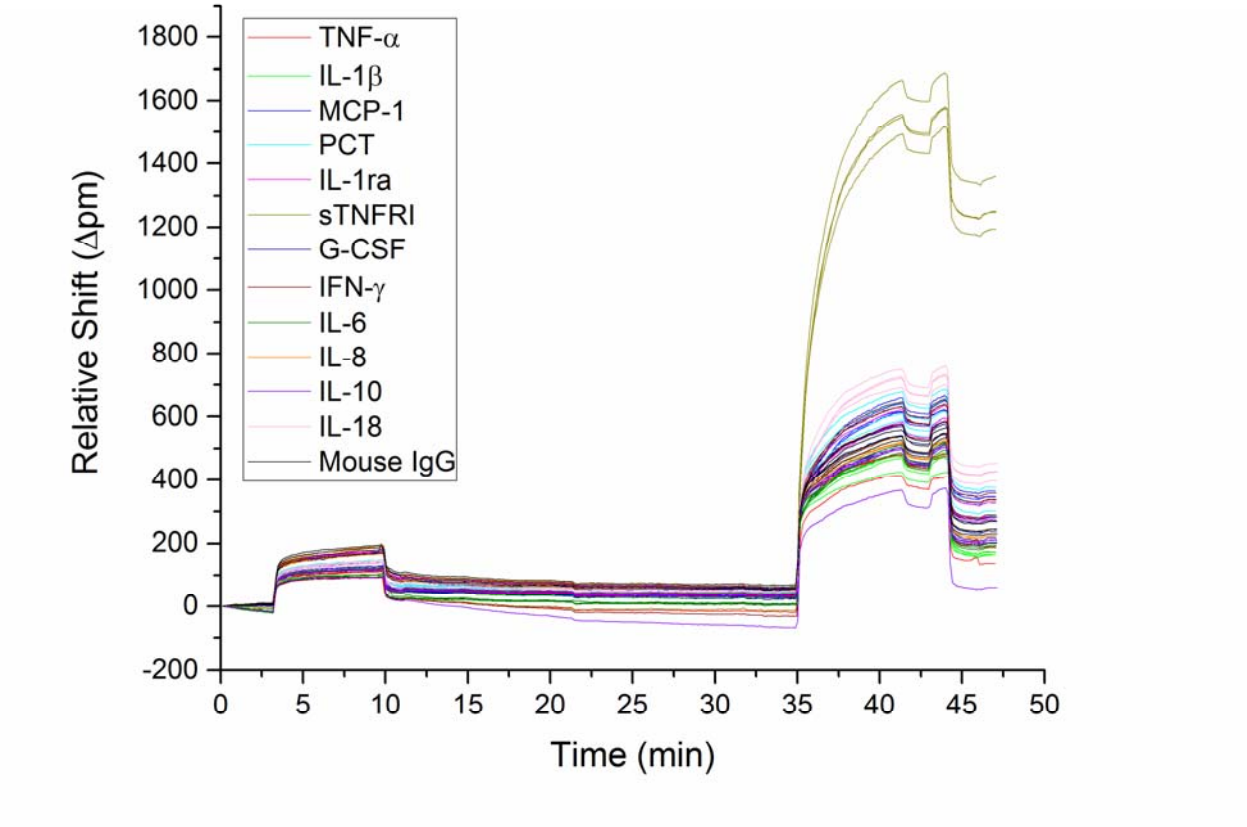

Figure 6.5 Sensogram of an assay testing 1:10 dilution of pooled human plasma. From the sensogram, it is evident that low levels of sTNFRI are present in the pooled plasma sample.

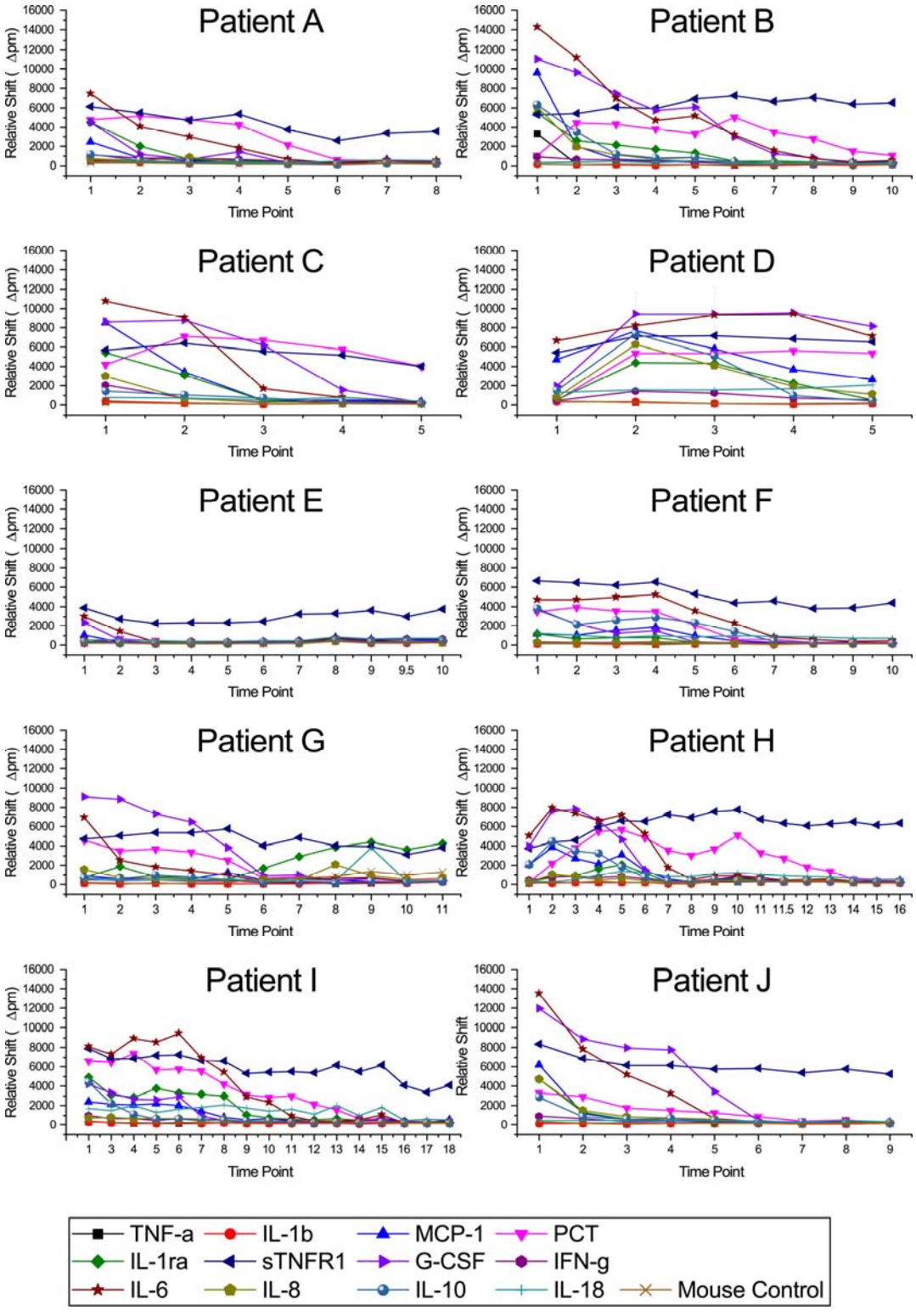

Figure 6.6 Assay response of 1:10 dilution of plasma samples from ten patients (Patients A-J) across variable time points. Error bars represent standard deviation of n=4 replicated measured response.

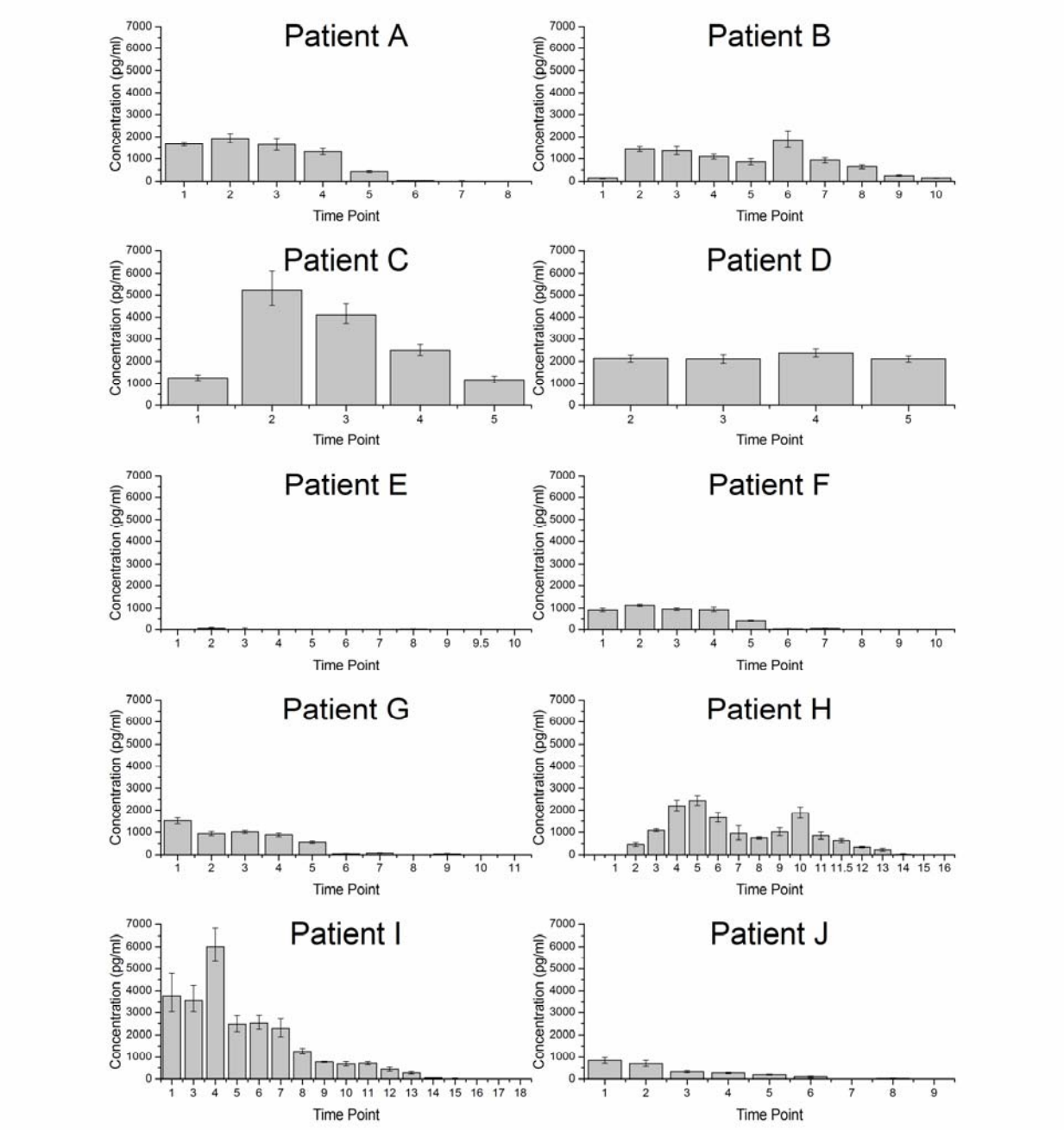

Figure 6.7 Interpolated PCT concentrations of the plasma samples from all ten patients. Error bars represent the upper and lower concentration range based on the interpolated results accounting for the standard deviation in response in Figure 6.6.

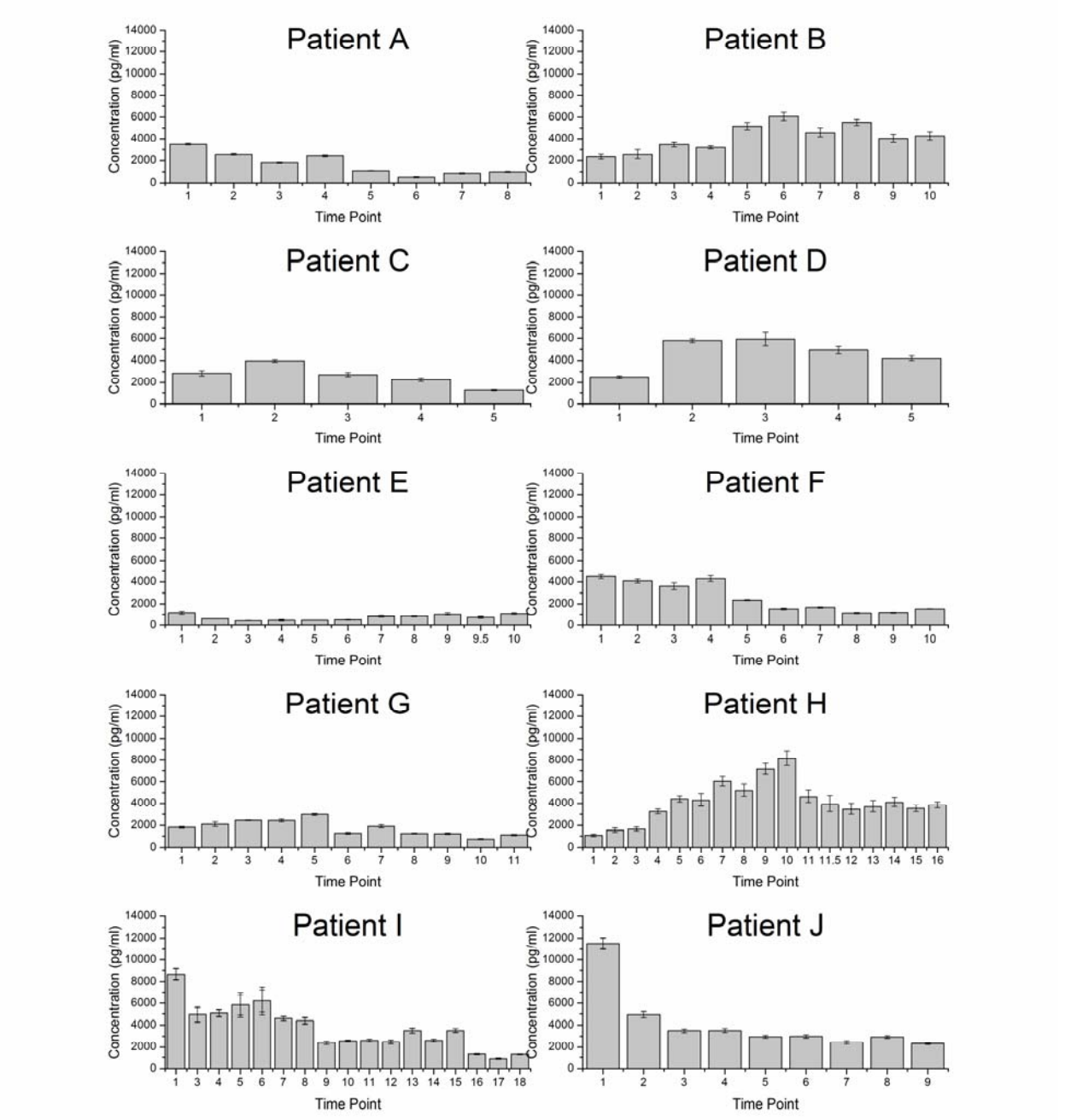

Figure 6.8 Interpolated sTNFRI concentrations of the plasma samples from all ten patients. Error bars represent the upper and lower concentration range based on the interpolated results accounting for the standard deviation in response in Figure 6.6.

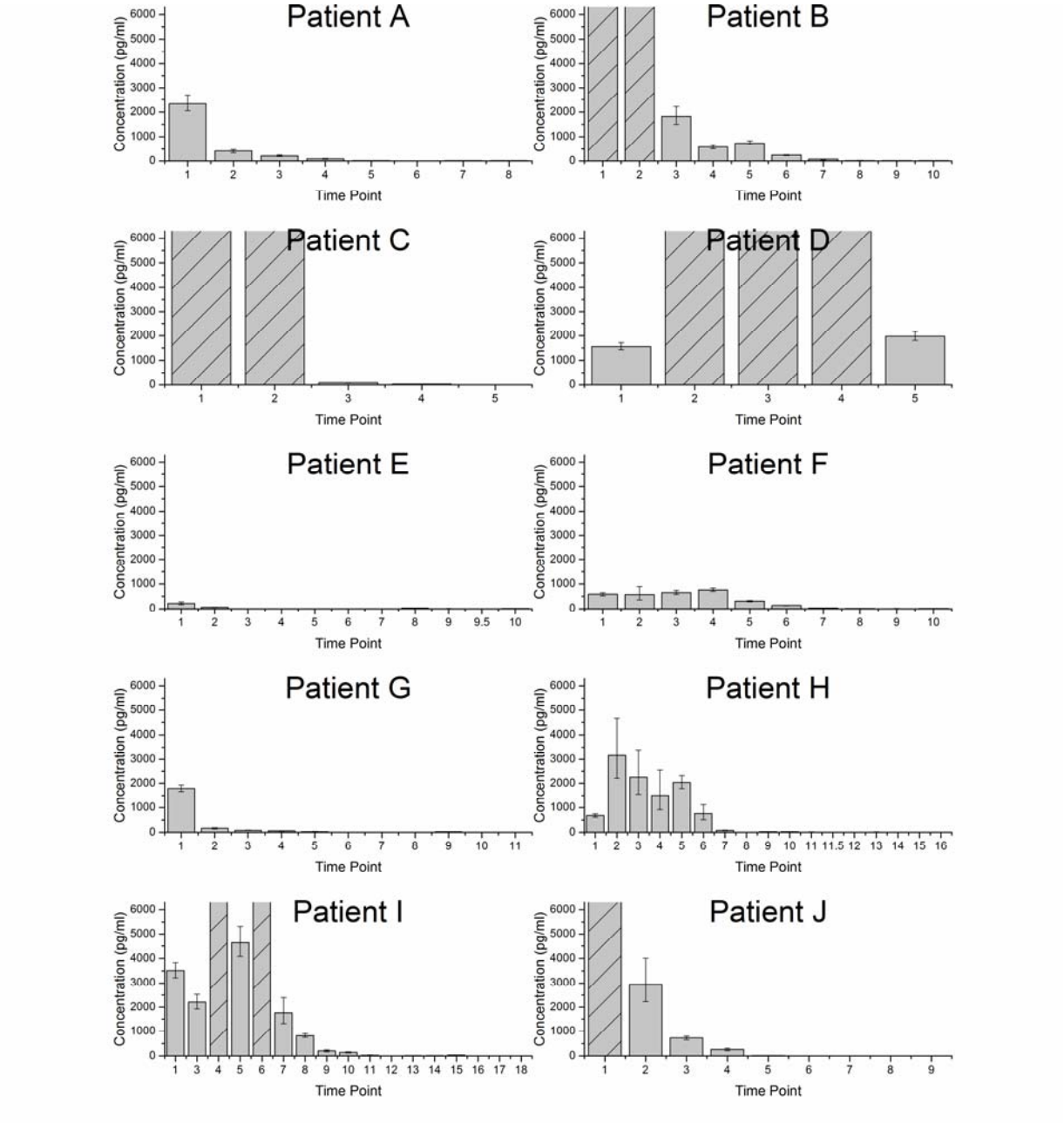

Figure 6.9 Interpolated IL-6 concentrations of the plasma samples from all ten patients. Columns shaded with diagonal lines indicate that the IL-6 levels exceeded the linear range of the calibration plot. Error bars represent the upper and lower concentration range based on the interpolated results accounting for the standard deviation in response in Figure 6.6.

Biomarker	Antigen Standard	Capture Antibody	Tracer Antibody #1	Tracer Antibody #2
TNF-α	Biolegend 510102	Biolegend 502802	Biolegend 502904	
IL-1β	eBioscience 14-8018	eBioscience 16-7018-85	eBioscience 13-7016-85	
MCP-1	ebioscience 14-8398-80	eBioscience 14-7099-85	eBioscience 13-7096-85	
PCT	Abbexa abx068668	Abbexa abx019247	Abbexa abx019248	
IL-1ra	Biolegend 714406	R&D Systems MAB280	R&D Systems BAF280	Biolegend 509501
sTNFRI	R&D Systems 636-R1-025	R&D Systems MAB625	R&D Systems BAF225	
G-CSF	Biolegend 713402	R&D Systems MAB214	R&D Systems BAF214	
IFN-γ	Mabtech 3420-10	Mabtech 3420-3-250	Mabtech 3420-6-250	
IL-6	eBioscience 14-8069	eBioscience 16-7069	eBioscience 13-7068	R&D Systems BAF206
IL-8	R&D Systems 208-IL	BD Biosciences 554716	BD Biosciences 554718	R&D Systems BAF208
IL-10	eBioscience 14-8109-80	eBioscience 16-7108-85	Biolegend 501501	Invitrogen AHC7109
IL-18	R&D Systems B001-5	R&D Systems D044-3	R&D Systems D045-6	

Table 6.1. Catalogue numbers and vendors for all purchased antibodies and antigen standards used for the assay panel.

	TNF-a	IL-1b	MCP-1	PCT	IL-1ra	sTNFR1	G-CSF	IFN-g	IL-6	IL-8	IL-10	IL-18
A1 [pm]	156	161	175	500	222	178	157	408	134	149	96	149
A2 [pm]	8409	9420	9657	8954	8822	10870	10024	10846	11155	9927	11885	10065
Slope	0.859	0.838	0.843	1.095	1.092	0.785	0.855	0.789	0.724	0.760	0.717	0.834
Avg. LOB [pg/ml]	5±6	3±1	4±4	50±20	500±100	3.6±0.8	5±4	9±3	0.4±0.2	0.8±0.8	6±9	9±9
Avg. LOD [pg/ml]	10±10	6±4	7±6	70±30	900±400	6.4±0.9	9±6	21±4	1.0±0.6	2±2	10±10	10±10
EC10 [pg/ml]	103	287	162	214	4815	159	162	108	45	104	113	177
Linear Range [pg/ml] †	266-1336	756-20658	423-11340	448-5641	10121-128270	447-15263	419-10733	303-10152	137-6295	302-11600	350-16701	467-12990
R^2	0.987	0.999	0.998	0.999	0.998	0.996	0.999	0.999	0.994	0.999	0.998	1.000

Table 6.2 Parameters of the dose response curve for each biomarker assay. A1 and A2 represents the bottom and upper asymptotes. †The linear range for all of the assays were defined as between the EC20 and EC80 concentrations of the curve.

6.6 References

1. Angus DC, Linde-Zwirble WT, Lidicker J, Clermont G, Carcillo J, Pinsky MR. Epidemiology of severe sepsis in the united states: Analysis of incidence, outcome, and associated costs of care. Critical care medicine 2001;29:1303-10.
2. Stevenson EK, Rubenstein AR, Radin GT, Wiener RS, Walkey AJ. Two decades of mortality trends among patients with severe sepsis: A comparative meta-analysis. Critical care medicine 2014;42:625-31.
3. Kumar G, Kumar N, Taneja A, Kaleekal T, Tarima S, McGinley E, et al. Nationwide trends of severe sepsis in the 21st century (2000-2007). Chest 2011;140:1223-31.
4. Martin GS. Sepsis, severe sepsis and septic shock: Changes in incidence, pathogens and outcomes. Expert review of anti-infective therapy 2012;10:701-6.
5. Torio CM, Andrews RM. National inpatient hospital costs: The most expensive conditions by payer, 2011. http://www.hcup-us.ahrq.gov/reports/statbriefs/sb160.pdf (Accessed August 02, 2015).
6. Bone RC, Balk RA, Cerra FB, Dellinger RP, Fein AM, Knaus WA, et al. Definitions for sepsis and organ failure and guidelines for the use of innovative therapies in sepsis. The accp/sccm consensus conference committee. American college of chest physicians/society of critical care medicine. Chest 1992;101:1644-55.
7. Iskander KN, Osuchowski MF, Stearns-Kurosawa DJ, Kurosawa S, Stepien D, Valentine C, Remick DG. Sepsis: Multiple abnormalities, heterogeneous responses, and evolving understanding. Physiol Rev 2013;93:1247-88.
8. Mancini N, Burioni R, Clementi M. Microbiological diagnosis of sepsis: The confounding effects of a “gold standard”. T sepsis, Vol. 1237:1-4.
9. Valles J, Rello J, Ochagavia A, Garnacho J, Alcala MA. Community-acquired bloodstream infection in critically ill adult patients: Impact of shock and inappropriate antibiotic therapy on survival. Chest 2003;123:1615-24.
10. Stone RB, Steele JCH. Impact of reporting gram stain results from blood cultures on the selection of antimicrobial agents. American Journal of Clinical Pathology 2009;132:5-6.
11. Uehara Y, Yagoshi M, Tanimichi Y, Yamada H, Shimoguchi K, Yamamoto S, et al. Impact of reporting gram stain results from blood culture bottles on the selection of antimicrobial agents. American Journal of Clinical Pathology 2009;132:18-25.
12. Jones AE, Heffner AC, Horton JM, Marchick MR. Etiology of illness in patients with severe sepsis admitted to the hospital from the emergency department. Clinical Infectious Diseases 2010;50:814-20.
13. Pradipta IS, Sodik DC, Lestari K, Parwati I, Halimah E, Diantini A, Abdulah R. Antibiotic resistance in sepsis patients: Evaluation and recommendation of antibiotic use. North American Journal of Medical Sciences 2013;5:344-52.
14. Kempf VAJ, Mändle T, Schumacher U, Schäfer A, Autenrieth IB. Rapid detection and identification of pathogens in blood cultures by fluorescence in situ hybridization and flow cytometry. International Journal of Medical Microbiology 2005;295:47-55.
15. Peters RPH, Savelkoul PHM, Simoons-Smit AM, Danner SA, Vandenbroucke-Grauls CMJE, van Agtmael MA. Faster identification of pathogens in positive blood cultures by fluorescence in situ hybridization in routine practice. Journal of Clinical Microbiology 2006;44:119-23.

16. Tsalik EL, Jones D, Nicholson B, Waring L, Liesenfeld O, Park LP, et al. Multiplex pcr to diagnose bloodstream infections in patients admitted from the emergency department with sepsis. Journal of Clinical Microbiology 2010;48:26-33.
17. Wallet F, Loiez C, Herwegh S, Courcol RJ. Usefulness of real-time pcr for the diagnosis of sepsis in icu-acquired infections. Infect Disord Drug Targets 2011;11:348-53.
18. La Scola B, Raoult D. Direct identification of bacteria in positive blood culture bottles by matrix-assisted laser desorption ionisation time-of-flight mass spectrometry. PLoS ONE 2009;4:e8041.
19. Clark AE, Kaleta EJ, Arora A, Wolk DM. Matrix-assisted laser desorption ionization–time of flight mass spectrometry: A fundamental shift in the routine practice of clinical microbiology. Clinical Microbiology Reviews 2013;26:547-603.
20. Liesenfeld O, Lehman L, Hunfeld K-P, Kost G. Molecular diagnosis of sepsis: New aspects and recent developments. European Journal of Microbiology and Immunology 2014;4:1-25.
21. Cohen J, Vincent J-L, Adhikari NKJ, Machado FR, Angus DC, Calandra T, et al. Sepsis: A roadmap for future research. The Lancet Infectious Diseases;15:581-614.
22. Reinhart K, Bauer M, Riedemann NC, Hartog CS. New approaches to sepsis: Molecular diagnostics and biomarkers. Clinical Microbiology Reviews 2012;25:609-34.
23. Zhao H-q, Li W-m, Lu Z-q, Sheng Z-y, Yao Y-m. The growing spectrum of anti-inflammatory interleukins and their potential roles in the development of sepsis. Journal of Interferon & Cytokine Research 2014;35:242-51.
24. Mera S, Tatulescu D, Cismaru C, Bondor C, Slavcovici A, Zanc V, et al. Multiplex cytokine profiling in patients with sepsis. APMIS 2011;119:155-63.
25. Novotny AR, Reim D, Assfalg V, Altmayr F, Friess HM, Emmanuel K, Holzmann B. Mixed antagonist response and sepsis severity-dependent dysbalance of pro- and anti-inflammatory responses at the onset of postoperative sepsis. Immunobiology 2012;217:616-21.
26. Gårdlund B, Sjölin J, Nilsson A, Roll M, Wickerts C-J, Wretlind B. Plasma levels of cytokines in primary septic shock in humans: Correlation with disease severity. The Journal of Infectious Diseases 1995;172:296-301.
27. Tschoeke SK, Oberholzer A, Moldawer LL. Interleukin-18: A novel prognostic cytokine in bacteria-induced sepsis. Critical care medicine 2006;34:1225-33.
28. Ritter C, Tomasi CD, Dal-Pizzol F, Pinto BB, Dyson A, de Miranda AS, et al. Inflammation biomarkers and delirium in critically ill patients. Critical care (London, England) 2014;18:R106.
29. Fischer E, Van Zee KJ, Marano MA, Rock CS, Kenney JS, Poutsiaka DD, et al. Interleukin-1 receptor antagonist circulates in experimental inflammation and in human disease. Blood 1992;79:2196-200.
30. Institute CaLS. Protocols for determination of limits of detection and limits of quantitation, approved guideline ep17-a. 2004;24, No. 34.
31. Armbruster DA, Pry T. Limit of blank, limit of detection and limit of quantitation. The Clinical Biochemist Reviews 2008;29:S49-S52.
32. Biancotto A, Wank A, Perl S, Cook W, Olnes MJ, Dagur PK, et al. Baseline levels and temporal stability of 27 multiplexed serum cytokine concentrations in healthy subjects. PLoS ONE 2013;8:e76091.

Chapter 7:

Future Directions

7.1 Introduction

In this thesis, I have presented a summary of my research progress towards biomarker immunoassays development on a microring resonator platform, leading up to the translation of these assays to clinical diagnostic applications. The translational of immunoassays to clinical usage is an iterative process that involves trial and error of identifying correct biomarkers, assay development, clinical trials and outcome assessments. Particularly, the final two projects in this dissertation that involved collaboration with hospital physicians (Chapters 5 and 6) have excellent potential for more clinical studies with patients in the future.

7.2 Future work of the troponin project

For the cardiac troponins analysis project described in Chapter 5, future work can be expanded to multiplexed detection of other troponin degradation subunits/fragments in addition to cTnI. The troponin molecule consists of three subunits, out of which both the cTnI and cTnT subunits are highly specific to myocardial injury.(1) However at present stage, no troponin tests are available to simultaneously detect both the I and T subunits of a sample. Moreover, troponins released into circulation are subjected to degradation by serum proteases, and having the ability to detect and quantitate these fragmentation products are useful to understand cardiac dysfunction and disease prognosis.(2) Previously, we performed experiments on microring arrays platform that demonstrated the ability to distinguish between cTnI and cTnT subunits (Fig. 7.1). In the future, we can expand upon this work to detect other troponin fragments through a careful design of capture and tracer antibodies used in assays.

Another future direction for the troponin project is in the detection of troponin autoantibodies. Troponin autoantibodies are known to be found in both healthy individuals or patients afflicted with heart diseases, and currently troponin autoimmunity is not well understood.(3) However, it is reported that these autoantibodies can interfere with antibodies that are used in immunoassays, thus leading to false negative results.(4) One possible way to utilize microring resonators for troponin autoantibodies detection is through the use of peptide arrays. As a proof-of-principle experiment, peptide sequences that correspond to epitopes targeted by anti-cTnI assay antibodies are immobilized on different microring clusters of a sensor chip. Each individual anti-cTnI antibody is then sequentially flowed across the peptide-immobilized ring

clusters. As illustrated in Figure. 7.2, the antibodies are only specific to the peptides that correspond to their respective targeted epitopes and do not cross-react with the mismatched peptide sequences. Thus, this peptide array can potentially be used for detecting troponin autoantibodies that have similar epitope targets.

7.3 Future work of sepsis biomarker panel project

The sepsis biomarkers panel project described in the previous Chapter 6 has great promise of applying to clinical settings for monitoring sepsis progression in patients. In the short term, dilution of plasma samples should be investigated to optimize the measured response within the linear range of the assays for determining the concentration of each marker. As the project achieves quantitative detection of the 12 biomarkers in the panel, more septic patients' samples should be analyzed, and at this stage the results of the measurements should be validated by an external established method, such as ELISAs or the Luminex™ assay platform. This will give a good assessment of the microring resonator platform's performance in quantitation of sepsis markers. With the biomarker concentrations in the patients' plasma samples determined, these results can be used along other physiological information collected by the treating physicians to correlate the measured biomarker levels with patients' outcomes, and hopefully this information can aid in improving treatment of sepsis.

Finally, it should be recognized that as a hallmark of translational study, various steps in this project, beginning from biomarker screening, assay optimization, clinical trials, to correlation of results to disease prognosis of the patient, all require cooperative efforts between physicians, laboratory technicians, as well as data scientists, and this collaboration should continue on in the future to have successful achievements.

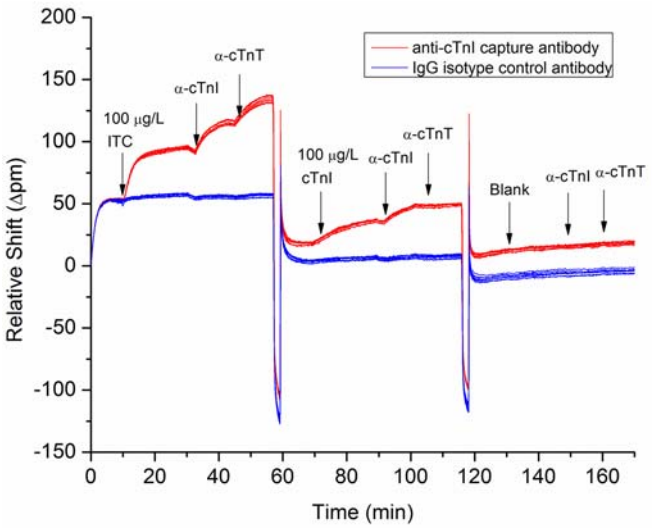

Figure 7.1 Sequential delivery of tracer antibodies specific against cTnI and cTnT demonstrates the ability to differentiate between troponin ITC complex and the cTnI subunit.

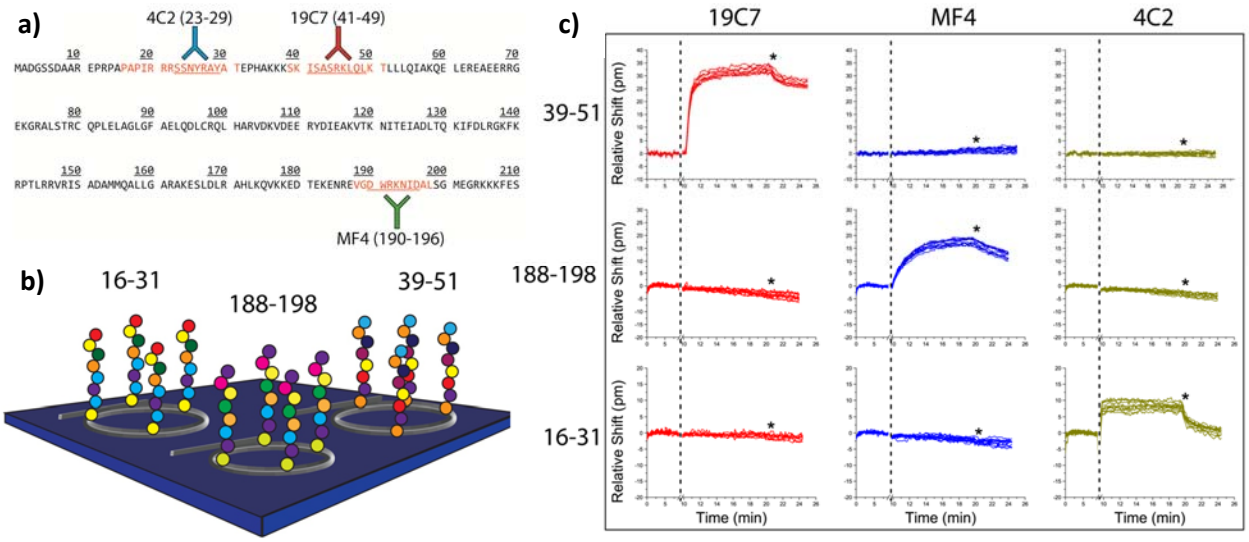

Figure 7.2 a) Schematic of the entire cTnI amino acid sequence, highlighting specific epitopes (residues 23-29, 41-49, and 190-196) that are targeted by anti-cTnI antibody clones 4C2, 19C7, and MF4. **b)** Schematic illustration of microring resonator arrays presenting the three selected peptide epitopes in a). **c)** Real-time microring resonator responses the three selected antibodies binding to their corresponding targeted peptide epitopes. Each columns represent the simultaneous probing of the three selected peptide sequences with a single antibody clone. From the figure, the antibody-peptide binding response are highly specific with minimal cross-reactivity observable. Thus, the same peptide array principle can potentially be applied to detecting autoantibodies that interfere with cTnI assays.

7.4 References

1. Gaze DC, Collinson PO. Multiple molecular forms of circulating cardiac troponin: Analytical and clinical significance. Annals of Clinical Biochemistry 2008;45:349-55.
2. Lippi G, Cervellin G. Degradation of troponin i in serum or plasma: Mechanisms, and analytical and clinical implications. Semin Thromb Hemost 2012;38:222-9.
3. Düngen H-D, Platzeck M, Vollert J, Searle J, Müller C, Reiche J, et al. Autoantibodies against cardiac troponin i in patients with congestive heart failure. European Journal of Heart Failure 2010;12:668-75.
4. Eriksson S, Halenius H, Pulkki K, Hellman J, Pettersson K. Negative interference in cardiac troponin i immunoassays by circulating troponin autoantibodies. Clinical Chemistry 2005;51:839-47.